1995-12

Synoptic and mesoscale influences on refraction during SHAREM 110

Byers, David John.

Monterey, California. Naval Postgraduate School

NAVAL POSTGRADUATE SCHOOL
MONTEREY, CALIFORNIA

THESIS

SYNOPTIC AND MESOSCALE INFLUENCES ON REFRACTION DURING SHAREM 110

by

David John Byers

December, 1995

Thesis Co-Advisors: Kenneth L. Davidson
Carlyle H. Wash

Approved for public release; distribution is unlimited.

REPORT DOCUMENTATION PAGE

Form Approved OMB No. 0704-0188

1. AGENCY USE ONLY *(Leave blank)*	2. REPORT DATE	3. REPORT TYPE AND DATES COVERED
	December, 1995	Master's Thesis

4. TITLE AND SUBTITLE	5. FUNDING NUMBERS
SYNOPTIC AND MESOSCALE INFLUENCES ON REFRACTION DURING SHAREM 110	
6. AUTHOR(S) David John Byers	
7. PERFORMING ORGANIZATION NAME(S) AND ADDRESS(ES) Naval Postgraduate School Monterey CA 93943-5000	8. PERFORMING ORGANIZATION REPORT NUMBER
9. SPONSORING/MONITORING AGENCY NAME(S) AND ADDRESS(ES)	10. SPONSORING/MONITORING AGENCY REPORT NUMBER

11. SUPPLEMENTARY NOTES The views expressed in this thesis are those of the author and do not reflect the official policy or position of the Department of Defense or the U.S. Government.

12a. DISTRIBUTION/AVAILABILITY STATEMENT	12b. DISTRIBUTION CODE
Approved for public release; distribution is unlimited.	

13. ABSTRACT *(maximum 200 words)*

Highly variable refractive conditions over the Persian Gulf and Gulf of Oman are studied during the SHAREM 110. Data collected during SHAREM 110, conducted in February 1995, included the Naval Operational Regional Atmospheric Prediction System (NORAPS), a large data base of upper air profiles, shipboard surface weather observations, and satellite imagery. Four different meteorological regimes occurred; pre-Shamal or Kaus, Shamal, Northeast Monsoon, and a short Shamal event. In addition to discussing the effects of synoptic meteorology on refraction during these periods, topography is also found to be a major factor in influencing refractive variability. The land/sea breeze was also found to be very important in modifying the low level refractive structure, especially in the Gulf of Oman.

14. SUBJECT TERMS Elevated Duct, Kaus, Land Breeze, Littoral Zones, Northeast Monsoon, Refraction, Sea Breeze, Shamal, Surface Based Duct	15. NUMBER OF PAGES 135
	16. PRICE CODE

17. SECURITY CLASSIFICATION OF REPORT	18. SECURITY CLASSIFICATION OF THIS PAGE	19. SECURITY CLASSIFICATION OF ABSTRACT	20. LIMITATION OF ABSTRACT
Unclassified	Unclassified	Unclassified	UL

NSN 7540-01-280-5500

Standard Form 298 (Rev. 2-89)
Prescribed by ANSI Std. 239-18 298-102

Approved for public release; distribution is unlimited.

SYNOPTIC AND MESOSCALE INFLUENCES ON REFRACTION DURING SHAREM 110

David John Byers
Lieutenant, United States Navy
B.A., University of Virginia, 1985

Submitted in partial fulfillment
of the requirements for the degree of

MASTER OF SCIENCE IN METEOROLOGY AND PHYSICAL OCEANOGRAPHY

from the

NAVAL POSTGRADUATE SCHOOL
December 1995

Author: [redacted]
David John Byers

Approved by: [redacted]
Kenneth L. Davidson, Thesis Co-Advisor

[redacted]
Carlyle H. Wash, Thesis Co-Advisor

[redacted]
Robert L. Haney, Chairman
Department of Meteorology

ABSTRACT

Highly variable refractive conditions over the Persian Gulf and Gulf of Oman are studied during the SHAREM 110. Data collected during SHAREM 110, conducted in February 1995, included the Naval Operational Regional Atmospheric Prediction System (NORAPS), a large data base of upper air profiles, shipboard surface weather observations, and satellite imagery. Four different meteorological regimes occurred; pre-Shamal or Kaus, Shamal, Northeast Monsoon, and a short Shamal event. In addition to discussing the effects of synoptic meteorology on refraction during these periods, topography is also found to be a major factor in influencing refractive variability. The land/sea breeze was also found to be very important in modifying the low level refractive structure, especially in the Gulf of Oman.

TABLE OF CONTENTS

I. INTRODUCTION

Two major roles of the U.S. Navy have always been power projection and protection of the sea lanes of communication and commerce. However, over the last several years, the way this mission has been met has drastically changed. Both the end of the Cold War along with the corresponding decrease in defense spending have ended the Navy's concentration on what was known as "blue water"or open ocean warfare. Deep water anti-submarine warfare (ASW) and large fleet to fleet engagements are not now considered the Navy's primary threat.

Today, the emphasis of the Navy's efforts has been directed to more localized regions where the primary national interests of the United States can be threatened. This new emphasis is stated quite clearly in Forward...From the Sea, a policy document signed by the Secretary of the Navy, the Chief of Naval Operations, and the Commandant of the Marine Corps (Dalton, 1994). It was intended to update and expand an earlier policy document, From the Sea (O'Keefe, 1992). Forward...From the Sea states:

> Because we are a maritime nation, our security strategy is necessarily a transoceanic one. Our vital interests-those interests for which the United States is willing to fight-are at the endpoint of "highways of the seas" or lines of strategic approach that stretch from the United States to the farthest point on the globe. Not surprisingly, these strategic lines and their endpoints coincide with the places to which we routinely deploy naval expeditionary forces: the Atlantic, Mediterranean, Pacific, Indian Ocean, Red Sea, Persian Gulf, and Caribbean Sea. Reductions in fiscal resources, however, dictate that we must refocus our more limited naval assets on the highest priorities and the most immediate challenges, even within these areas of historic and vital interest to the United States.

These new areas for Navy operations are in what is generally described as littoral regions. Littoral regions are basically thought of as "near land" regions and can be defined as comprising two segments of the battle space. The first is known as the seaward segment. It is the area from the open ocean to the shore which must be controlled to support operations ashore. The second is the landward segment. It is the area inland from shore that can be supported and defended directly from the sea (O'Keefe, 1992). O'Keefe (1992) further describes the littoral region as an area of,

> ...confined and congested water and air space occupied by friends, adversaries, and neutrals--making identification profoundly difficult. This environment poses varying technical and tactical challenges to Naval Forces. It is an area where our adversaries can concentrate and layer their defenses. In an era when arms proliferation means some third world countries possess sophisticated weaponry, there is a wide range of potential challenges.

Littoral regions bring with them unique operating environments especially as far as electromagnetic propagation is concerned. These include terrain effects causing backscatter, land-sea breeze circulations which can produce surface based ducts, and distinct air mass differences as different synoptic systems cross the land/water border. All of these environmental factors can dramatically affect how well a particular sensor will be able to detect a target and the range at which it will be seen.

Recently the Persian Gulf littoral region, in particular, has proven itself to be of vital interest to the United States. Now the U.S. Navy finds itself operating there continuously. As described above, this is a region where the Navy operates surrounded by allies, neutrals, and potentially hostile enemies. It is crucial that operational commanders have confidence in their ability to tell the difference between all of these possible contacts. Since the atmosphere

can have a major influence in determining radar detection ranges, it is very important to understand the changing meteorology of a region and how it affects atmospheric propagation.

This thesis will look in particular at the recent fleet exercise, called SHAREM 110, that was conducted in the Persian Gulf in February 1995. A detailed discussion of the changing synoptic situation during this period will be presented. The effect these changes had on the upper air profiles with respect to temperature, dew point, and the refraction conditions will be discussed.

II. ATMOSPHERIC PROPAGATION

A. GENERAL

To date, the best methods of detecting objects above the surface involve the use of sensors that exploit some portion of the electromagnetic (EM) spectrum. The EM spectrum contains such useful frequencies/wavelengths as visible light, x-rays, and those making up the radar band. While all EM frequencies are subject to some amount of refraction, this thesis is concerned mainly with those that make up the radar bands as summarized in Table 1 below.

		(Frequency)	300 GHz
EHF (Extreme High Frequency)	Radar, space exploration	(Wavelength)	1 mm 30 GHz
SHF (Super High Frequency)	Radar, satellite communication		1 cm 3 GHz
UHF (Ultra-high Frequency)	Radar, TV, navigation		10 cm 300 MHZ
VHF (Very High Frequency)	Radar, TV, FM, police, air traffic control		1 m 30 MHZ
			10 m

Table 1. Electromagnetic Spectrum (after Craigie, 1993).

Predicting detection ranges for a particular sensor system would be easy if the earth's atmosphere were horizontally homogeneous and well-mixed in the vertical. Instead the atmosphere is comprised of different air layers with different temperature, and moisture characteristics. It is these differences that cause EM rays to bend or refract. As these air masses move horizontally, they bring with them their own unique refraction characteristics.

In littoral environments, the prediction problem becomes more difficult due to rapid air mass changes due to land-sea interactions.

In free space, the rays traced by EM waves travel in straight lines and radars are basically line of sight. This is not true for EM waves traveling in the atmosphere. Even with the assumption of a "normal" atmosphere (i.e. homogenous in the horizontal and normal vertical decreases in pressure, temperature, and moisture with height), radars would have slightly extended over the horizon detection ranges. These extended ranges are due to the fact that the index of refraction (n) also generally decreases with height. EM waves "bend" toward higher values of n, so rays traveling through the earth's atmosphere are bent toward the surface instead of traveling straight out into space thereby allowing over the horizon detection. The temperature and moisture differences due to different air masses, both in the vertical and horizontal, mentioned above compound the problem by changing n with distance and altitude.

B. REFRACTION

EM waves can be described by Snell's Law. This law makes it possible to predict the path a ray (EM, acoustic, etc.) will follow as it propagates through a medium with varying indices of refraction. It basically predicts the new direction a ray will take as it transitions into a different layer in the medium if the direction of the ray in the first layer is known.

The index of refraction, n, is defined as the ratio of the velocity of a wave in a medium, v, to its velocity in a vacuum, c, or n=c/v. For air, n is a function of barometric pressure, temperature, and water vapor pressure. Snell's law can be used to show that the radius of the ray is determined by the gradient of n using the relationship:

$$r = -\frac{1}{\frac{dn}{dz}} \qquad \textbf{(1)}$$

The index of refraction for the atmosphere generally has a value that lies between 1.000250 and 1.000400. Because the index of refraction of VHF/UHF/microwave frequencies in the atmosphere is very close to 1, it is convenient to define a new measure of refraction based on the difference from 1, which is called the "refractivity", or N, defined as:

$$N \equiv (n-1) * 10^6. \qquad \textbf{(2)}$$

N may be derived for any altitude from atmospheric pressure, P, the temperature, T, and the partial pressure of water vapor, e, by:

$$N = \frac{(77.6P)}{T} + \frac{(5.6e)}{T} + \frac{(3.73*10^5 e)}{T^2}. \qquad \textbf{(3)}$$

Both P and e must be in millibars (mb), and T must be in degrees Kelvin (K).

There is a third and more useful way to describe atmospheric refraction known as the modified refractivity index (M). This index can be calculated from the following expression:

$$M = N + 10^6 \frac{z}{R_e} \tag{4}$$

where z is height above the earth in kilometers (km)., N is the refractivity at that height and R_e is the radius of the earth in km. When the vertical gradient of M is zero (or dN/dz = -157/km.) the ray radius equals the earth's radius. The modified refractivity index will increase with height in the standard atmosphere defined earlier. The importance of using M is that for a trapping layer (defined later) to occur, dM/dz must be negative. This makes it much easier to find trapping layers and ducts when M is actually plotted against height.

There are basically four different regimes for refraction; normal, subrefraction, super-refraction, and trapping. Figure 2.1 gives a basic graphical description of them. Since pressure always decreases with height, how a ray is refracted depends mainly with how temperature and moisture vary along the propagation path. Normal refraction occurs when dN/dz goes from -79 to 0/km and dM/dz goes from 79 to 157/km. Subrefraction occurs when temperature and moisture factors combine to cause N to increase with height and dM/dz > 157/km. The effect on EM rays is to cause them to actually bend upward or bend downward less than normal. The effect on EM sensor systems is reduced detection ranges. Superrefraction occurs when temperature and moisture factors cause rays to bend downward more than normal. This results in extended range detection for radars. For these first three conditions, any downward bending of EM rays is less or equal to the earth's curvature.

Trapping occurs when there is a very sharp negative gradient in N (or $dM/dz < 0$). EM waves now bend downward with a curvature equal to or greater than the earth's curvature. They will then either reflect off the earth's surface or be refracted back upward after entering a region of standard refraction. The waves are effectively trapped in what amounts to a waveguide and extremely extended ranges are possible. Table 2 below summarizes the various refractive conditions for vertical gradients of N and M.

	N - Gradient	M - Gradient
Subrefractive	> 0/km	> 157/km
Normal	-79 to 0/km	70 to 157/km
Super-refractive	-157 to -79/km	0 to 79/km
Trapping	< -157/km	< 0/km

Table 2. Conditions of Refractivity (after Craigie, 1993).

C. DEFINITION OF DUCTING CONDITIONS

Of the situations summarized in Table I above, trapping conditions are the most useful operationally. Over the past several years, much research has gone into detecting and predicting the presence of trapping layers and how they can affect radar propagation. Trapping layers are formed when temperature increases and/or moisture decreases with height at a very rapid rate.

One way for such a condition to occur is under large scale subsidence which occurs after a cold frontal passage. As air sinks it will warm due to compression. Also, air aloft generally contains very little moisture. Hence, as this air sinks, it warms and dew points remains low. When this air caps cooler, moist air (such as the air over a body of water) a distinct boundary is formed producing strong temperature (inversion) and moisture gradients.

Another way for a trapping layer to form is for the generally drier and warmer air over a land mass to be advected out over a body of water. There may not be much of a temperature inversion formed but the drier air over the moist ocean air can produce a strong enough moisture gradient to produce a trapping layer.

The entire duct includes the trapping layer and extends downward until the same value for M as that at the top of the trapping layer is encountered again. If this happens before the earth's surface is reached, it is known as an elevated duct. If the duct reaches the earth, then it is known as a surface based duct. Figures 2.2 and 2.3 illustrate this phenomena.

Evaporation ducts are a special type of surface based duct. They are caused by the sharp decrease in atmospheric moisture at the air-sea boundary. Because of this, M decreases with height but a relative minimum quickly occurs (Figure 2.4), usually under 30 m. with a worldwide average of 13 m. (Craigie, 1993). They can also be embedded in a thicker surface based duct. Evaporation ducts are very hard to measure so generally some sort of model based on sea surface temperature and relative humidity has to be employed. Measurement of these parameters, however, are subject to shipboard influences and instrument error making analysis and prediction more difficult and possibly unreliable.

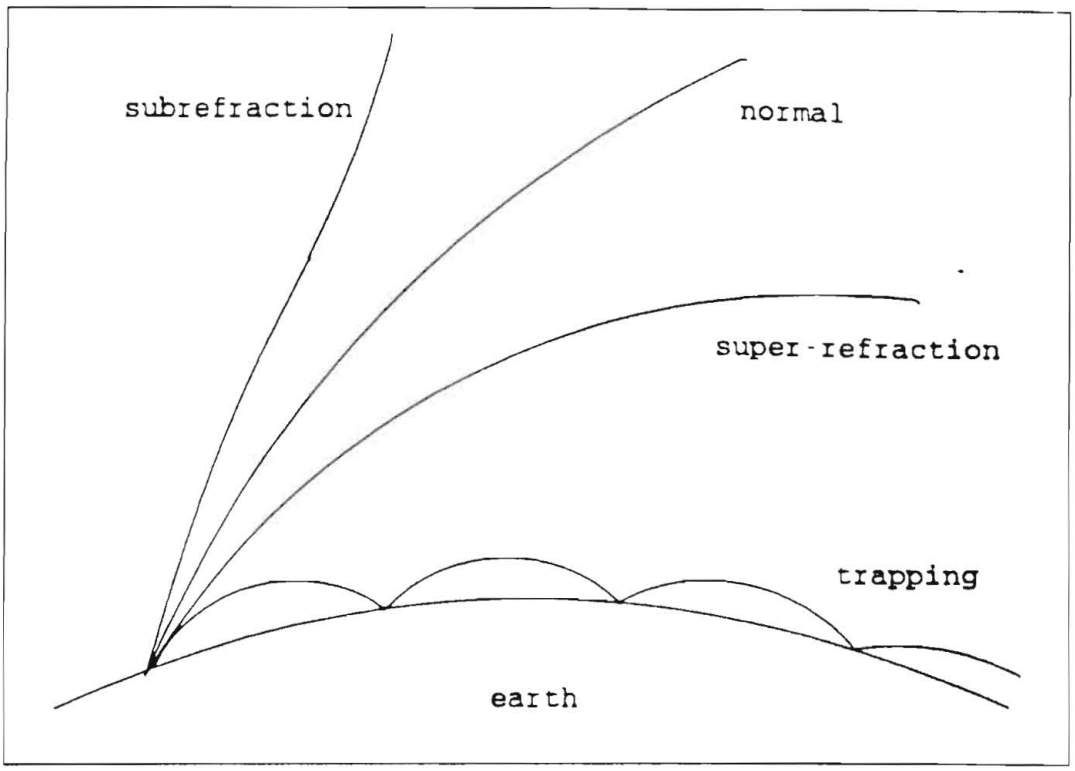

Figure 2.1 Electromagnetic Wave Paths for Various Refractive Conditions (from Craigie, 1993).

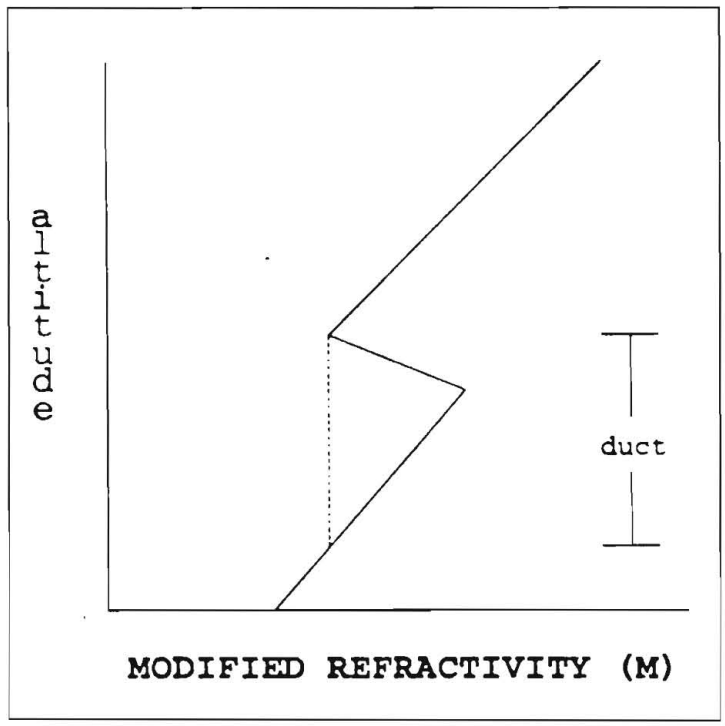

Figure 2.2 Elevated Duct (from Craigie, 1993).

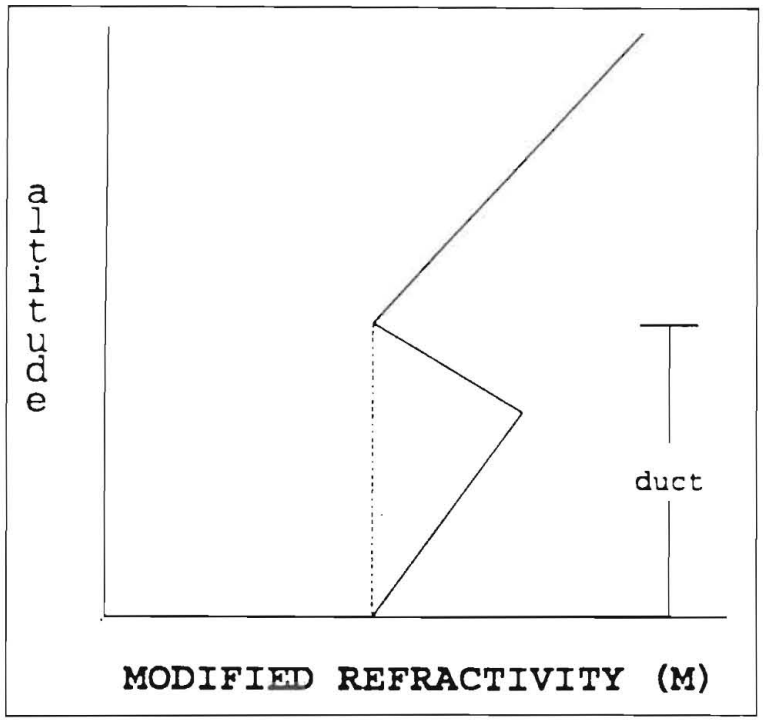

Figure 2.3 Surface-based Duct (from Craigie, 1993).

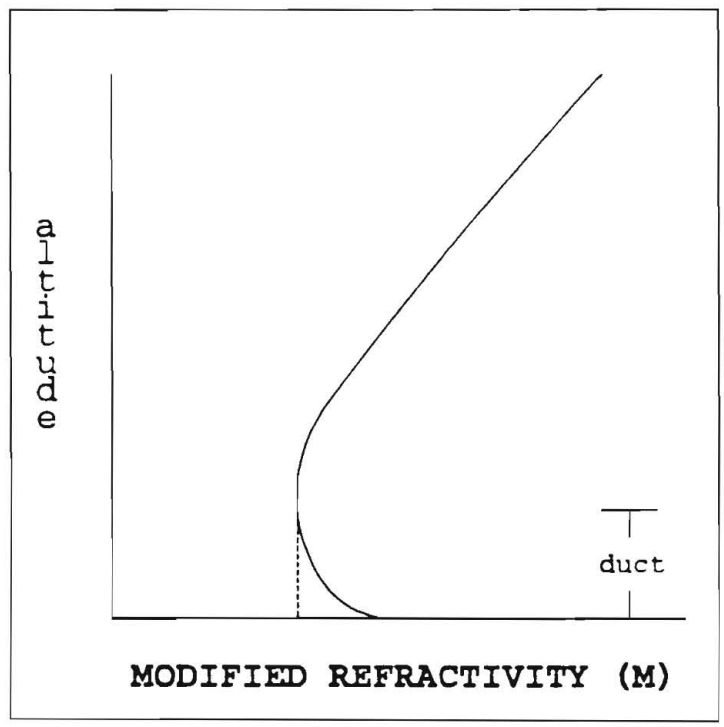

Figure 2.4 Evaporation Duct (from Craigie, 1993).

III. SHAREM 110 OVERVIEW

Fleet exercises are used to construct an operational environment for developing and testing new tactics. Until recently, the Ship ASW Readiness and Effectiveness Measuring (SHAREM) Program series of exercises were exclusively the test bed for anti-submarine warfare (ASW) tactics. However, SHAREM 110, conducted in the Commander, US Naval Central Command's (COMUSNAVCENT) area of responsibility from 5 to 17 February, 1995, was one of recent expanded SHAREMs including other naval threats. The revised exercise structure has grown to include a multi-threat, multi-warfare scenario.

Integral to understanding this multi-threat, multi-warfare environment is the deployment of an electromagnetic/electro-optic (EM/EO) support system capable of depicting the physical atmosphere and how it will affect sensor and weapon systems. The primary purpose of SHAREM 110 phase 1 was to demonstrate, in a tactically significant theater of operations, an end-to-end meteorological and oceanographic (METOC) EM/EO support system. This system consisted of two components, the SPAWARSYSCOM METOC Shipboard Forecast Tactical Atmospheric Capability (STAFC) and Sensor Performance Prediction Advanced Development Model (SPP-ADM).

The support system process, utilized during the exercise, was initiated by high resolution Fleet Numeric Meteorology and Oceanography Center (FNMOC) models transmitted to Bahrain where they were to be interfaced with in situ measured environmental inputs and transmitted to the EM/EO test ship. This data was combined on the ship *with the*

most recent meteorological measurements and measured clutter data to finally result in shipboard generated radar performance predictions. The EM/EO support system made use of state-of-the-art prediction models such as the Naval Operational Regional Atmospheric Prediction System (NORAPS) and the Navy's Radio Physics Optics (RPO) propagation model, extensive and exhaustive measurements using sophisticated measurement devices, and exchange of substantial amounts of data (both modeled and measured) to provide near real-time predictions of combat system performance. Figure 3.1 depicts the overall data flow for the EM/EO support system.

The surface ships which participated in SHAREM 110 were the USS Lake Erie (LKE), USS David R. Ray (DRR), USS Vandegrift (VAN) and the USNS Silas Bent (BNT). The Officer in Tactical Command (OTC) was Commander, Destroyer Squadron Fifty (COMDESRON 50) embarked on the USS David R. Ray. There were two operating areas during SHAREM 110. The first half of the exercise was conducted in the southern Persian Gulf and the second half was conducted just outside the Strait of Hormuz in the western Gulf of Oman. In order to meet thesis objectives, upper air profiles calculated from radiosondes launched from all three of these platforms as well as dropsondes and rocketsondes launched from the Lake Erie will be studied. Approximately 140 profiles in all were collected.

The local terrain plays a major role in the weather of the Persian Gulf region. Figure 3.2 depicts the general geography and topography of the Persian Gulf and the Gulf of Oman, the area of interest for SHAREM 110. The Persian Gulf extends 530 nautical miles from the Euphrates River delta southeastward to the Strait of Hormuz. The width of the Gulf averages from 130 nm to 150 nm from its northern end to Abu Dhabi. East of Abu Dhabi, the Gulf

rapidly narrows to 70 nm. Further east, the Gulf narrows even further to become the Strait of Hormuz. The strait averages 50 nm in width, however, it is only 30 nm across at its narrowest point. The Gulf of Oman extends from the Strait of Hormuz into the Arabian Sea where it ends at a line drawn from Jiwani on the Iran-Pakistan border to the easternmost point of Oman. (Walters and Sjoberg, 1988)

The topography surrounding the Persian Gulf on its northwestern, southwestern, and southeastern sides is basically flat. The northwestern shore is dominated by salt marshes with desert lying beyond. The southwestern shore is basically flat with sand dunes inland. South of Dhahran elevations rise slowly inland to about 1,700 feet. The northeastern shore of the Persian Gulf Gulf, however, is dominated by numerous mountain ranges oriented parallel to the Persian Gulf-Gulf of Oman. These mountains are called the Zagros Mountains with peaks ranging from 11,000 to over 14,000 feet. They are a major influence in lower level wind directions.

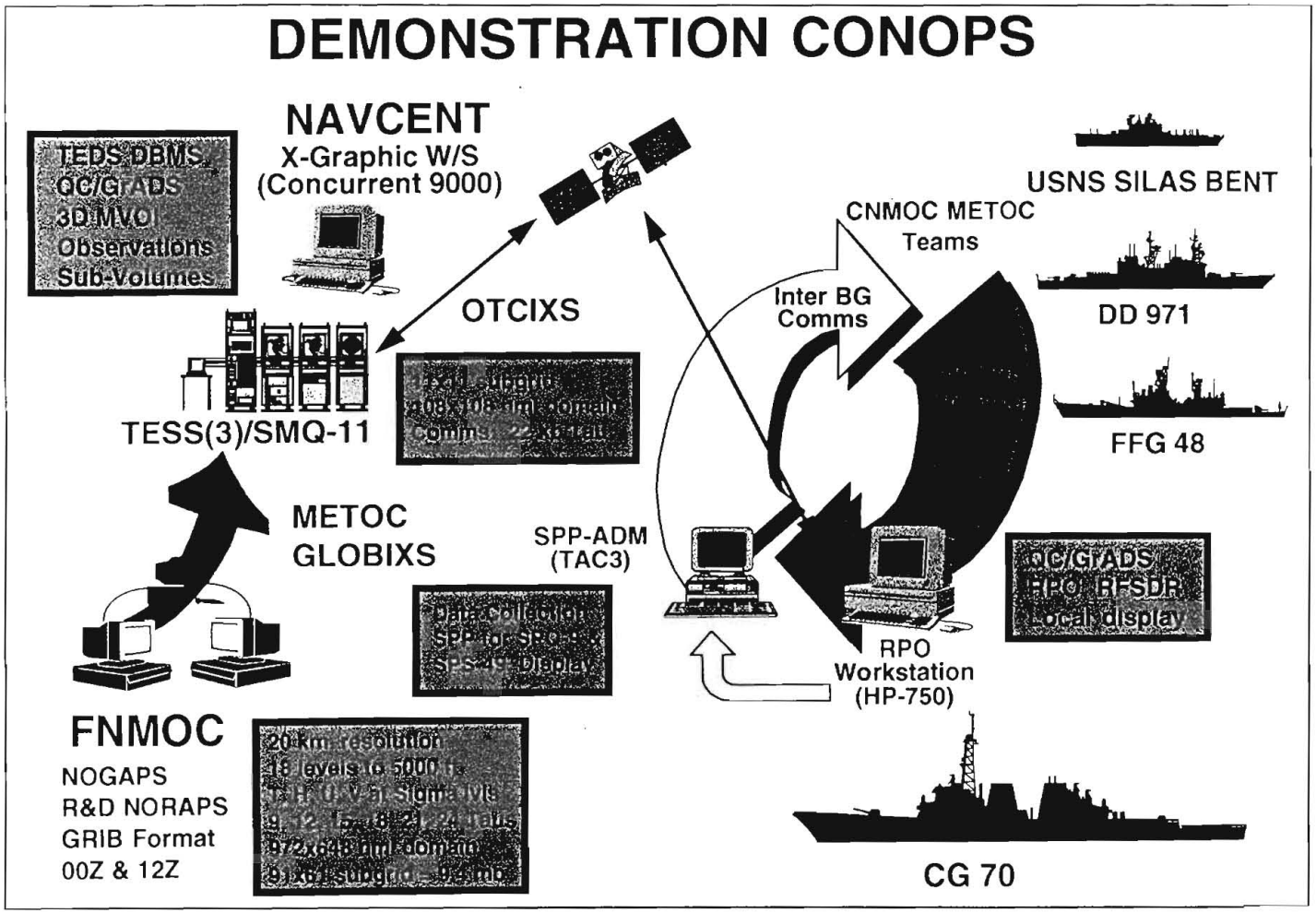

Figure 3.1 Communications Connectivity During SHAREM 110 (Cook, 1995).

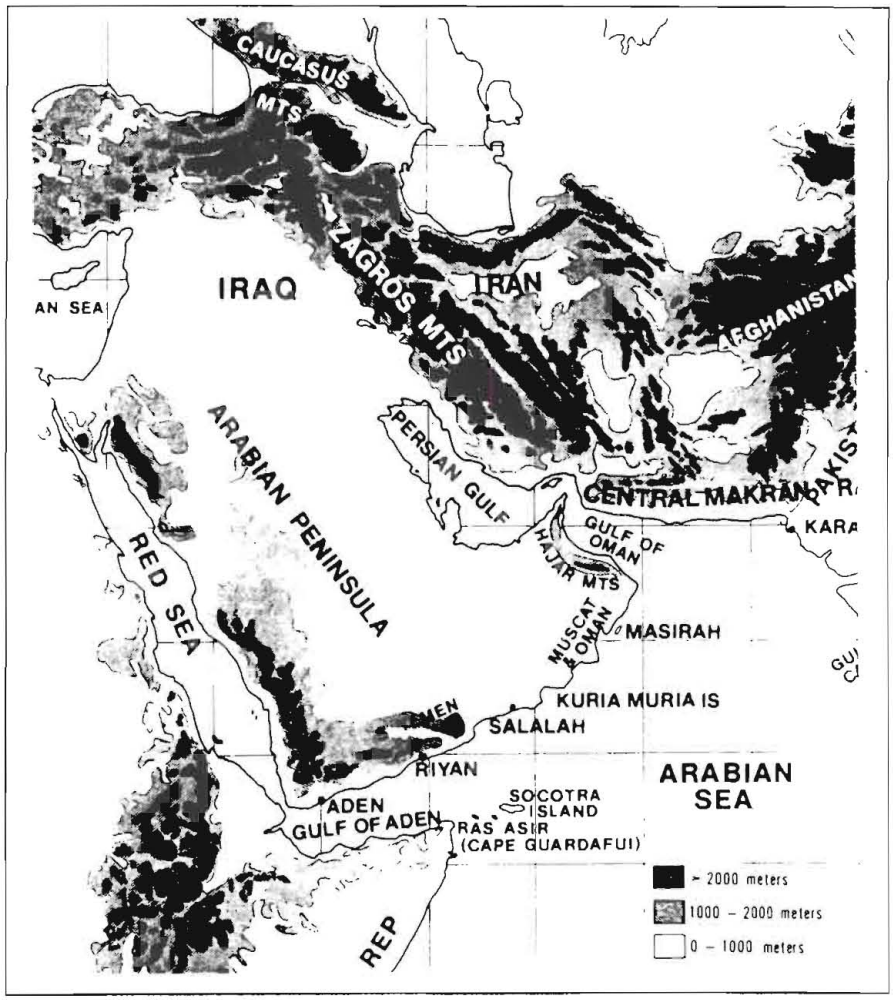

Figure 3.2 Locator Map of the Arabian Sea (after Brody, 1979).

IV. PERSIAN GULF PORTION OF SHAREM 110

A. GENERAL

The first half of SHAREM 110, from 6 to 13 February, was conducted just off the coast of Iran in the southeastern portion of the Persian Gulf. During this eight day period the participating ships launched a combined total of 60 radiosondes and rocketsondes. These were to support various exercises designed to evaluate detection of low flying aircraft and submarine periscopes. One of the desired goals was to evaluate how knowledge of the refractive nature of the atmosphere could affect the detection of such targets.

The Persian Gulf experienced a Shamal during this period. The Shamal is a well known meteorological phenomena for this area and has been described and documented by Perrone (1979). It is important to understand how Shamals can affect atmospheric refractivity in this region since they are a frequent winter event.

While general refractive studies of the Persian Gulf have been completed (Farrell, 1988), this is the only time, to the author's knowledge, that such a large number of frequent vertical profiles have been obtained before and during a Shamal The synoptic progression of the Shamal during SHAREM 110 is described using NORAPS model data archived by the Naval Research Laboratory, Monterey. It should be noted here that the meteorological charts with time of 03Z and 15Z used in this study are actually the tau = 15 hr. run of the NORAPS model even though they are occasionally referred to and "analyses". This thesis will address the ability of NORAPS to capture the significant meteorological events as reflected in the actual vertical profiles collected during SHAREM 110.

B. WINTER SHAMAL DEFINED

The word Shamal comes from the Arabic language and means north. It refers to strong northerly and northwesterly winds that occur in the Persian Gulf just after a southward moving cold front passes through the area. During the winter, these Shamals are generally responsible for the very hazardous weather conditions due to winds. The strong northerly surface winds are caused by an intense pressure gradient that develops behind the cold front. This gradient is formed by a strong high pressure area over western Saudi Arabia and Iraq. The northwesterly surface winds are then reinforced by upper level northwesterly winds behind the middle level trough present over the area. (Walters and Sjoberg, 1988)

There are basically two types of Shamals that have been identified, a short 24 to 36 hour Shamal and the longer lasting 3 to 5 day Shamal. During SHAREM 110, the Persian Gulf experienced a Shamal of the 3-5 day variety. This type of Shamal occurs only one to three times a winter and can produce the highest winds and seas found in the Gulf over the whole year. Sustained winds over the exposed Gulf have been known to reach 50 kts. producing 12 to 15 ft. seas (Walters and Sjoberg, 1988).

The 3-5 day Shamal arises due to the stagnation of a 500 mb trough over the Strait of Hormuz. In addition, a surface low is often induced in the Gulf of Oman by this trough. This coupled with high pressure to the north can lead to a 6 to 8 mb pressure gradient from Saudi Arabia to the Gulf of Oman. The Zagros Mountains (Figure 3.2) also play a major role in that they induce a lee trough that lies right along the Iranian coast. This trough serves to deform the surface pressure gradient to a northwest-southeast orientation. Figure 4.1 shows a typical surface pressure pattern associated with the 3 to 5 day Shamal. The Shamal ends

once the upper level trough moves off eastward allowing subsidence over northern Saudi Arabia to decrease and a relaxation of the surface pressure gradient (Perrone, 1979).

C. PRE-SHAMAL PERIOD

1. Synoptic Weather

Perrone (1979) states that the first indication of the possible formation of Shamal conditions is the presence of a upper level trough with a corresponding surface low moving over Syria from the eastern Mediterranean. NORAPS surface and 500 mb. analysis (Figures 4.2 and 4.3) show this situation developing at 12Z 7 Feb. In addition, an area of high surface pressure lies along the eastern shore of the Persian Gulf over western and northern Iran. To the north of this high lies another area of low pressure over the Caspian Sea, separate from the low to the west over Syria.

As the low over Syria moves east, it merges with the low over northern Iran. Also, the high pressure over Iran becomes less intense. By 03Z 8 Feb. this transition eastward of the Syrian low led to a nearly "classical" synoptic situation of southeasterly winds over the Persian Gulf known as Kaus winds. As Perrone (1979) states:

> Before the onset of the Shamal, winds in the area ahead of the approaching cold front blow from the south to southeast. These southerly winds (called "Kaus" in Arabic or "Shakki" in Persian) slowly increase in intensity as the front approaches, and may reach gale force before the frontal passage. The strongest southerly winds tend to occur on the eastern side of the Gulf, due to channeling of the lower level flow by the Zagros Mountains in western Iran...These southerly winds bring thick, gloomy weather, often with considerable rain.

More detailed presentations of the sea level pressure pattern and general wind flow are shown in Figures 4.4 and 4.5. Figure 4.4 presents the 03Z 8 Feb. NORAPS sea level

pressure chart. It shows low pressure over the south central Arabian peninsula and high pressure dominating central Iran. Figure 4.5 depicts the streamlines present during this time and shows Kaus winds covering the entire Persian Gulf.

The presence of these winds is supported by weather observation data collected onboard each ship. The time series in Figure 4.6 covers the Persian Gulf portion of SHAREM 110. It depicts changes over time of temperature, dew point depression, pressure, wind direction, and wind speed. Both NORAPS and ship data show easterly to southeasterly winds persisted over the southern Persian Gulf from the start of the exercise until about 00Z 9 Feb. Associated with these winds were warm temperatures between 70 and 76 degrees Fahrenheit and a slight general decrease in dew point depression and pressure.

2. Upper Air and Refraction

For the first half of the exercise, the ships generally operated in the area just west of the Strait of Hormuz shown in Figure 4.7. Vertical soundings reveal interesting and rather significant meteorological events affecting atmospheric refraction occurred during the pre-Shamal period. Under normal operating conditions, the subtle yet important changes in atmospheric refractivity to be described would probably have been overlooked. It is only due to the large number of vertical soundings that, for the first time, refraction changes with the onset of a Shamal can be studied.

The very first balloon launch of the exercise was from the USNS Silas Bent at 12Z 6 Feb and is shown in Figure 4.8. The first panel is a plot of temperature (Ta) in red and dew point temperture (Td) in blue in °C. The center panel shows wind direction and speed with height. The longer flags on the direction vectors signify 10 kts. and the shorter flags equal

5 kts. The map inset is of the southern Persian Gulf with a "+" marking the position where the radiosonde was launched. The third paned shows refractivity (N) in blue and modified refractivity (M) in green values with height and are unitless. This figure shows winds below 1500 m. are generally southerly. Winds at higher levels veer to the southwest as would be expected given the position of the upper level trough shown earlier. From the plot of temperature and dew point, it can be seen that the atmosphere is fairly well mixed in the lower levels with some drying starting at about 2200 meters. This situation lead to an M profile depicting near normal refractive conditions.

The wind profile from the next Silas Bent sounding, six hours later at 18Z, shows a subtle yet profound change (Figure 4.9). The lower level winds in the profile have backed and are now out of the northeast. Wind reports from the other ships also indicate this change in surface wind direction. Considering the time (2100 local time) at which these winds occurred, it is likely that these northeasterly winds were the result of a land breeze circulation due to rapid cooling of the Iranian land mass to the north. As the land cooled to a lower temperature than the water in the Persian Gulf, a low level circulation could have formed just like a sea breeze except reversed. Figure 4.4 indicates that at this time surface pressure gradient was weak so synoptic influences were minimal. This allowed the land breeze signal to become dominate in the local area.

Given the position of the ship, these lower level winds were offshore winds. Since offshore winds are generally dry, this lead to a strong moisture gradient in the vertical as can be seen in the temperature-dew point plot of Figure 4.9. These light offshore winds would also be subsiding due to down slope flow causing a temperature inversion. As a result, a

surface based duct formed as seen in the M unit profile also plotted in Figure 4.9. If exploited effectively by the operational commander, this duct would allow greatly increased detection ranges of just about every threat including submarine periscopes, low flying aircraft, and small, fast moving surface craft.

The Lake Erie launched a sounding three hours later at 21Z (Figure 4.10) and the results show that a low level layer of fairly strong easterlies had developed by this time extending from the surface to about 1400 m. Figure 4.6 and this sounding both show that the surface winds have picked up speed again at this time. The easterlies seen in this sounding were probably the result of the low level winds interacting with the local topography and are seen in roughly half of the soundings launched from 21Z 6 Feb. to 21Z 8 Feb. The other half of the soundings show the southerly to southeasterly lower level winds.

Whether or not a particular sounding indicated low level easterlies or not was due to its position in the box shown in Figure 4.7. NORAPS streamlines (Figure 4.5) during this time period illustrate the reason for varying wind directions. In this figure, the winds are out of the southeast for the most part. However, winds coming from the Gulf of Oman and the southeastern corner of the Saudi Arabian Peninsula are forced by the southern end of the Zagros Mountains (Figure 3.2) into a more easterly path. The result is the confluent asymptote (and, therefore, the fairly strong low level winds) seen over the eastern portion of the Persian Gulf in the figure. Generally, the closer to shore and the further east a ship was when it launched its balloon, the better chance the vertical wind profile would indicate low level easterlies. This would be particularly true during the night time land breeze hours. The further west and offshore a ship was would result in southerly to southeasterly winds.

The sounding from the Lake Erie at 21Z 6 Feb. (Figure 4.10) shows some drying with height and a slight temperature inversion below 500 m. This did not result in a trapping layer but produced a layer where dM/dz was approximately zero. The sounding from the Silas Bent (Figure 4.11) at 03Z 7 Feb. shows a well-mixed marine layer starting to develop topped by a decrease in moisture and a temperature inversion with southeasterly winds. This resulted in a fairly weak trapping layer from about 250 m. to 300 m.

At 06Z 7 Feb. a second layer of drying began to make its appearance at around 1500 m. Both layers were well developed by 15Z 7 Feb. as shown by the sounding launched at this time by the Silas Bent (Figure 4.12). There is a well developed marine layer extending from the surface to around 300 m. The second layer of drying starts at around 1000 m. and appears to be associated with the easterly winds shifting and coming out of the south. Southerly winds drying out the sounding are not surprising as their source region would have been over the dry Saudi Arabian peninsula. The M profile of this figure indicates that the weak trapping layer seen in the last figure is still present. However, because of the additional drying taking place at 1000 m., a new trapping layer is found also at 1000 m.

At 18Z 7 Feb. both the Silas Bent and the David R. Ray launched soundings from the positions shown in Figure 4.13 and some interesting comparisons can be made from them. Figure 4.14 is the sounding from the David R. Ray and Figure 4.15 is the sounding from the Silas Bent. The David R. Ray was further to the west at this time than the Silas Bent. Figure 4.14 shows that the lower level winds were, for the most part, from the south-southeast while the lower level winds in Figure 4.15 were from the east. This is not unexpected as discussed previously above. This difference in low level wind directions are the reason the low level M

profiles are different in the two soundings. The drying starting right at the surface in the David R. Ray's sounding was due to dry air coming directly from the interior of Saudi Arabia influencing the lower levels at this position. On the other hand, the Silas Bent was in a position further east where air that started out in the Gulf of Oman was also influencing the lower levels. This caused the Silas Bent to have a better mixed marine layer as moist air from the Gulf of Oman moved over its position. Both sounding indicate drying associated with southerly winds taking place at slightly higher levels. Once again this would be dry air directly from the interior of Saudi Arabia and at least in the Silas Bent's sounding led to the formation of an elevated duct. The implication of this is that soundings launched in an area affected by the Zagros Mountains as discussed above will show stronger ducting conditions than a sounding launched further to the west away from topographic effects.

By 06Z 8 Feb., the Silas Bent sounding only shows the previously described lower elevated duct and it has grown weaker and shallower. In addition, the upper levels became moister since the 18Z 7 Feb. as southwesterly upper level wind advected moisture in advance of the front. This can be seen in satellite imagery shown later.

This lack of trapping layers caused by mesoscale or synoptic scale influences during this time period seem to be tied to the disappearance of the surface layer easterly winds dominate in previous soundings and a general decrease in low level wind speed seen both in the soundings and Figure 4.6. In addition, all of these later soundings show a more mixed and moist boundary layer as the time of the Shamal onset approached (approximately 00Z on the 9th). This is depicted very well by Figure 4.16, the last sounding before the appearance of the Shamal from the Silas Bent.

It should be noted here that a number of the balloon soundings during the entire SHAREM 110 indicate the presence of a very shallow surface based duct with a top around 20 to 30 meters (such as the one seen in Figure 4.16). At first glance, these ducts would appear to be evaporation ducts. However, it is also possible that the duct depicted in these soundings are the result of shipboard influences. This is not to say that an evaporation duct is not present but rather that a balloon usually launched anywhere from 10 to 30 meters above the water from a ship whose deck can be warmer and drier than the ambient temperature is not an appropriate sensor to detect the presence of an evaporation duct.

In general, results in this section have shown that refractive conditions varied greatly both in time and space during the pre-frontal period of SHAREM 110. Perhaps the most important lesson presented in this section is the fact that low level flow in the Persian Gulf, especially in the southeast portion, is subject to topographical influences that can cause large differences in both the elevation and strength of a trapping layer. It was also shown during weak synoptic flow the land/sea breeze regimes develop and also significantly affect low level refraction. Finally, it was shown that as the front associated with the Shamal winds approaches, one can expect the atmosphere to become more and more mixed with a corresponding decrease in the occurrence of trapping layers and ducts.

D. SHAMAL PERIOD

1. Synoptic Weather

The Shamal during SHAREM 110 lasted from approximately 00Z 9 Feb. to about 03Z 14 Feb. The ships moved into the Gulf of Oman by the end of the Shamal. Hence, this section only covers the effects of the Shamal while the ships were still in the Persian Gulf (to approx. 00Z 13 Feb.). Chapter V will continue this discussion for the remaining period.

The synoptic situation continued to follow the "classic" description of a Shamal as described by Perrone (1979). This description indicates that by the onset of Shamal winds in the Persian Gulf , a new low pressure center will form on the front to the south of the original low that was moved from the eastern Mediterranean and that the upper level trough, shown previously in Figure 4.3, will progress eastward. In this case the new low develops over south-central Iran, as shown by the NORAPS 03Z 9 Feb. surface pressure analysis presented in Figure 4.17. This analysis also shows low pressure dominating the southern Saudi Arabian peninsula and high pressure in the Gulf of Oman and northern Saudi Arabian peninsula. Figure 4.18 shows the surface streamlines for the same time and indicates the front extending from the low in south-central Iran southwest to the Strait of Hormuz and continuing over the southern Saudi Arabian peninsula. Behind the front are the north-westerly Shamal winds. Upper air analysis at 00Z 9 Feb. (Figure 4.19) shows that the upper level trough has indeed progressed eastward from its position shown in Figure 4.3.

The mature period of the Shamal also agrees with Perrone's (1979) description. Although not shown, the new low was moved east into Pakistan and the front continued to push to the southeast into the Arabian Sea. High pressure continued to build down from the

north into Saudi Arabia as well as central Iran. The interaction of these two high pressure areas with the Zagros mountains induced a lee trough along the eastern Persian Gulf. By 03Z 11 Feb., this trough was fully developed according to NORAPS surface analysis (Figure 4.20). It continued unchanged, for the most part, until the end of the Persian Gulf portion of SHAREM 110.

The appearance of the Shamal, as well the frontal passage, can be seen readily in the time series presented previously in Figure 4.6. All four of the ships experienced decreasing (Kaus) winds out of the east-southeast just before the Shamal. With the passage of the front, winds shifted to from the north and rapidly picked up speed. Frontal passage occurred with the wind shift from the southwest to the northwest took place at around 00Z 9 Feb. Towards the end of the Persian Gulf portion of SHAREM 110, winds decreased considerably in speed (Figure 4.6) but still remained out of the northwest.

The time series also shows that temperatures began to fall with the wind shift as colder air was advected into the area of interest behind the front by these northerly winds. With the passage of the front, dew point depression rose. This is not unexpected as generally there is rapid clearing and subsidence behind a cold front. Figure 4.6 also indicates that surface pressures generally began to rise right after the frontal passage. The rise in pressure agrees with the NORAPS analysis of high pressure moving into the area behind the front during this time.

2. Upper Air and Refraction

Perrone (1979) states, "At the first penetration of cold air into the Gulf region, the lower levels of the troposphere experience strong but shallow northwesterly flow, while at

middle and upper tropospheric levels, the flow remains southwesterly." This is illustrated by the 00Z 9 Feb. sounding (Figure 4.21) from the Silas Bent. These northwesterly winds extending from the surface to about 400 meters are the first appearance of colder air of the Shamal in the upper air soundings.

Comparison of this sounding with the Silas Bent's previous sounding, Figure 4.16, shows the wind shift at lower levels typically associated with a frontal passage. This sounding plus the wind direction data in the time series, Figure 4.6, indicate that frontal passage was occurring this time, at least at the Silas Bent location. The two soundings are similar in that the lower levels shown are well mixed and the M value profile shows normal refractive conditions. The 0257Z DMSP infra-red satellite image, Figure 4.22, show the frontal band positioned directly over the operating area.

The next sounding, not shown, was three hours later from the David R. Ray. It showed the post frontal subsidence discussed above had begun and the low level northwesterly Shamal wind layer had deepened to about 1000 meters. This subsidence was much more prevalent by the 06Z 9 Feb. sounding from the Silas Bent (Figure 4.23). This sounding shows drying in the atmosphere taking place at about 1500 meters. This drying was probably associated with circulation around the front itself. This subsidence lead to the low dew point temperatures and the temperature inversion shown starting at about 1500 meters (Figure 4.23) with a fairly well mixed boundary layer remaining below 1500 meters. This, in turn, resulted in a thin trapping layer forming at around 1500 meters.

By 09Z 9 Feb. the Lake Erie's sounding shows the top of the boundary layer down to around 600 meters (Figure 4.24). Correspondingly, the trapping layer top was also at 600

meters. Comparing this M profile with the previous M profile in Figure 4.23, one can see that dM/dz is greater in the 09Z sounding which in turn lead to a stronger trapping layer and thicker elevated duct. The layer of northwesterly Shamal winds had also become thicker by this time, extending up to 2000 meters. Winds in this sounding are also stronger at all levels than winds in the previous sounding. These stronger winds were due to the pressure gradient over the operational area becoming tighter due to high pressure moving into the area as discussed above.

Subsidence aloft is analyzed in the sounding (Figure 4.25) launched from the Silas Bent at 12Z 9 Feb. The temperature-dew point plot indicates a second "surge" of subsidence at around 3500 meters as evidenced by the slight temperature inversion and the rapid drying shown by these two variables. Also, upper level winds were starting to have a more westerly component than the previous soundings. This is due to the upper level trough axis approaching the location of the ships. This second dry layer is the result of synoptic scale subsidence produced by high pressure building into the area as discussed previously. The lower boundary layer is still present with its associated trapping layer at around 700 meters and the Shamal winds still extend from the surface to 2000 meters with fairly strong wind speeds.

This upper level of subsidence continued to push down to lower levels over the next nine hours until it "merged" with the lower level subsidence and produced the Silas Bent's 06Z 10 Feb sounding shown in Figure 4.26. The result of this "merging" was to form one boundary layer with a top at about 1200 meters and a much drier atmosphere above the boundary layer than seen in previous soundings. The resulting trapping layer is higher and

associated with negative vorticity advection associated with the upper level trough was present in the sounding twelve hours after frontal passage. This synoptic scale subsidence continued to sink with time resulting in an extremely dry layer above the aforementioned marine layer. This situation produced an extremely strong trapping layer and a thick elevated duct. This duct disappeared once the ships moved into the Strait of Hormuz.

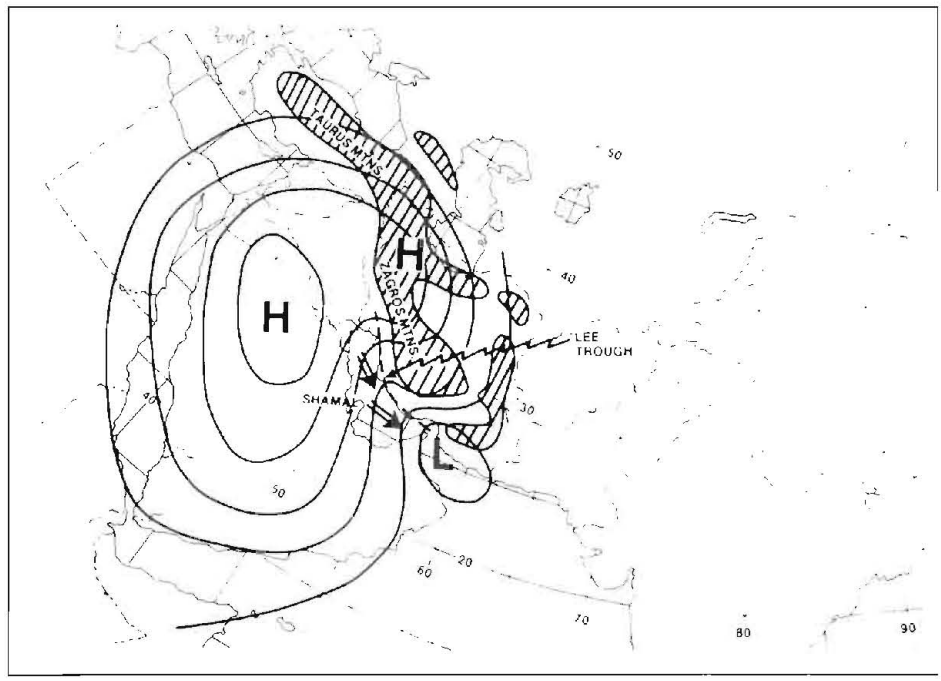

Figure 4.1 Typical Surface Pressure Pattern During a 3-5 day Sahmal (from Perrone, 1979).

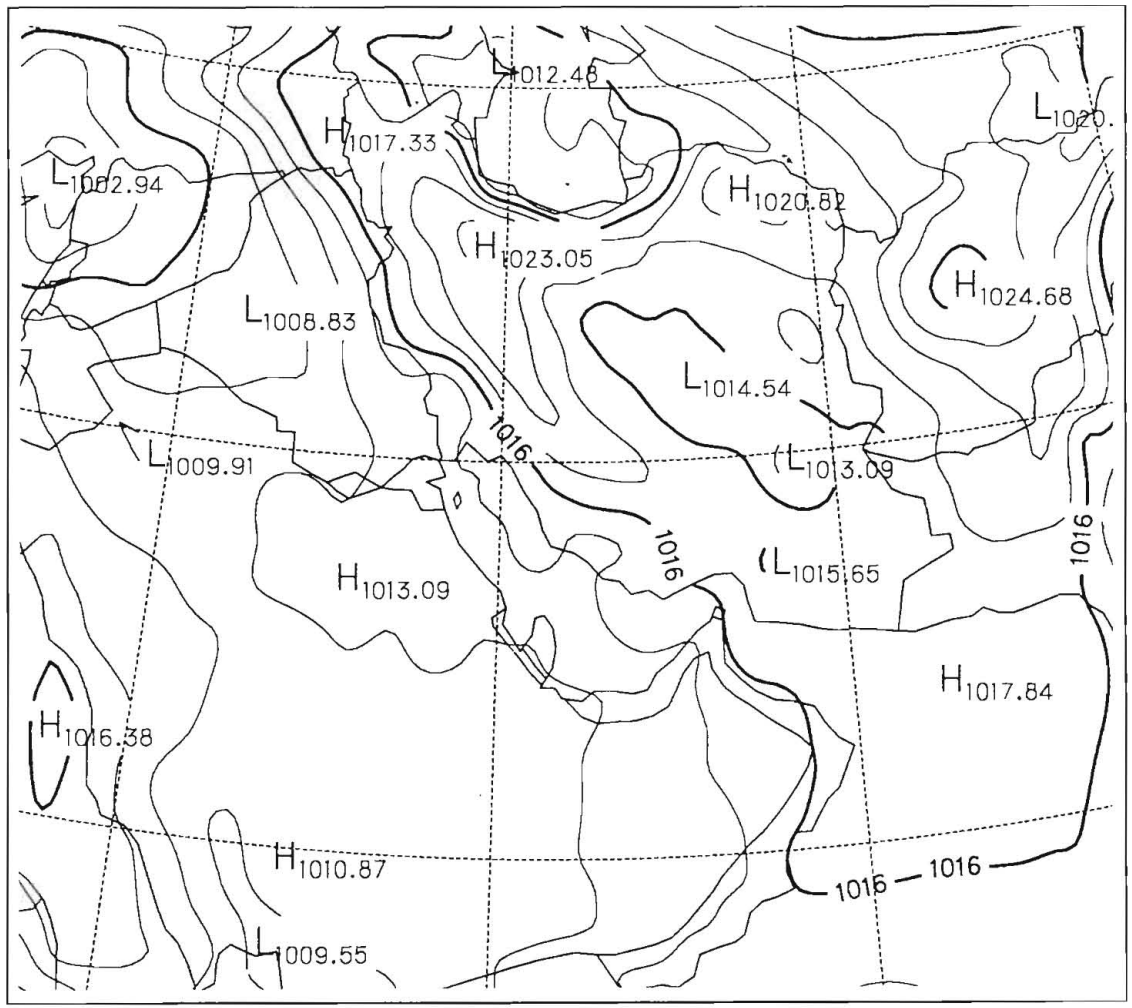

Figure 4.2 NORAPS 12Z Mean Sea Level Pressure Analysis for 07 Feb., 1995.

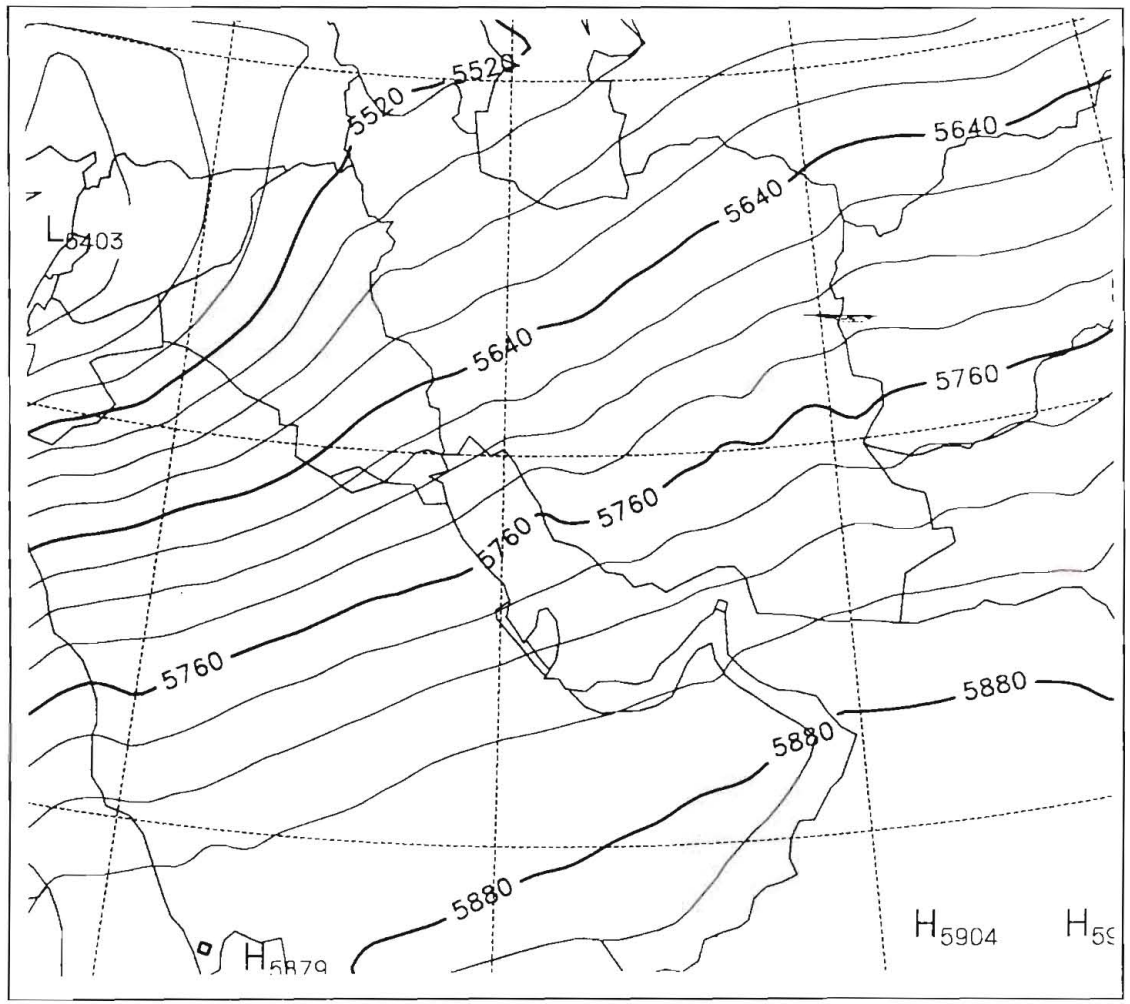

Figure 4.3 NORAPS 12Z 500 mb. Height Analysis for 07 Feb., 1995.

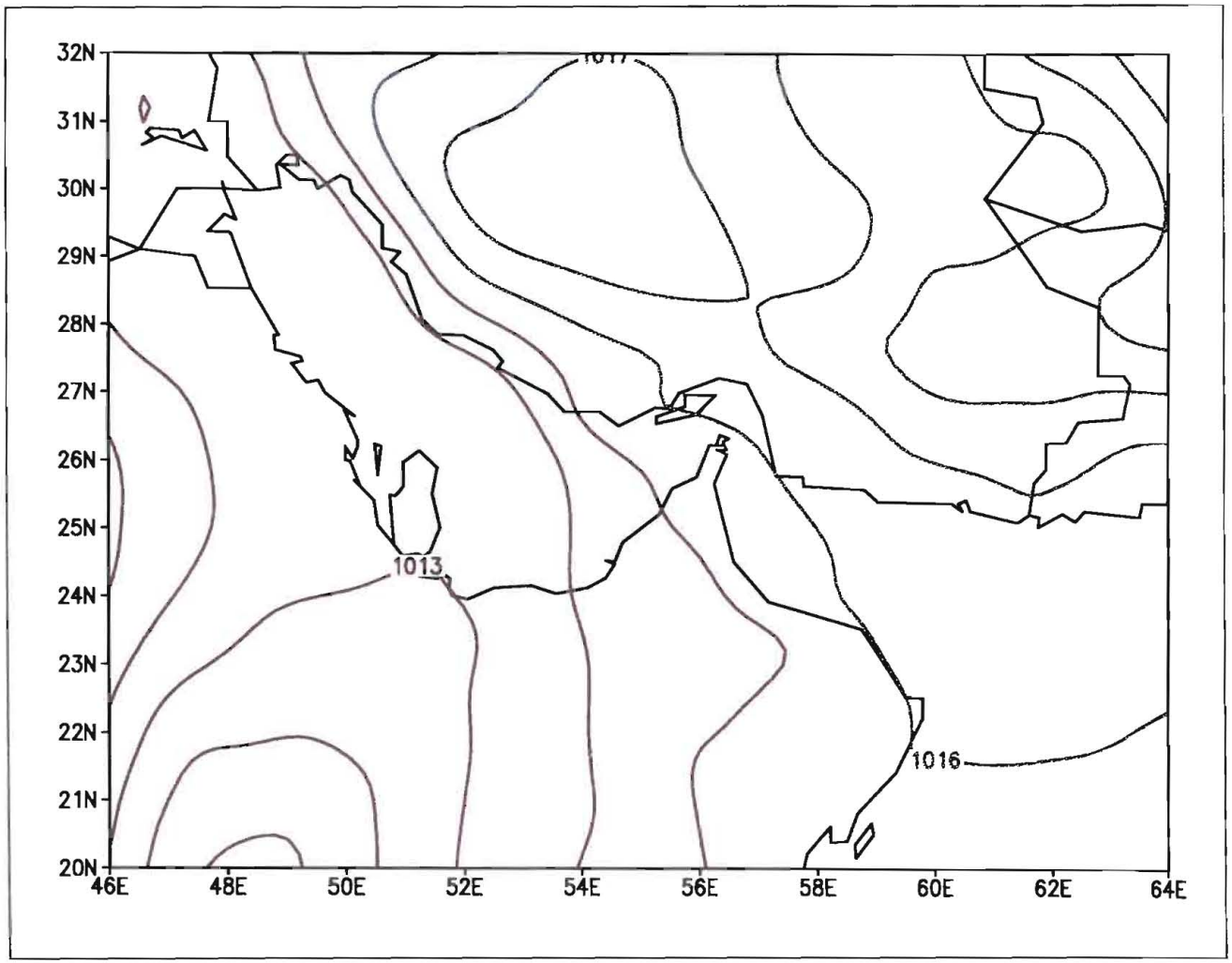

Figure 4.4 NORAPS (τ=15 hr.) 03Z Sea Level Pressure for 08 Feb., 1995.

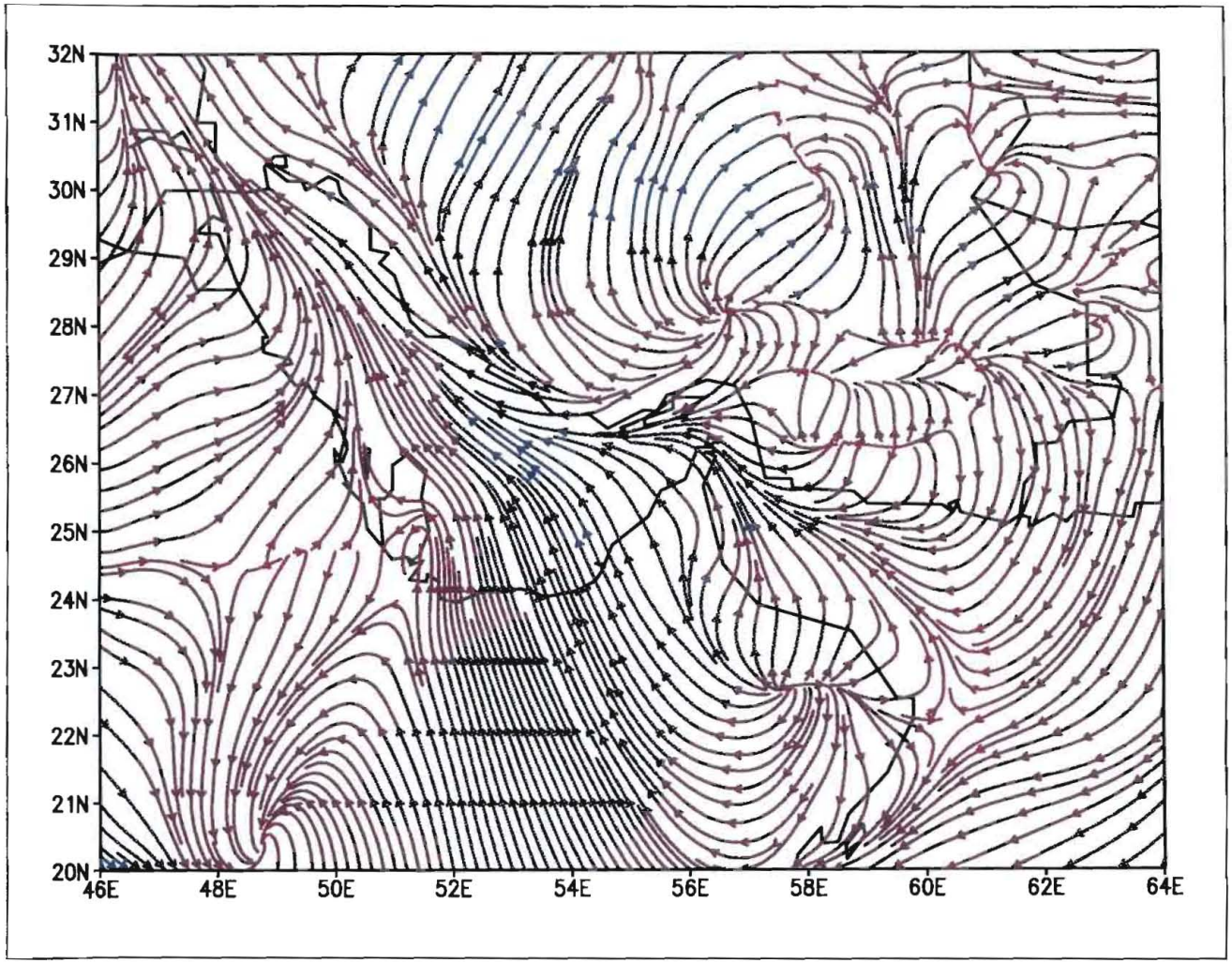

Figure 4.5 NORAPS (τ=15 hr.) 03Z Surface Streamlines for 08 Feb., 1995.

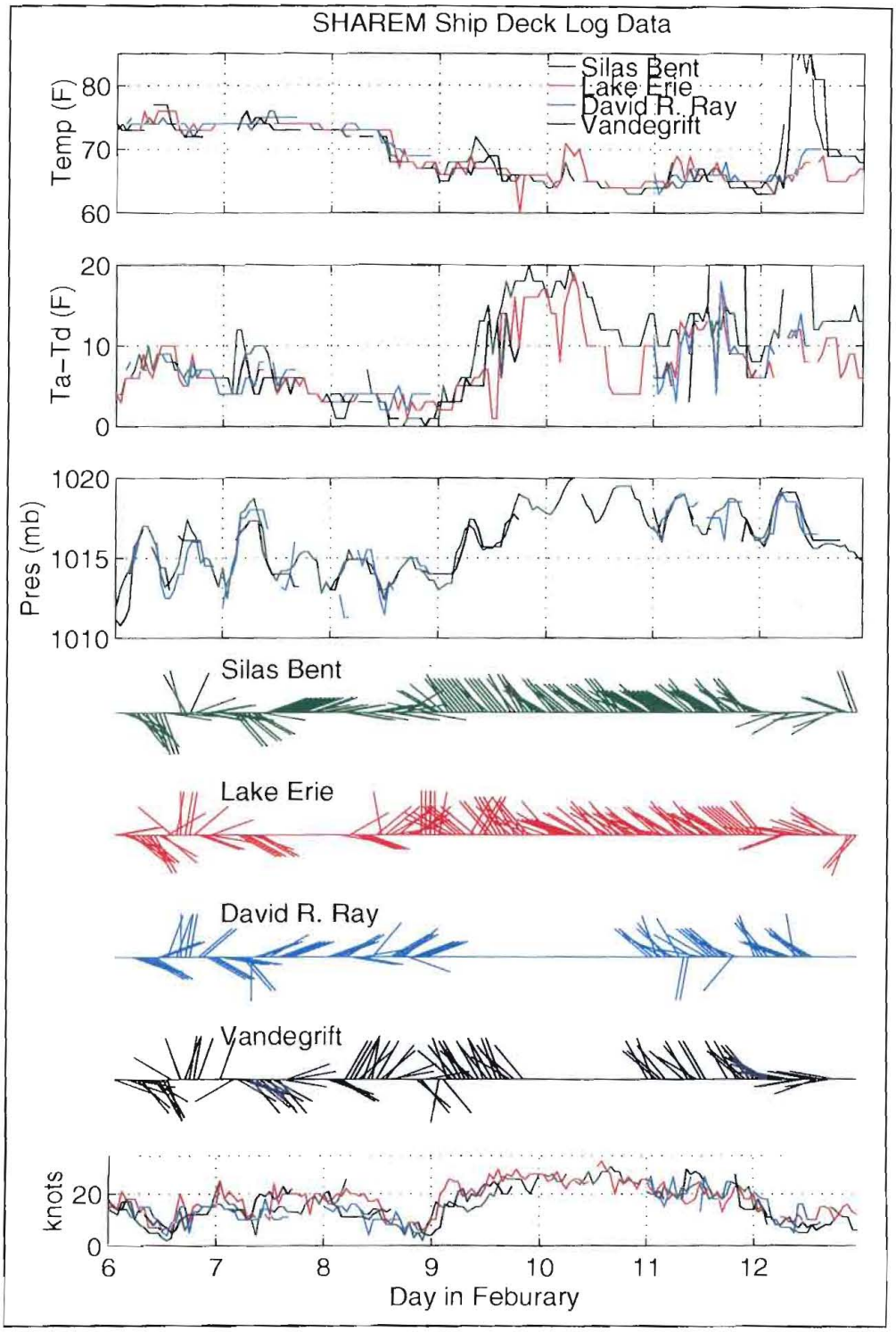

Figure 4.6 SHAREM Ship Surface Weather Observation Data.

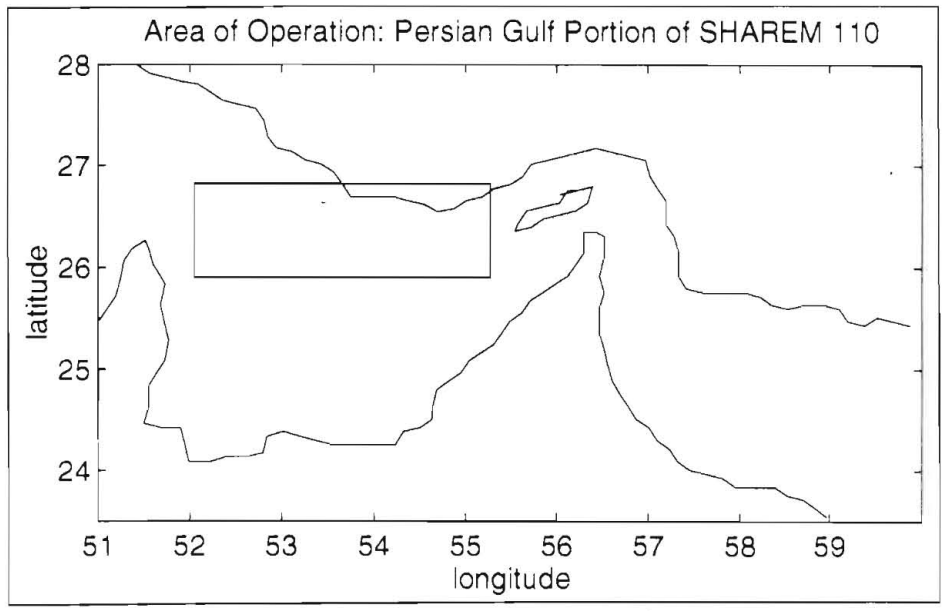

Figure 4.7 Area of Operation: Persian Gulf portion of SHAREM 110

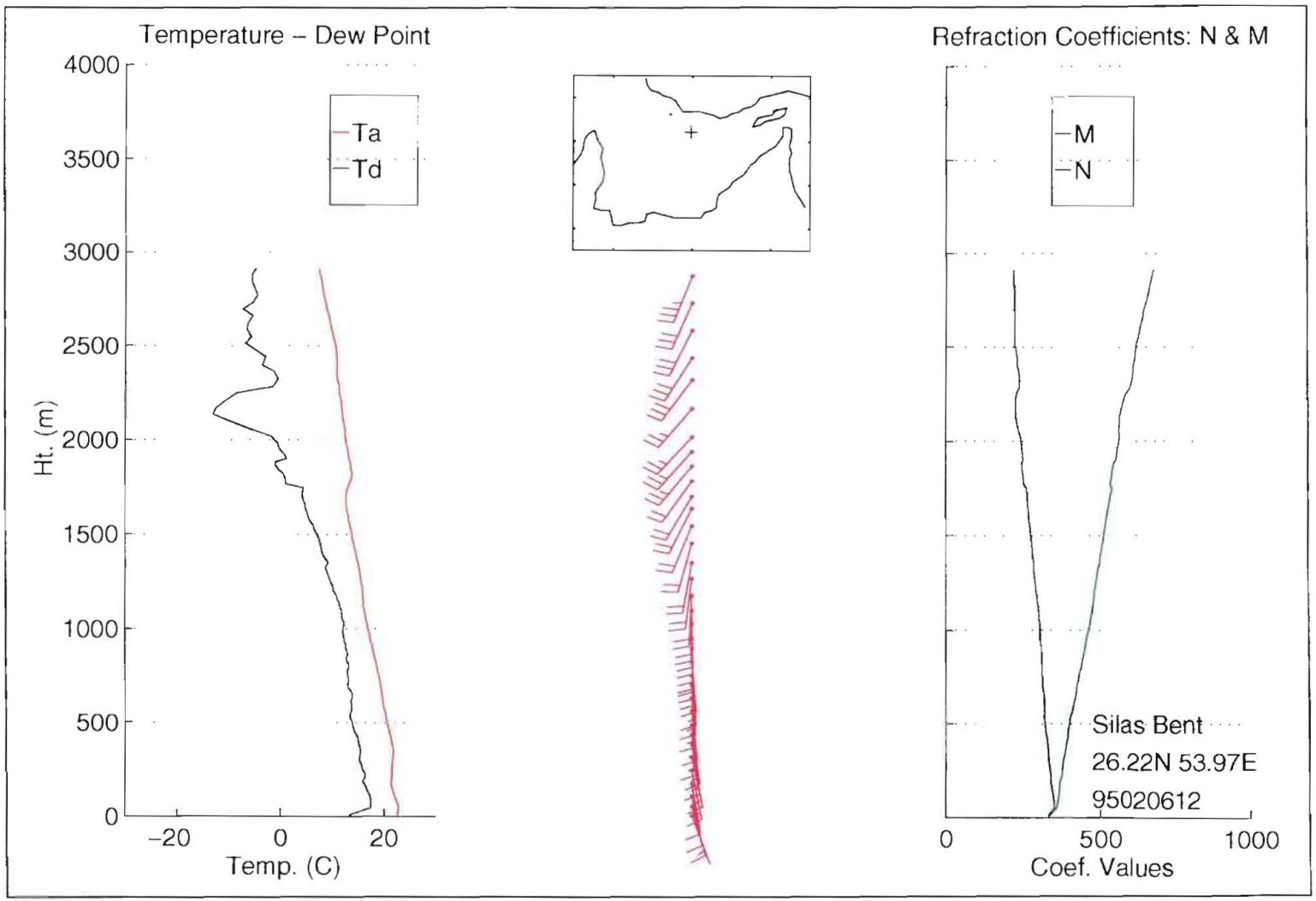

Figure 4.8 12Z Radiosonde Launched from the Silas Bent on 06 Feb., 1995. See text for description of contents.

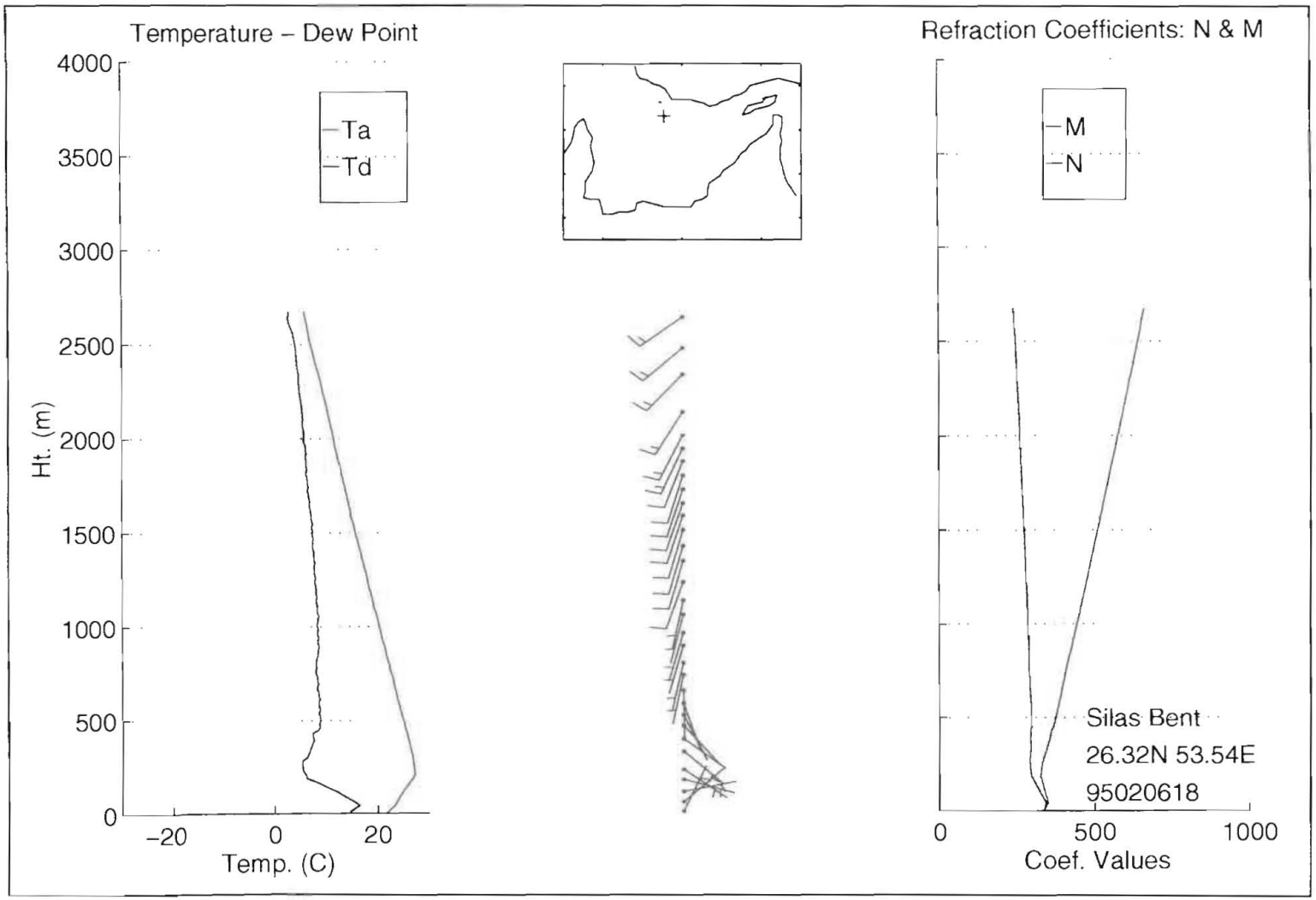

Figure 4.9 18Z Radiosonde Launched from the Silas Bent on 06 Feb., 1995.

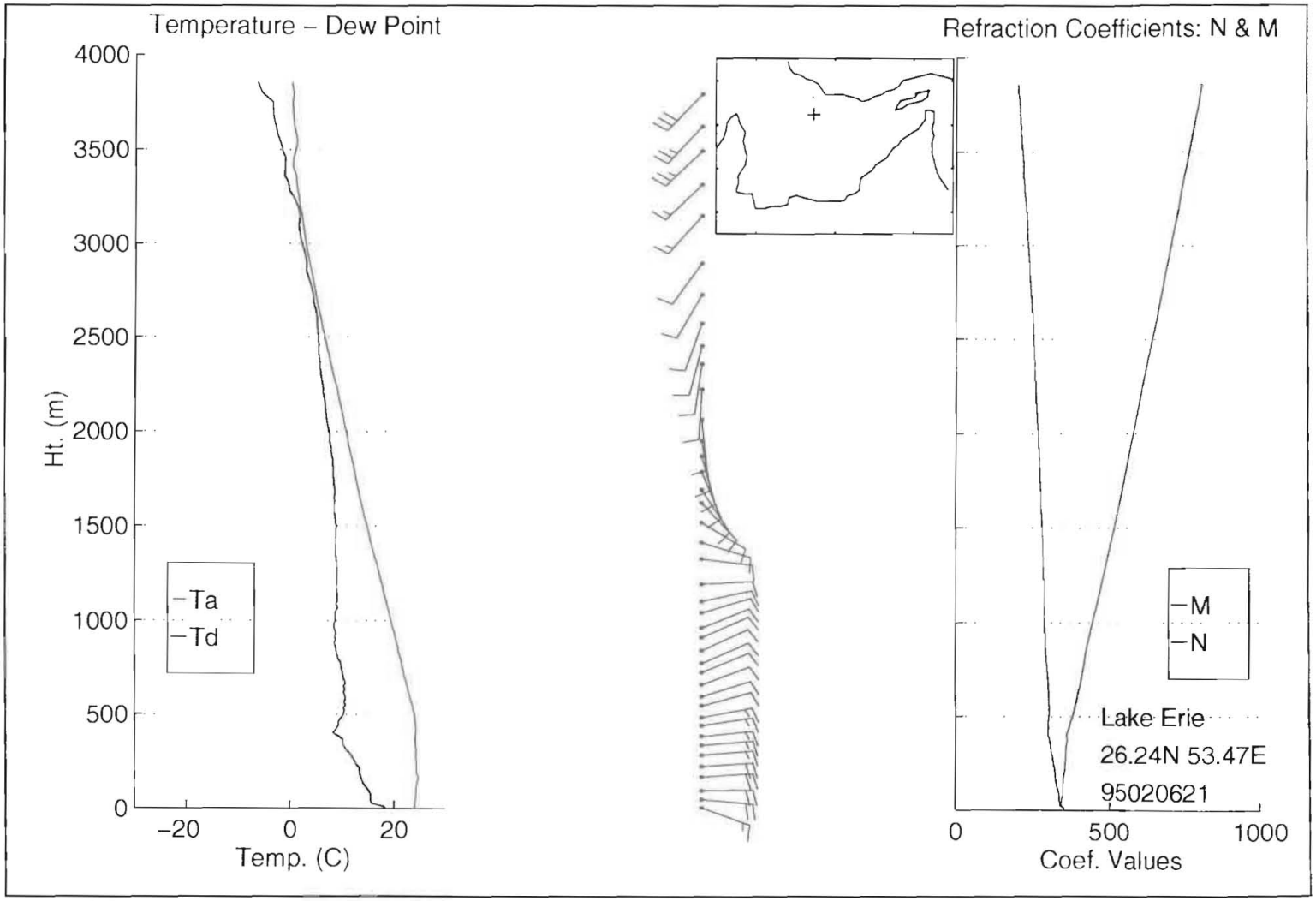

Figure 4.10 21Z Radiosonde Launched from the Lake Erie on 06 Feb., 1995.

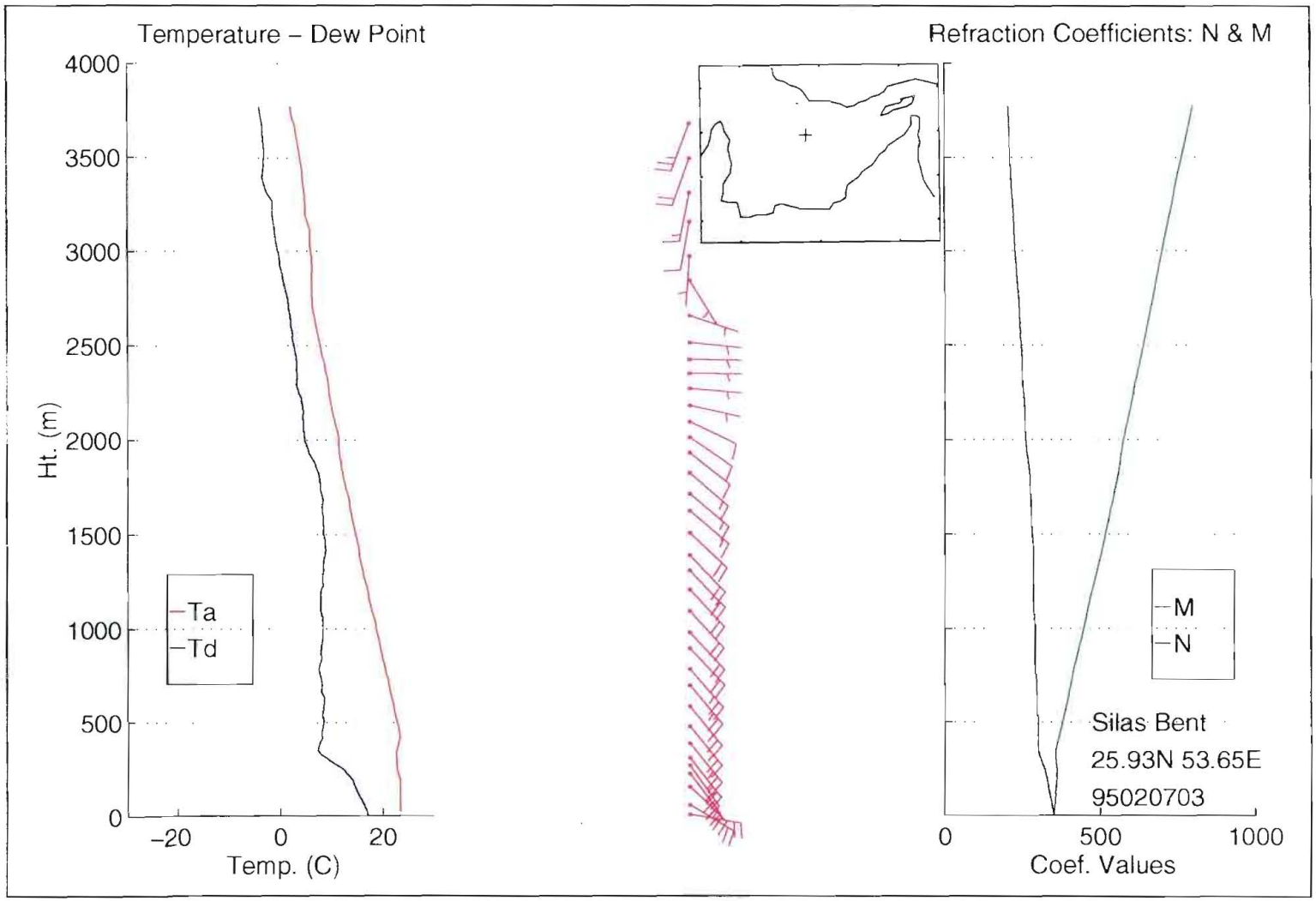

Figure 4.11 03Z Radiosonde launched from the Silas Bent on 07 Feb., 1995.

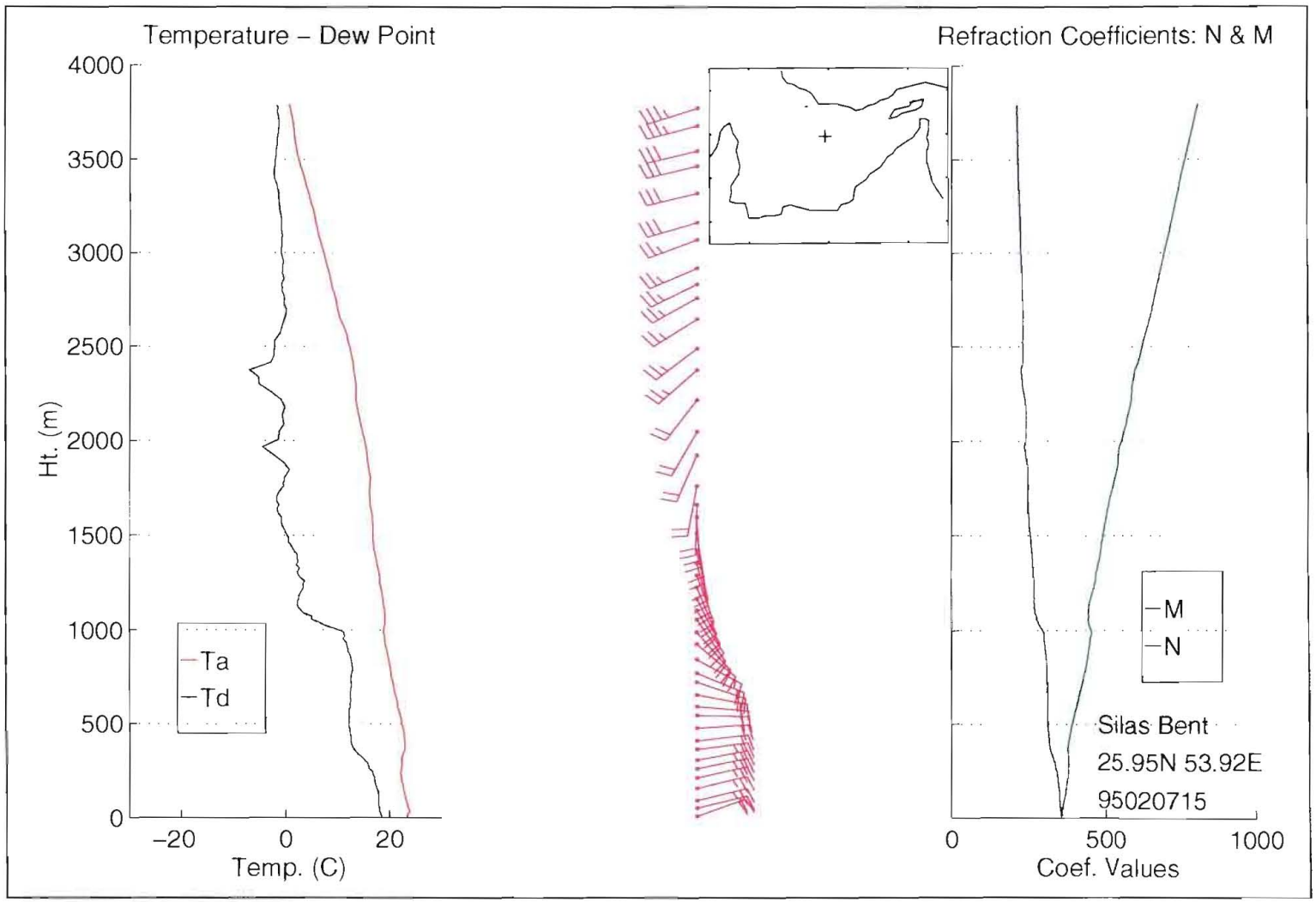

Figure 4.12 15Z Radiosonde Launched from the Silas Bent on 07 Feb., 1995.

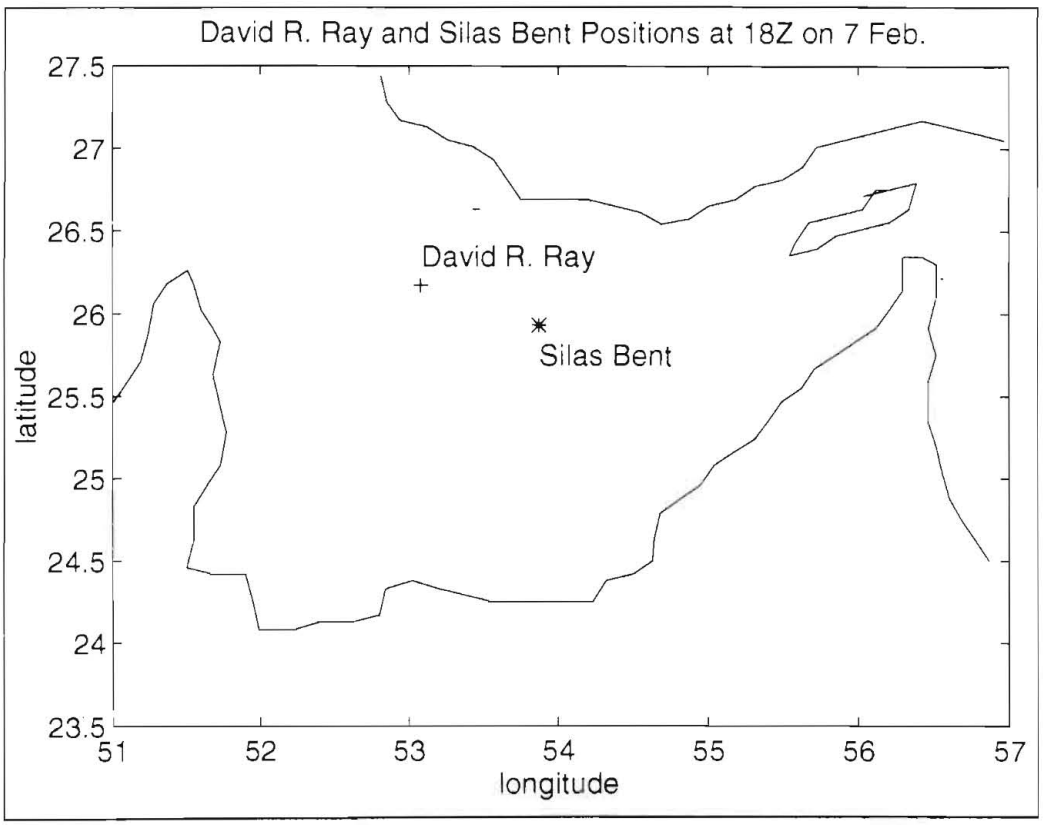

Figure 4.13 David R. Ray and Silas Bent Positions at 18Z on 07 Feb., 1995.

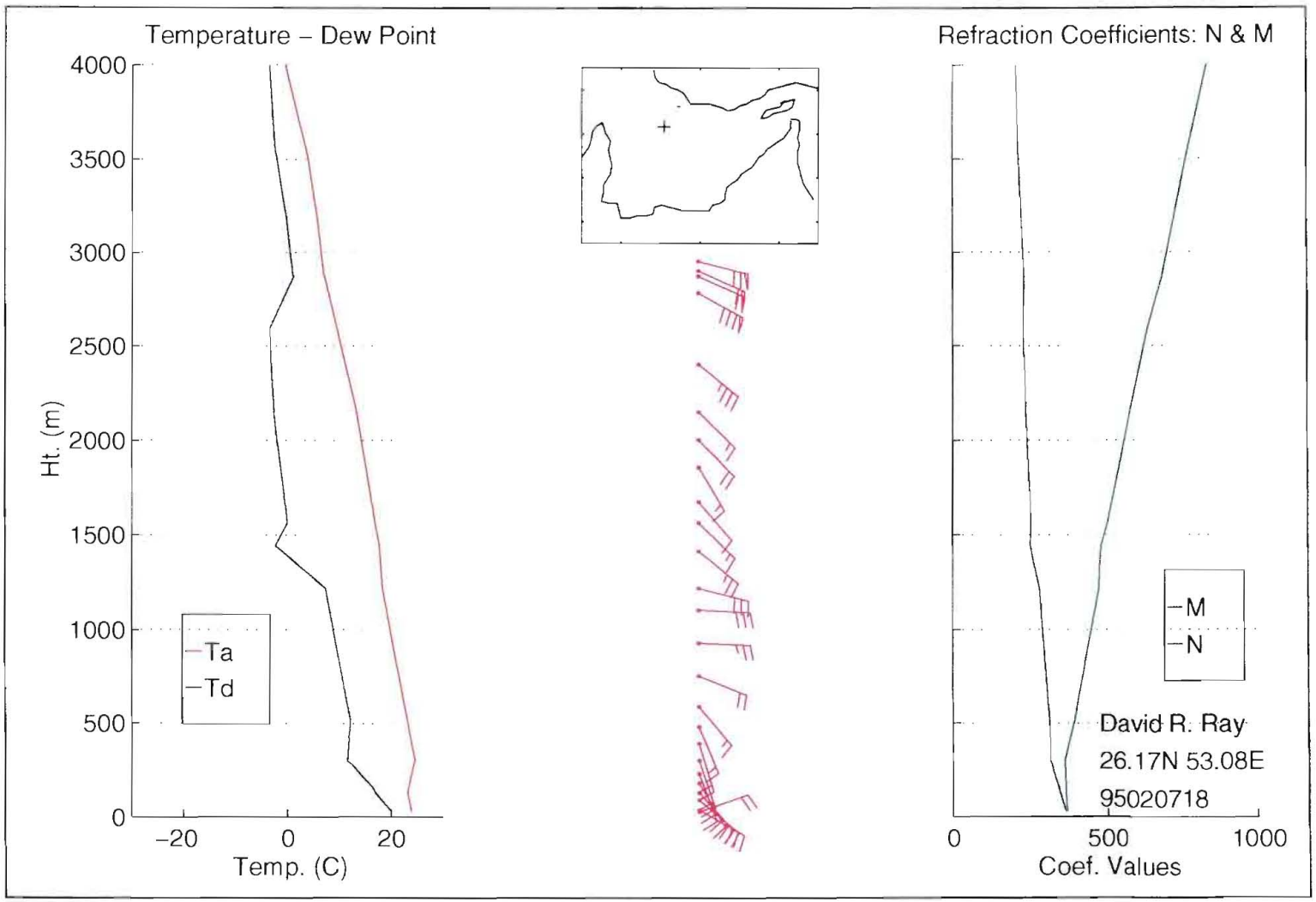

Figure 4.14 18Z Radiosonde Launched from the David R. Ray on 07 Feb., 1995.

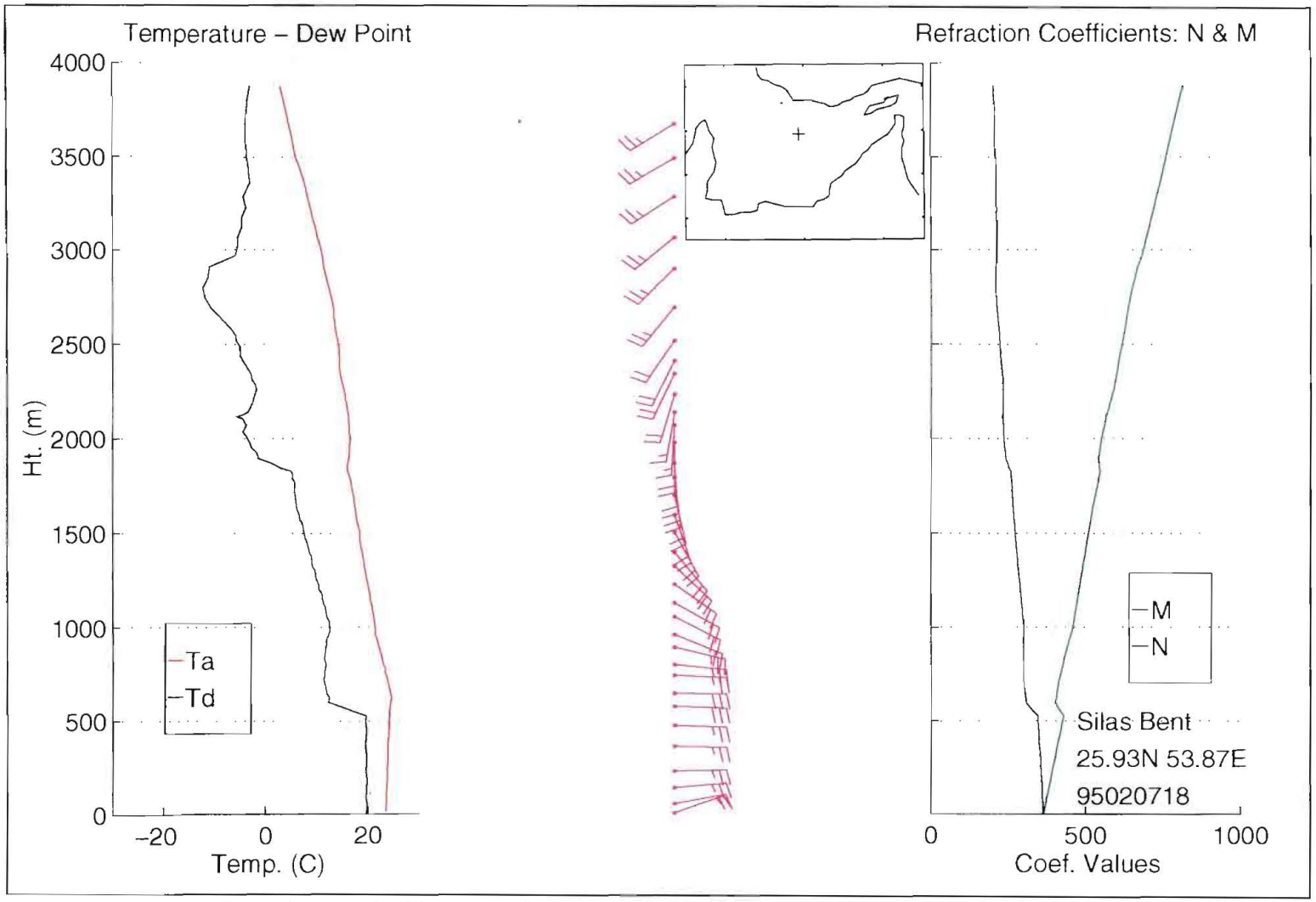

Figure 4.15 18Z Radiosonde Launched from the Silas Bent on 07 Feb., 1995.

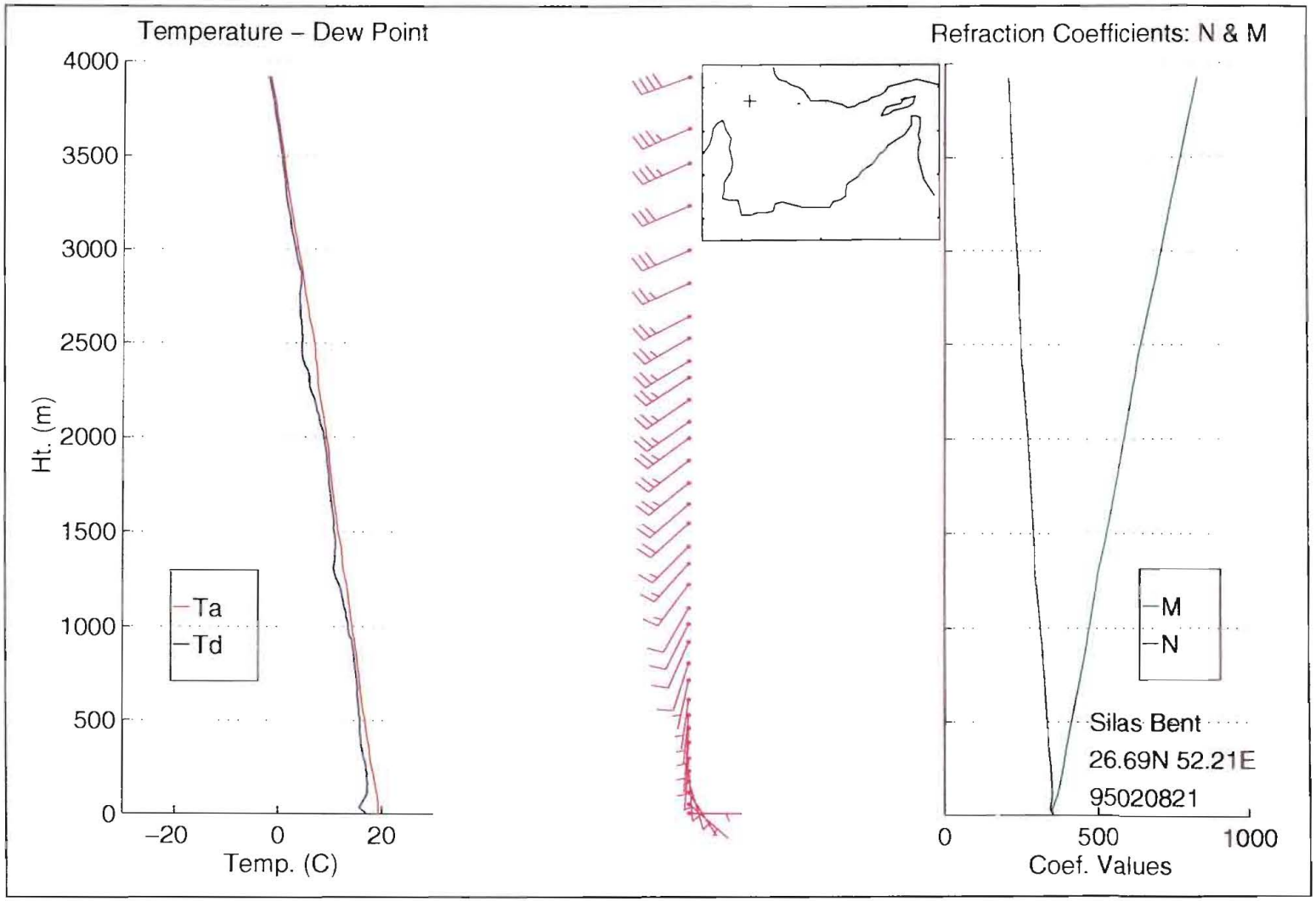

Figure 4.16 21Z Radiosonde Launched from the Silas Bent on 08 Feb., 1995.

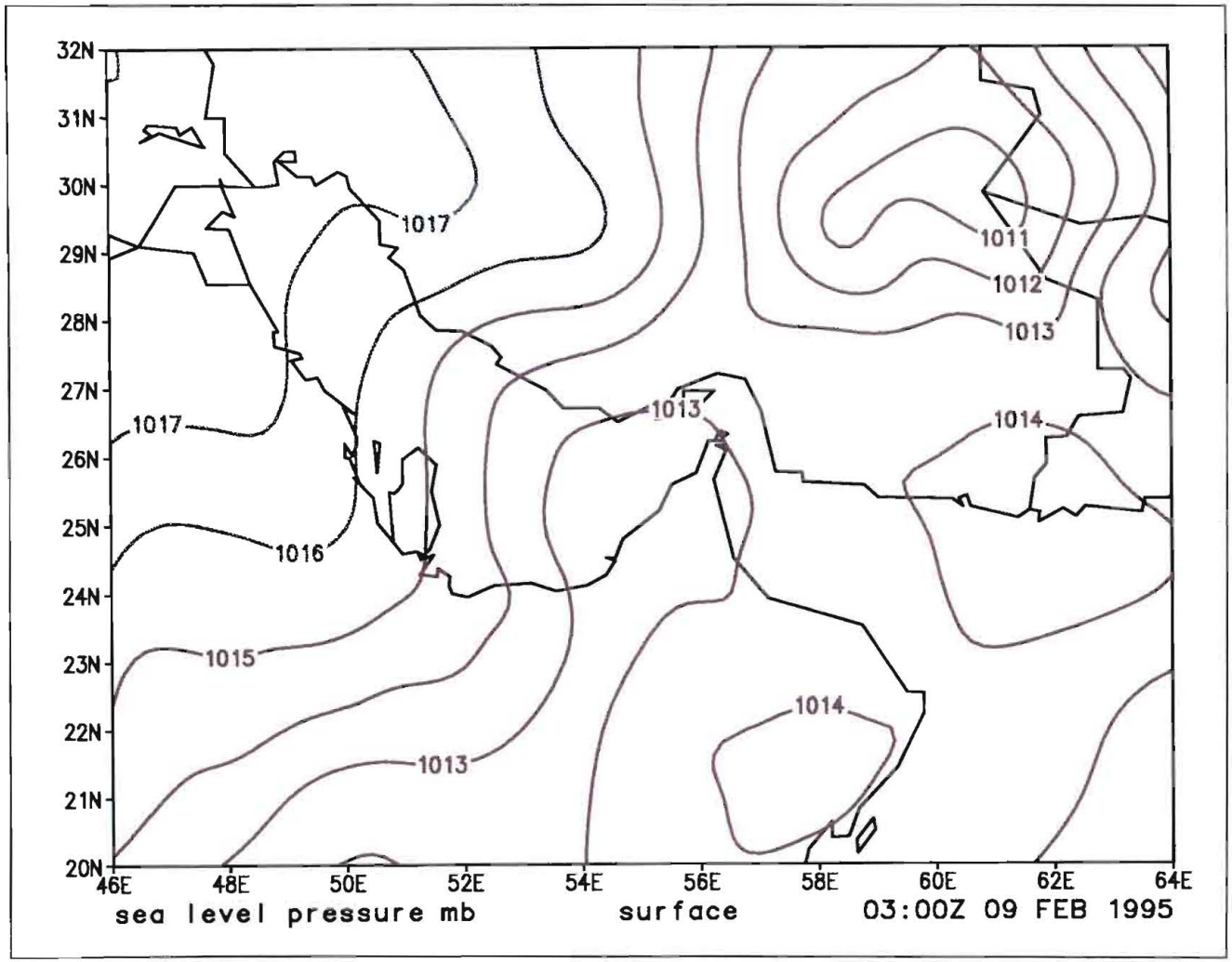

Figure 4.17 NORAPS (τ=15 hr.) 03Z Sea Level Pressure for 09 Feb., 1995.

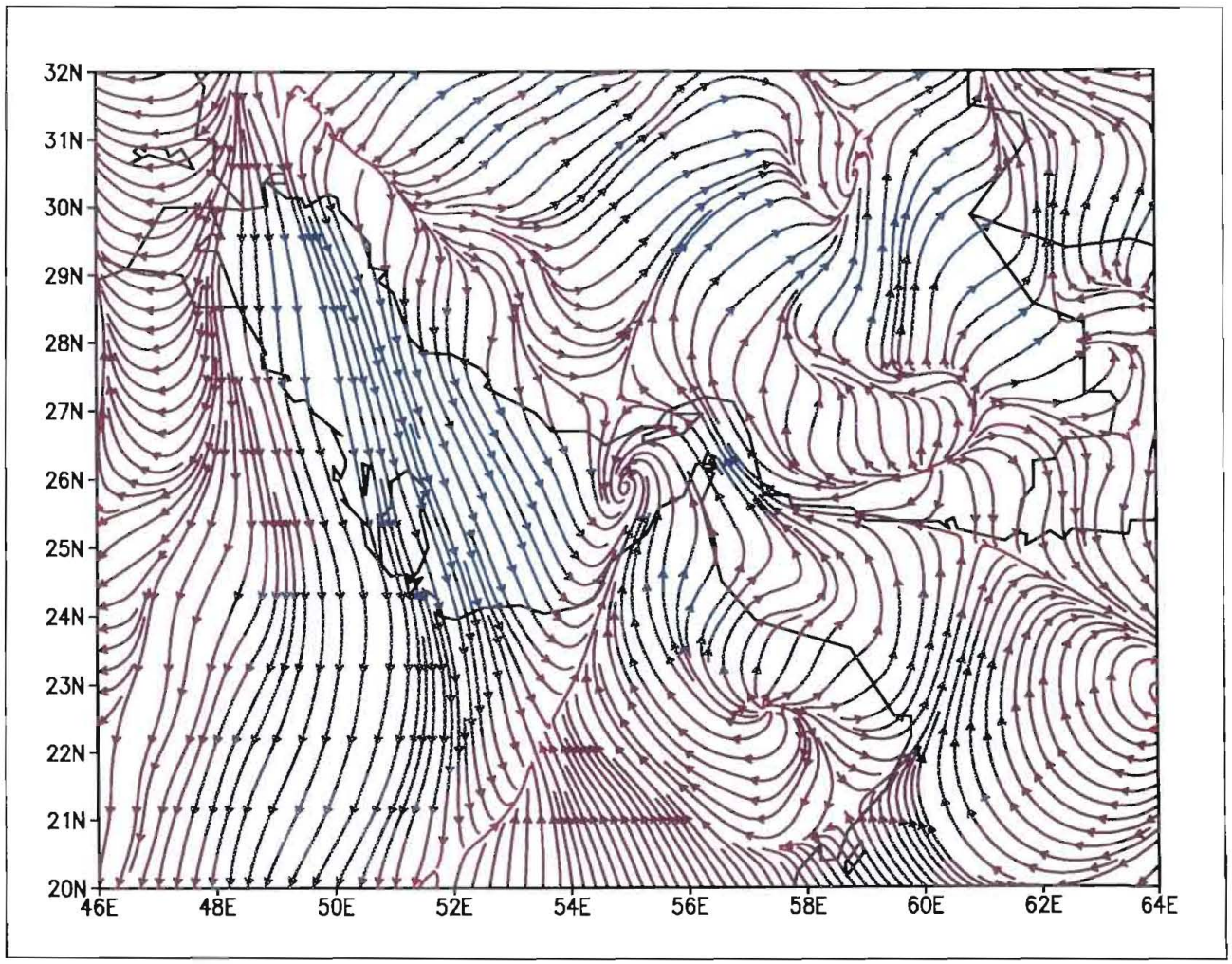

Figure 4.18 NORAPS (τ=15 hr.) 03Z Surface Streamlines for 09 Feb., 1995.

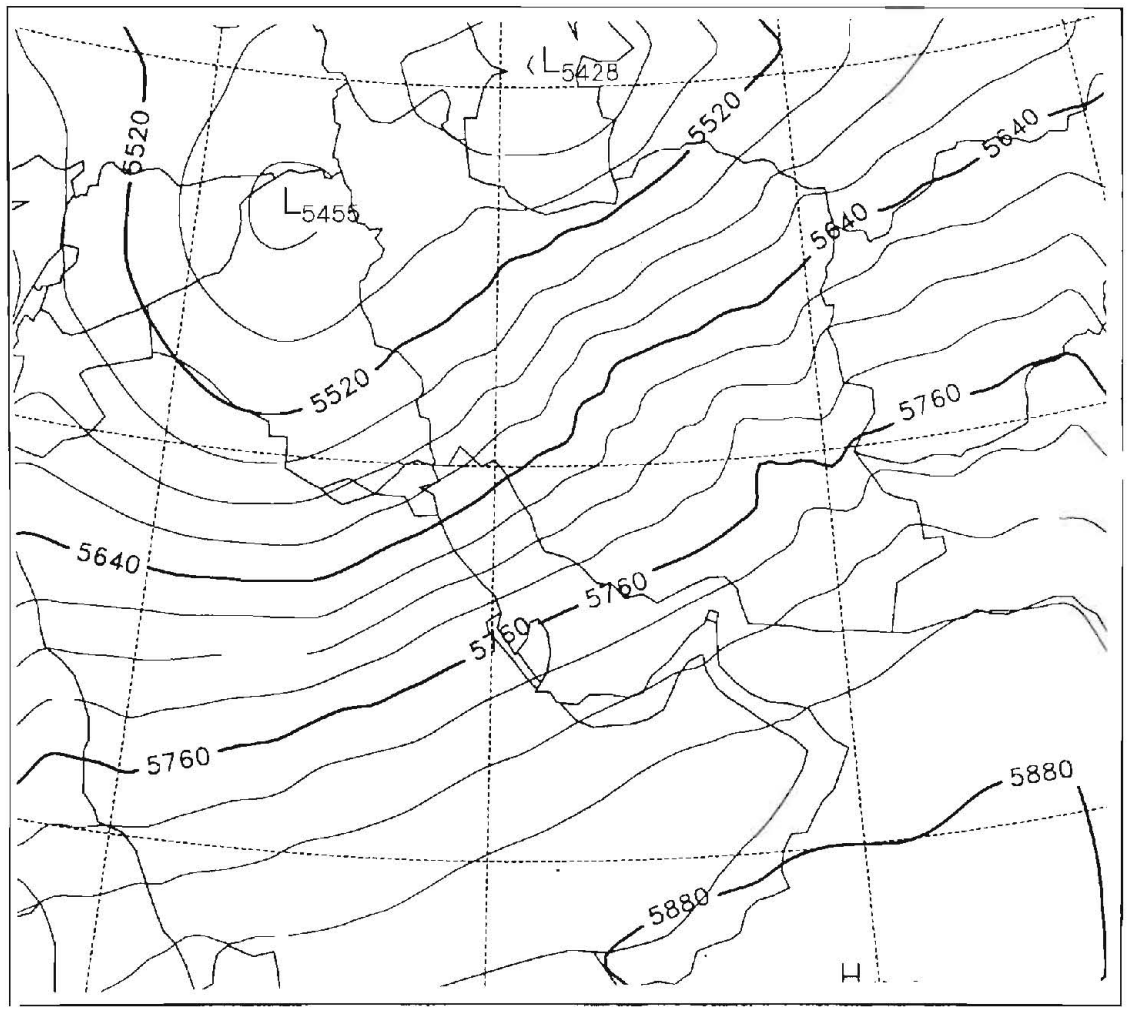

Figure 4.19 NORAPS 00Z 500 mb. Height Analysis for 09 Feb., 1995.

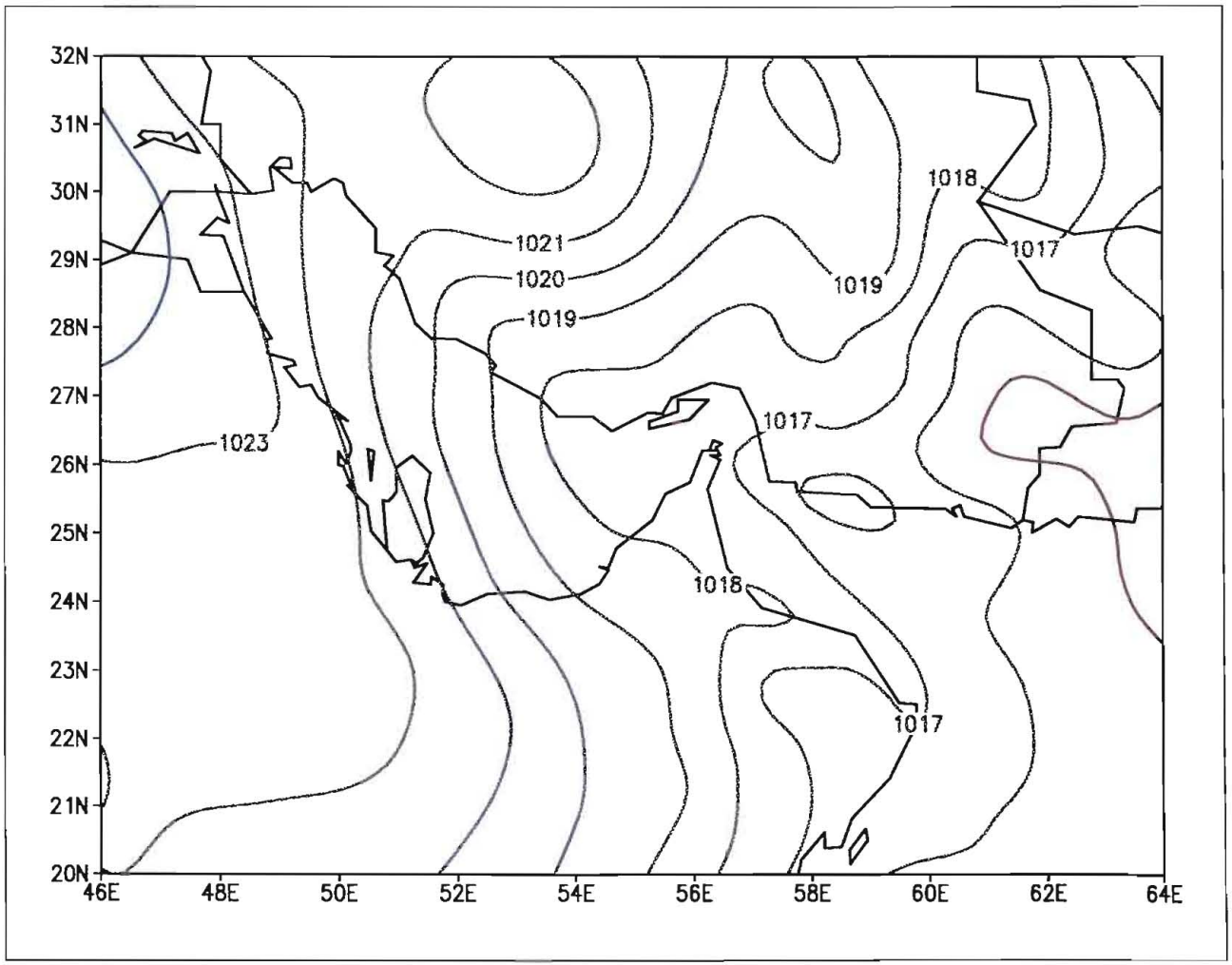

Figure 4.20 NORAPS (τ=15 hr.) 03Z Sea Level Pressure for 11 Feb., 1995.

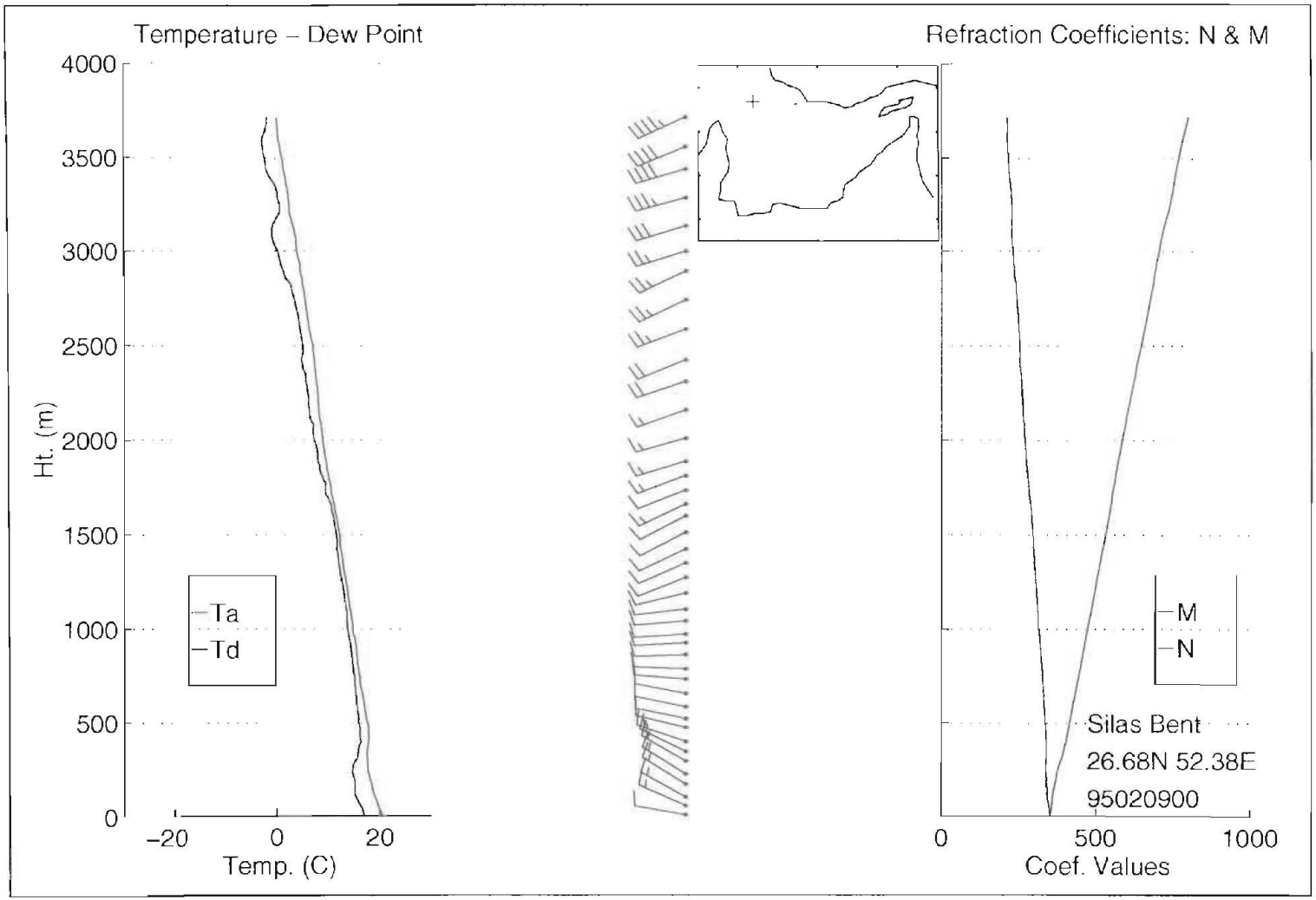

Figure 4.21 00Z Radiosonde Launched from the Silas Bent on 09 Feb., 1995.

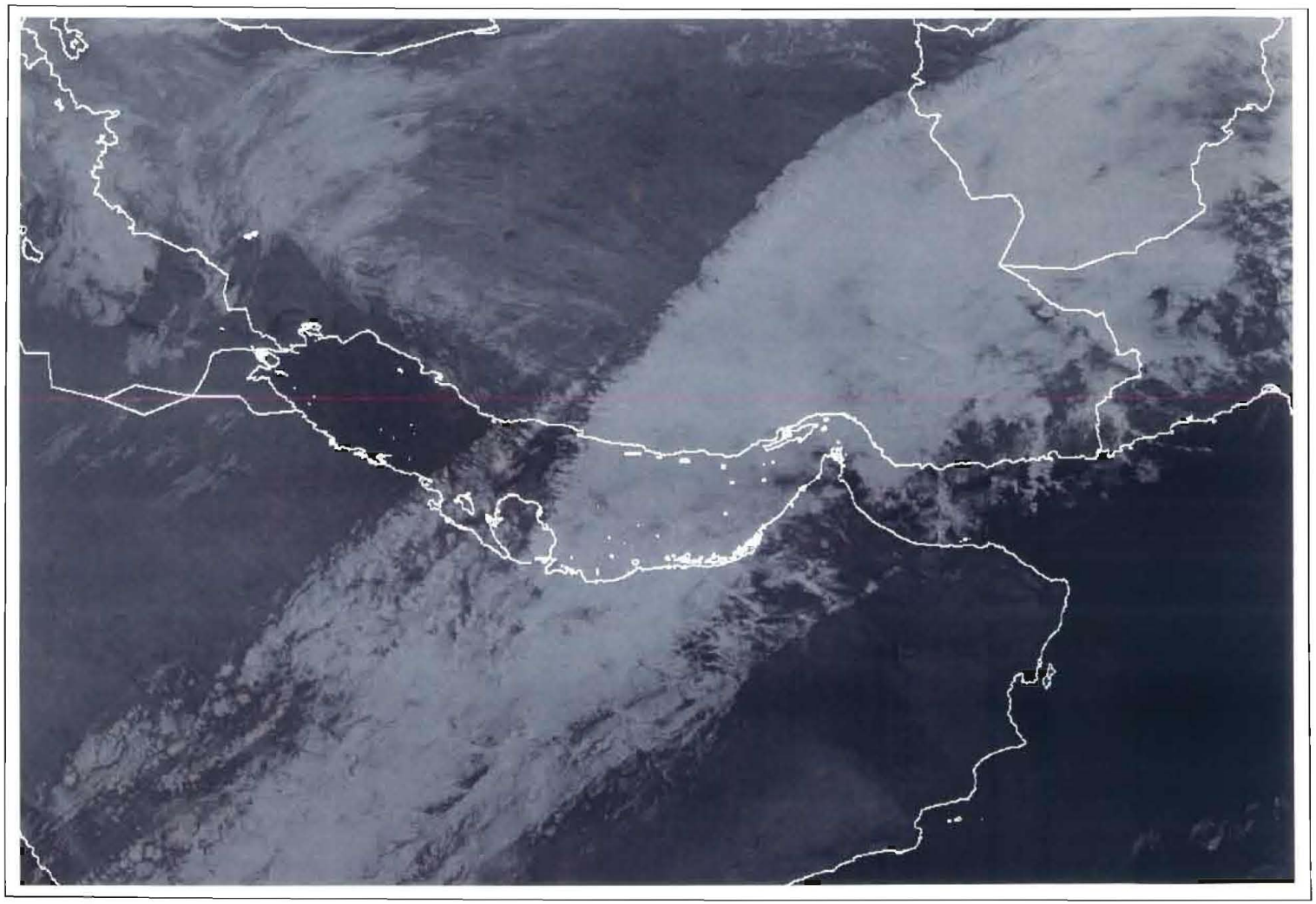

Figure 4.22 0257Z DMSP Infra-red Image from 9 Feb., 1995

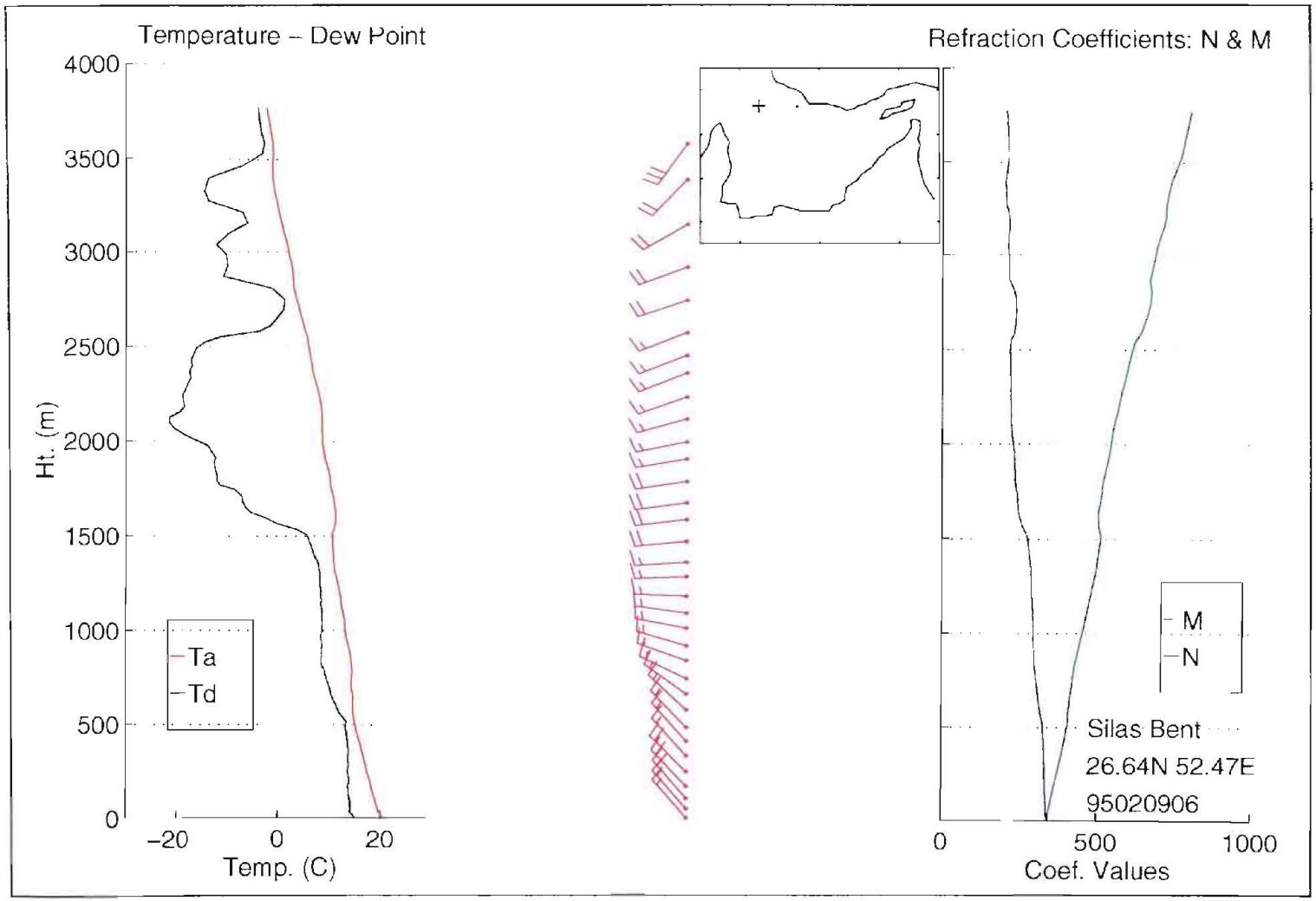

Figure 4.23 06Z Radiosonde Launched form the Silas Bent on 09 Feb., 1995.

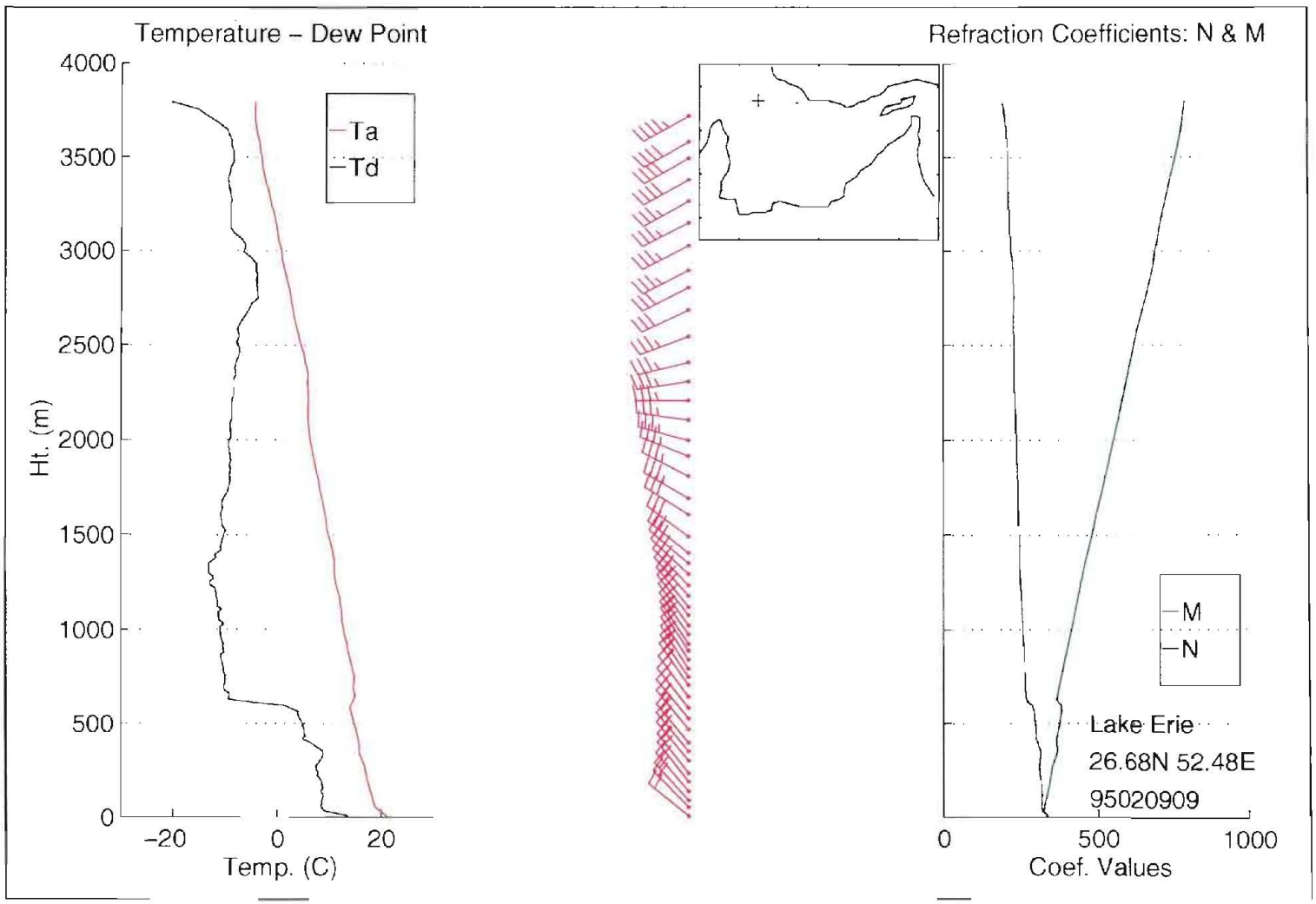

Figure 4.24 09Z Radiosonde Launched from the Lake Erie on 09 Feb., 1995.

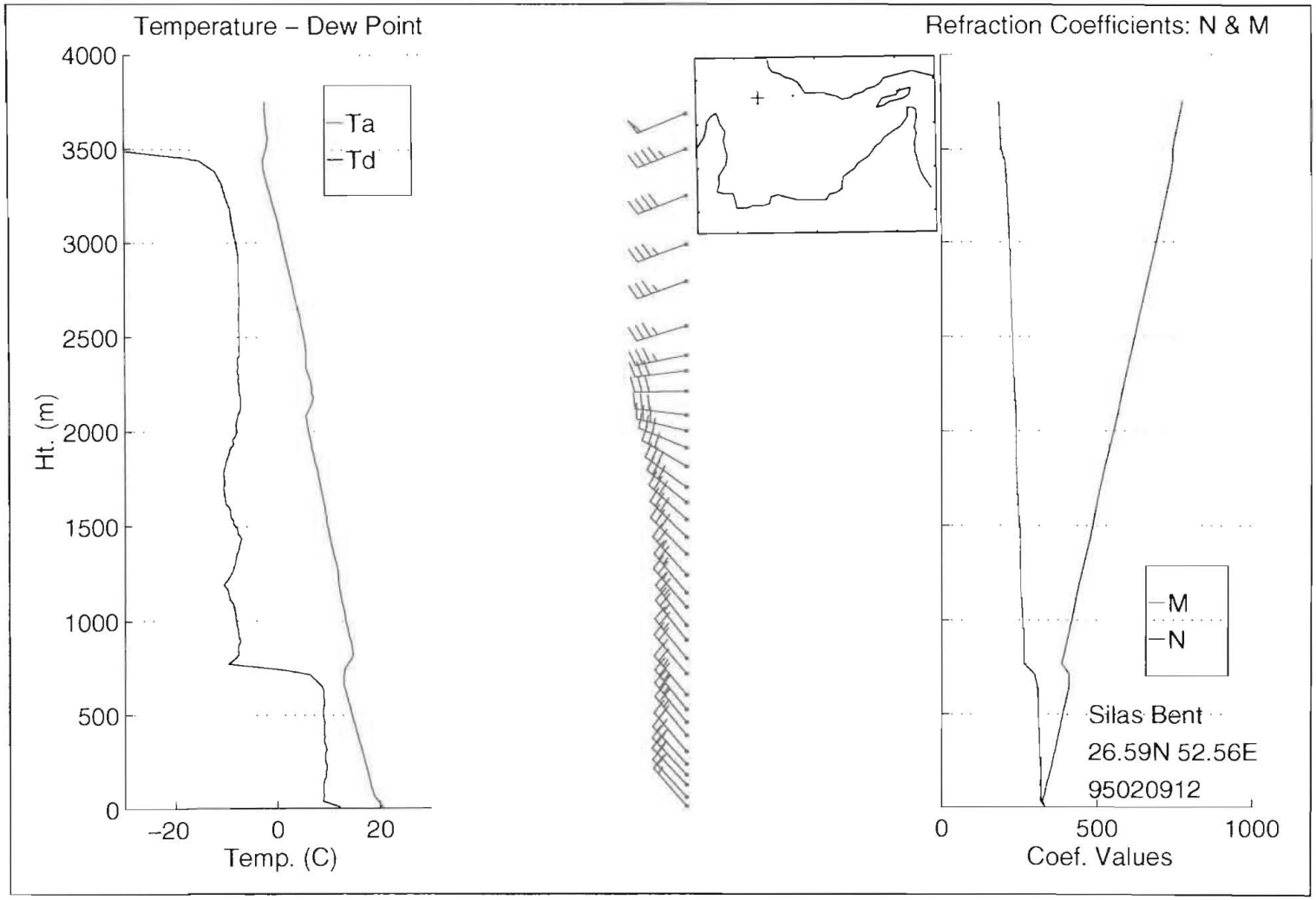

Figure 4.25 12ZRadiosonde Launched from the Silas Bent on 09 Feb., 1995.

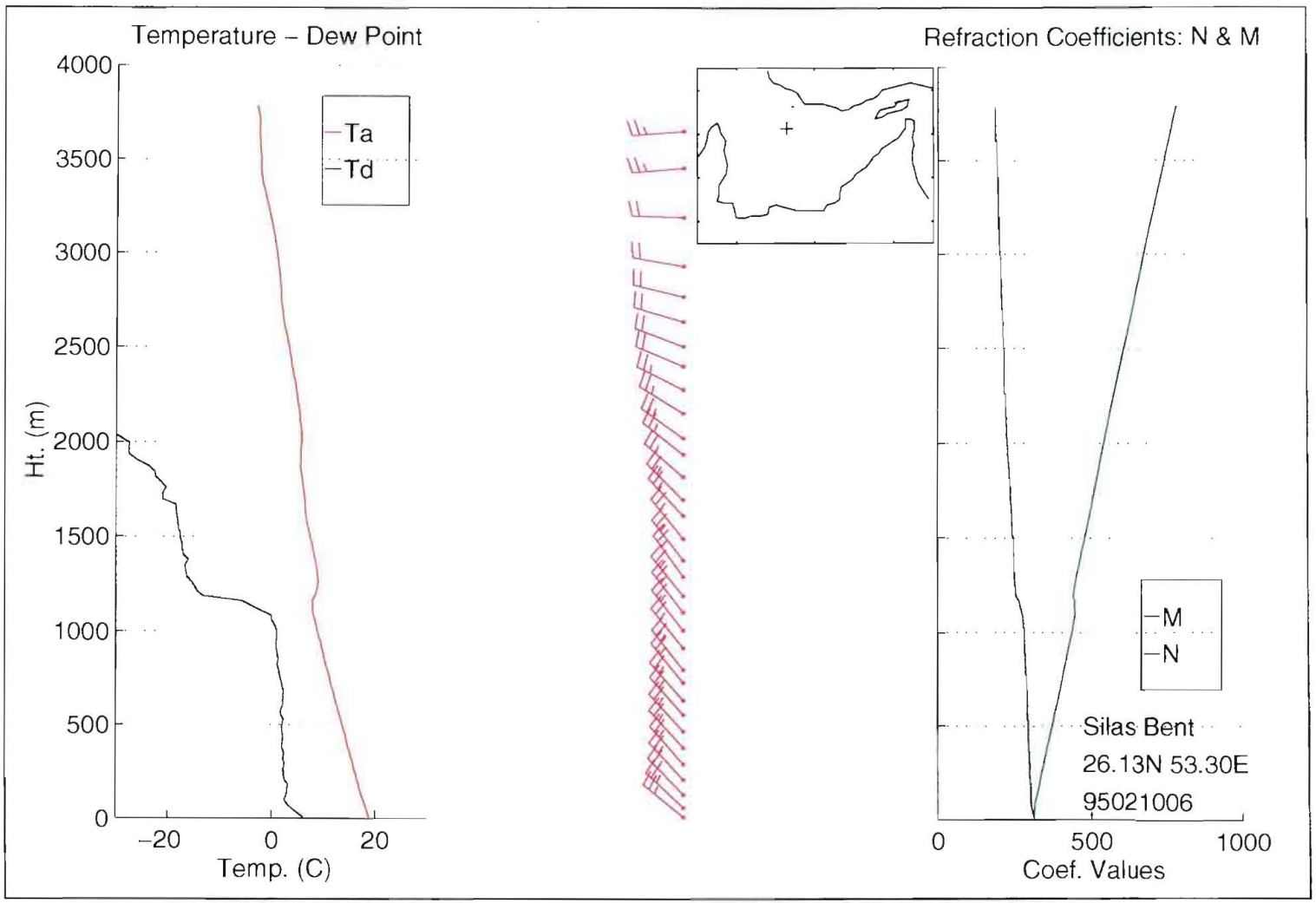

Figure 4.26 06Z Radiosonde Launched from the Silas Bent on 10 Feb., 1995.

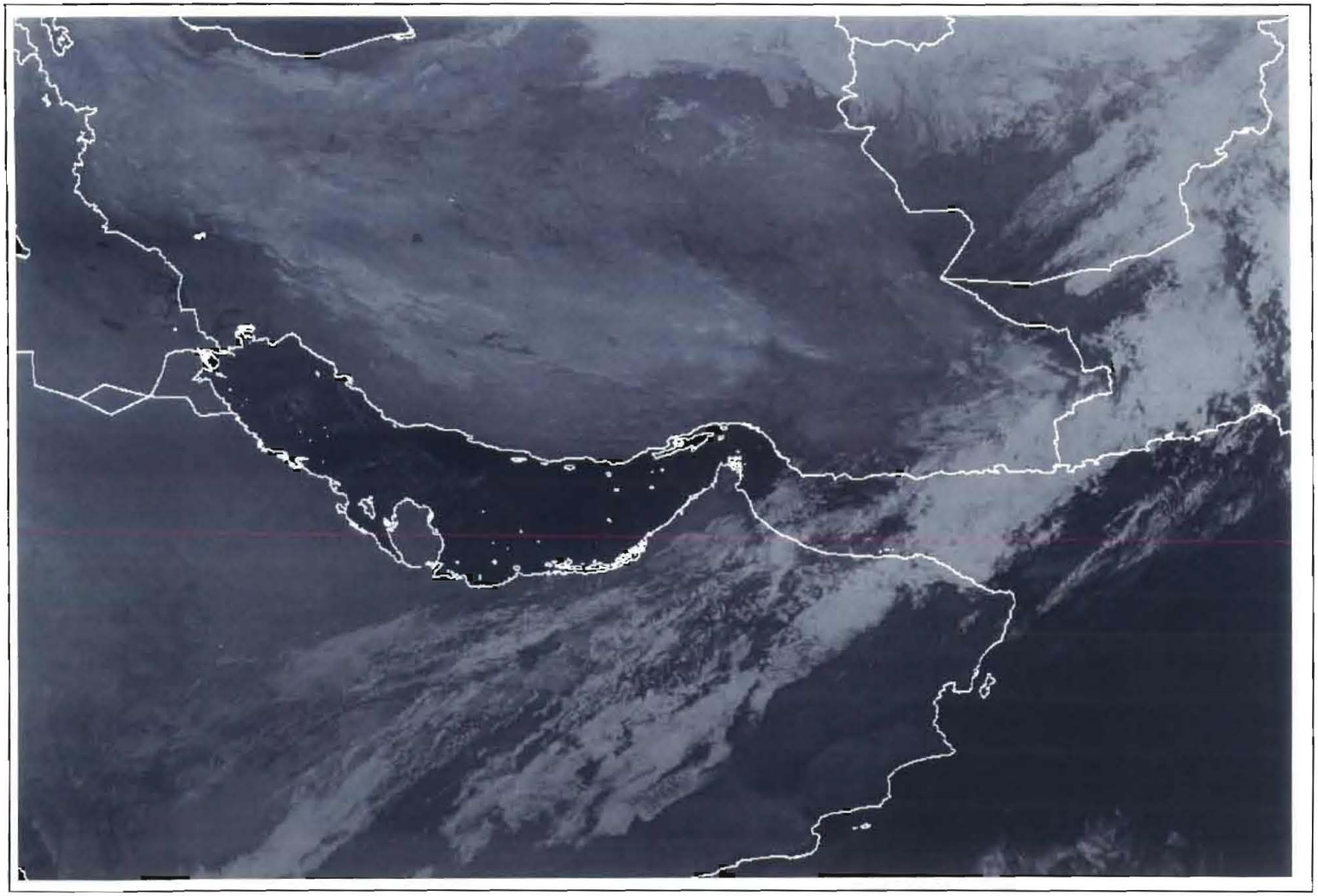

Figure 4.27 0243Z DMSP Infra-red Image from 10 Feb., 1995.

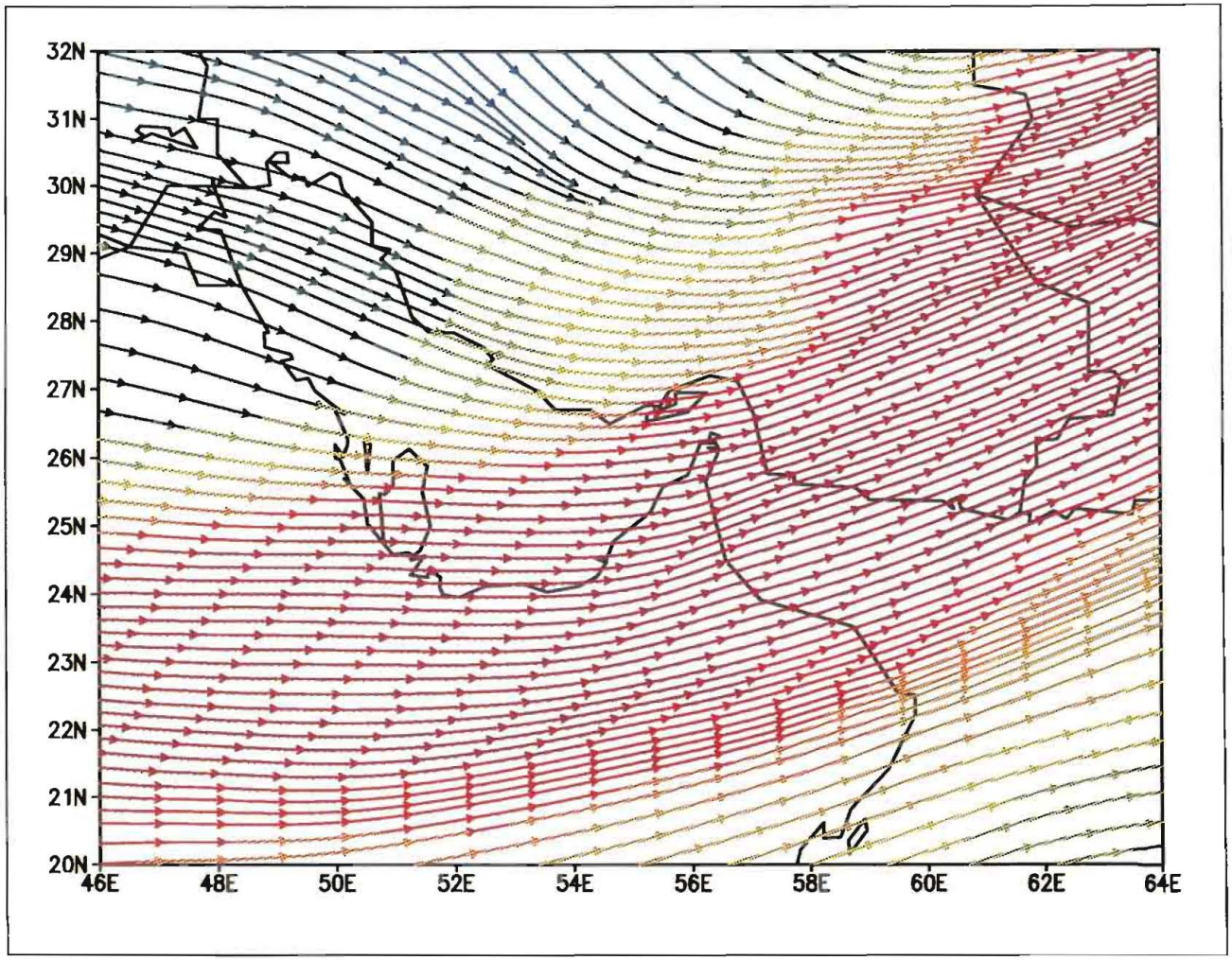

Figure 4.28 NORAPS (τ=15 hr.) 15Z Streamlines at 5500 m for 10 Feb., 1995.

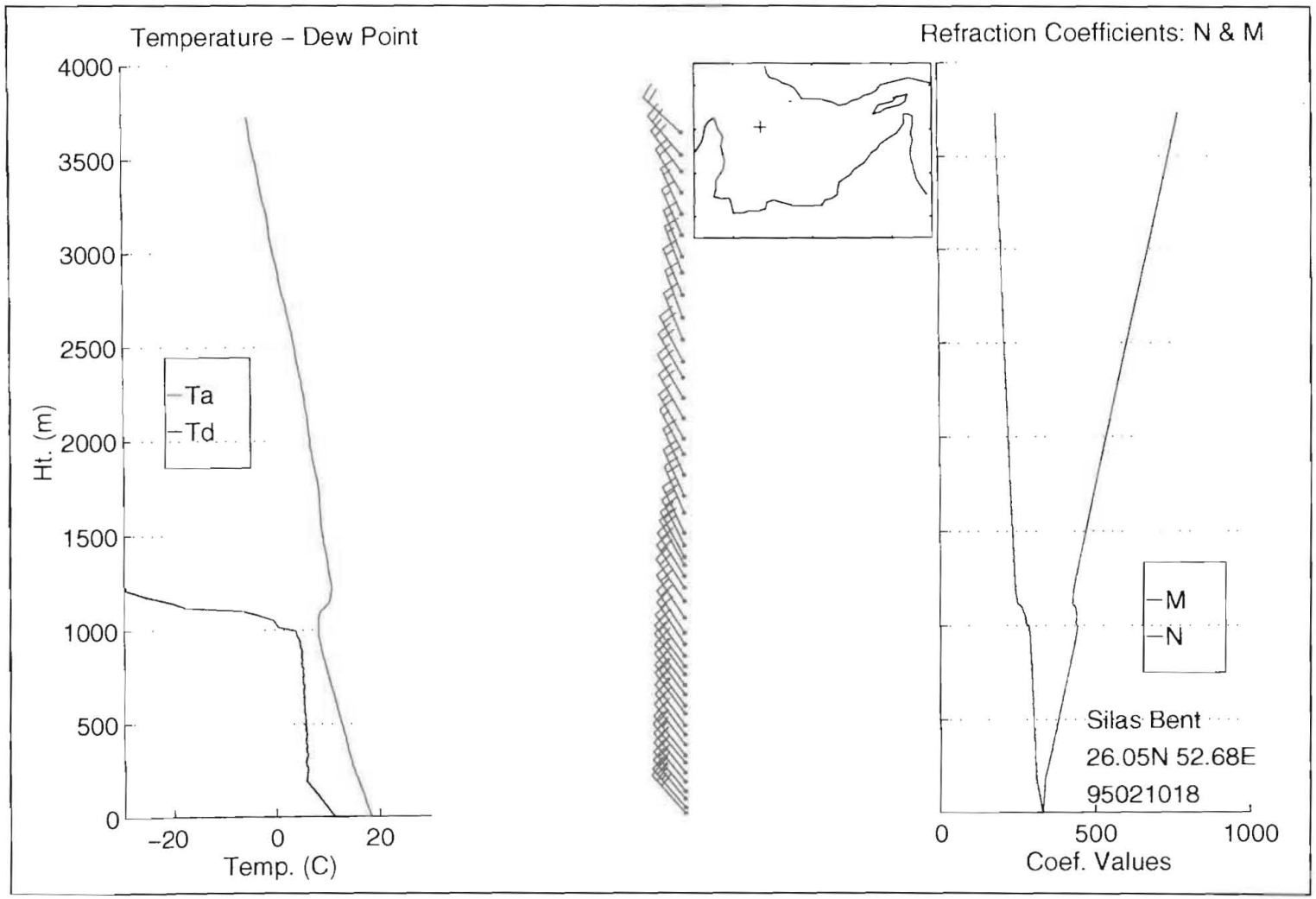

Figure 4.29 18Z Radiosonde Launched from the Silas Bent on 18 Feb., 1995.

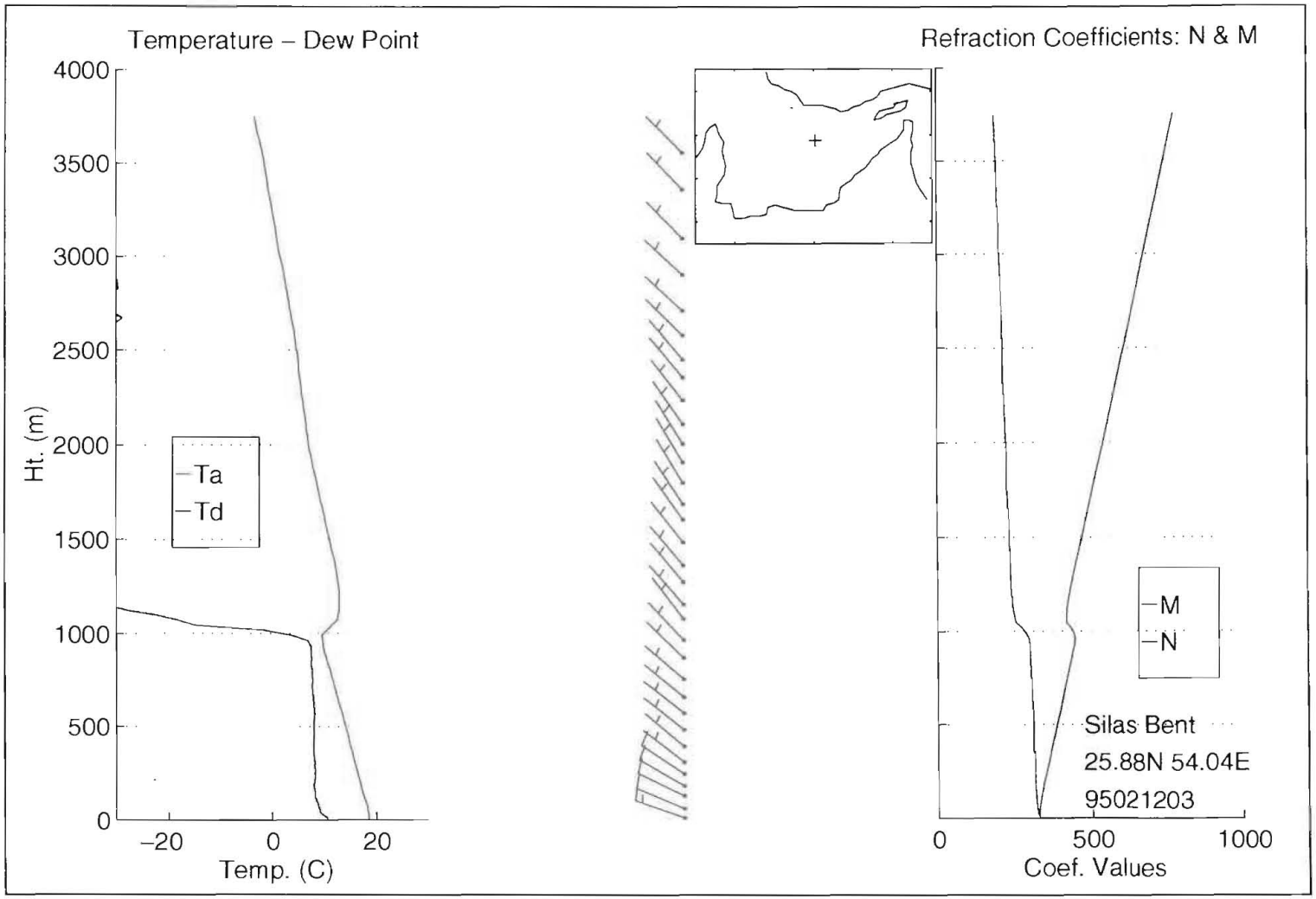

Figure 4.30 03Z Radiosonde Launched from the Silas Bent on 12 Feb., 1995.

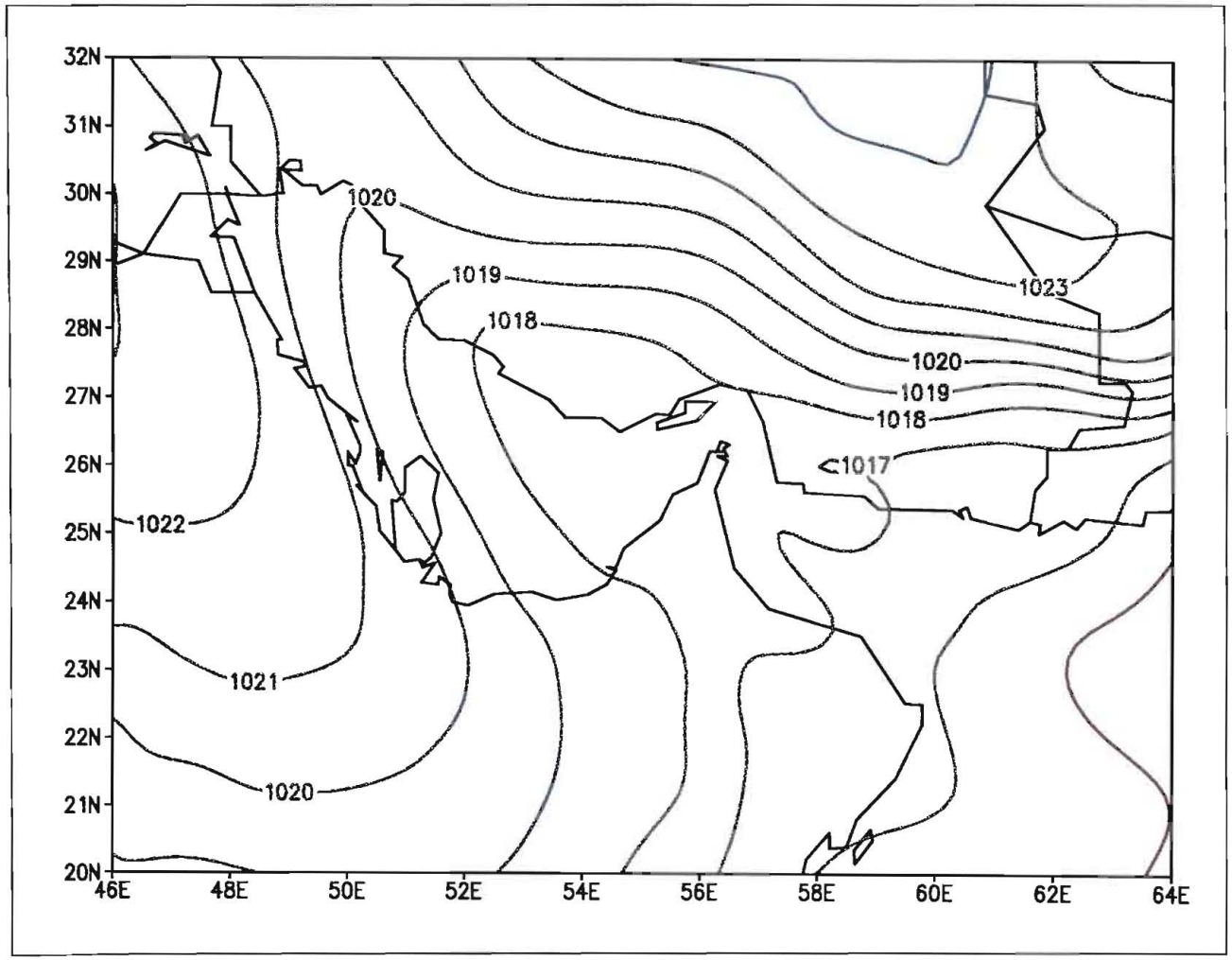

Figure 4.31 NORAPS (τ=15 hr.) 03Z Sea Level Pressure for 12 Feb., 1995.

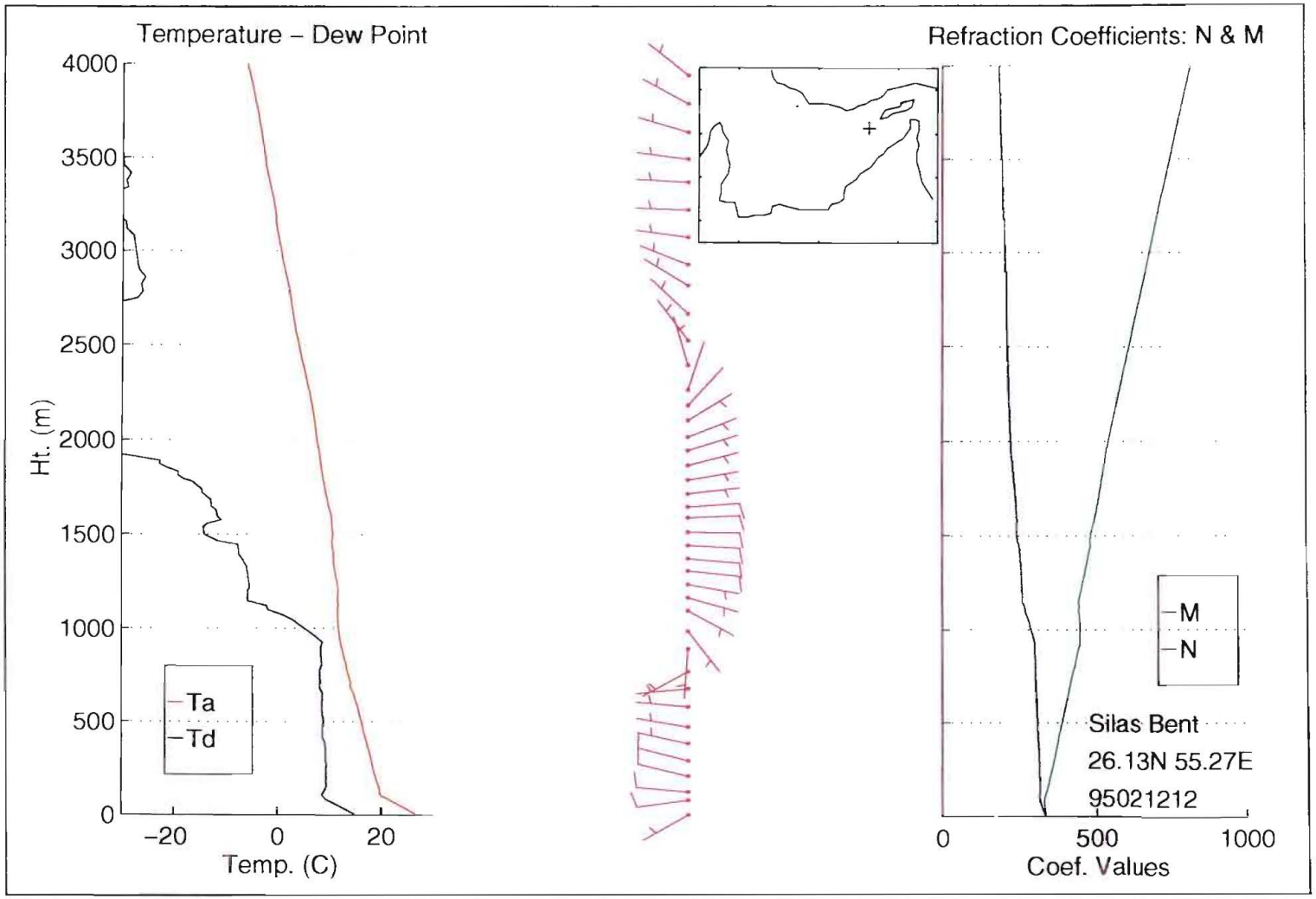

Figure 4.32 12Z Radiosonde Launched from the Silas Bent on 12 Feb., 1995.

V. GULF OF OMAN PORTION OF SHAREM 110

A. GENERAL

The second half of SHAREM 110 occurred in the Gulf of Oman (GOO) from approximately 13 to 18 February 1995. The SHAREM ships collectively launched a total of 57 radiosondes and 12 rocketsondes during this period. Twelve dropsondes were also deployed at from the Lake Erie's helicopter for a combined total of 81 upper air profiles.

The exercise was confined to the western end of the GOO with all of the upper air recordings taking place west of 59.27E. The northern shore of the GOO rises quickly into mountainous terrain known as the Central Makran Range. The southern shore of the GOO is bordered by the Hajar Mountains (Figure 3.2).

The GOO typically experiences a monsoonal type climate when not under the influence of an extratropical cyclone. Normally the Northeast Monsoon dominates the GOO in the winter. The Middle East and Arabian Sea can experience outbreaks of cold air such as the Shamal discussed in the previous chapter. However, the Himalayan and Caucasus Mountains block many of these outbreaks causing the monsoonal flow to be less intense over this region than over the South China Sea. (Hubert, et al, 1983).

Perrone (1979) depicts a typical surface analysis (Figure 5.1) during the Northeast Monsoon. Typically high pressure is centered over southern Asia with ridges over the Saudi Arabian Peninsula and North Africa with inverted lee troughs located over the Persian Gulf and GOO. Winds in the southern Arabian Sea during the Northeast Monsoon are mostly out of the northeast and are generally less than 21 kts. They are usually light and variable and

under the influence of land/sea breeze effects in the northern Arabian Sea and GOO. During the monsoon the gradient wind (which at the surface is actually cross gradient due to friction) tends to enhance the land breeze. This means that offshore winds are usually present except during afternoon hours. Higher winds are typically found off the Iranian coast, especially during the morning hours. In addition, winds in the Strait of Hormuz and the GOO are very much influenced by the mountain ranges surrounding both of these bodies of water. Venturi effects and down/upslope winds are quite common during the northeast monsoon (Walters and Sjoberg, 1988).

B. TRANSITION TO NORTHEAST MONSOON

1. Synoptic Weather

The previously described Shamal persisted as the ships moved into the GOO for the second half of SHAREM 110. However, at this time the Shamal was weakening with wind speeds decreasing to generally around 10-15 kts. Figure 5.2 presents the NORAPS surface analysis for 03Z 13 Feb. and it shows that the lee trough formed during the Shamal is still present over the eastern shore of the Persian Gulf extending into the GOO.

The surface streamlines associated with this surface pattern are depicted in Figure 5.3. The Persian Gulf is still experiencing northwesterly Shamal winds. Winds over the Strait of Hormuz are out of the northeast as they are funneled through the pass between the Zagros Mountains and the Central Makran Range (Figure 3.2). The wind flow then turns to the northwest as it encounters the the pressure gradient of the northwesterly Shamal winds and are drawn toward the lower pressure of the northern Arabian Sea after passing over the Omani peninsula. Surface winds over flowing from southern Iran and into the GOO are

northeasterly over land. Once over water, they quickly turn northwesterly and converge with the winds coming out of the Persian Gulf. Off shore winds in the GOO are aided by the fact that this is early morning so the land breeze effect (discussed below) is at its strongest. The Hajar Mountains enhance this convergence by channeling the winds and acting as a "wall" that causes the streamlines to bunch up and form a confluent asymptote. The result is a cloud line known as a Convergence Cloud Line (Hubert, et al, 1983). It can be seen in DMSP satellite imagery as a thin line of cloud running from northwest to southeast (Figure 5.4).

The transition from Shamal to Northeast Monsoon is consistent with other studies. Figure 5.5 is the 03Z 13 Feb. NORAPS 5500 m. streamline analysis. At this time, the upper level trough is moving eastward to be replaced by an upper level ridge with its corresponding northwesterly winds. True monsoonal flow had reestablished itself by 00Z 14 Feb. The NORAPS surface analysis (Figure 5.6) for this time shows high pressure dominating the region north and east of the Persian Gulf and the GOO. A second but less intense area of high pressure was in place over the Saudi Arabian Peninsula. This figure agrees very well with the typical synoptic picture presented in Figure 5.1.

When not under the influence of a strong extratropical cyclone, low level wind flow in the GOO is greatly affected by the the land/sea breezes and up/downslope winds as well as the surrounding topography. This is very obvious when surface streamlines from various parts of the day are compared. During the day the sea breeze effect plays a large role in low level wind flow. The 15Z 13 Feb. NORAPS surface streamline analysis (Figure 5.7) clearly shows what effect the heating of the northern and southern shores of the GOO has on low level wind flow.

Even though the Shamal is still present at this time, it has grown weak and synoptically the situation in the vicinity of the GOO is much as it would be during a monsoon. The low level synoptic pressure gradient would be expected to lead to off shore winds from southern Iran and Oman. Instead, Figure 5.7 shows that winds are actually onshore during this time due to daytime heating over land. The result is confluent asymptotes aligned with the mountain ranges on both shores and a diffluent asymptote generally in the middle of the GOO.

The land cools faster than the adjacent waters at night and the result is off shore flow known as a land breeze. The NORAPS surface streamline analysis for 03Z 14 Feb. (Figure 5.8) indicates the off shore winds from southern Iran are no longer immediately drawn into the northern Arabian Sea. Instead the streamlines follow a more southerly route over the GOO. They are still turned out of the northwest in the central GOO but this is solely because of their interaction with the Hajar Mountains and offshore winds from Oman. Once they are out over the Arabian Sea they become northerly again. Part of the velocity vector for the winds coming off both shores is due to a land breeze effect. Also, both shores are mountainous and at night cold air formed on the higher slopes flows downward and would augment any land breeze present.

In general, the diurnal effect of heating and cooling the surrounding land mass of the GOO is present most of the time to some magnitude. It takes a large disruption of the normal Northeast Monsoon pressure pattern for this signal not to occur. This did occur during the height of the Shamal described previously. The low level winds depicted in the streamline analysis by NORAPS during the strongest part of the Shamal, of which Figure 5.9 is a good

example, show no discernible onshore flow that would be normally expected in the GOO during this time of day. Instead the synoptic pressure pattern and steering do to topography seem to be the major influences in wind direction.

Shown in Figure 5.10 are time series of temperature, dew point depression, pressure, and wind direction and speed for each ship during the GOO portion of SHAREM 110. The figure shows wind direction at each ship varying greatly. This is not surprising as a ship's position relative to the confluent and diffluent asymptotes mentioned above would have and important effect on wind direction. During the early hours of the 13 Feb. the winds at each ship are generally out of the north-northwest and are in agreement with the streamlines of Figure 5.3. Later, during the afternoon and early evening hours of 13 Feb., the surface wind observations take on a more westerly component. This is generally in agreement with the streamlines of Figure 5.7. In all, the time series does show daily changes in wind direction during the entire period shown. Since the ships did not remain stationary during the exercise and considering model errors, it would be very difficult to reconcile every windbarb shown with model streamlines. Comparison of the shipboard observation data, however, does seem to be in general agreement with the model in most cases.

The temperature time series (Figure 5.10) indicates that with the end of the shamal, a warming period occurred over the GOO. Starting in the morning hours of 13 Feb. there do not appear to be any long term trends in the temperature plot such as the trends that were seen in Figure 4.6. Temperatures apparently varied only due to diurnal effects. The time series of dew point depression shows variations but that generally depressions were large. Surface pressure shows a slight rise (other than diurnal effects) until approximately 00Z 15

Feb. This was due to the Shamal ending as high pressure ridged in and the Northeast Monsoon set up as described above. Surface pressure then falls until the 17 Feb. and remains fairly constant for the rest of the period. This drop in pressure was due to a short lived Shamal event to be described later.

2. Upper Air and Refraction

The first sounding of the GOO portion of SHAREM 110 was launched by the Silas Bent at 03Z 13 Feb. The sounding (Figure 5.11) revealed northerly surface winds quickly veering to the north at approximately 1400 m. Figure 5.3 indicates that northerly winds at this location were due to channeling around the local topography as discussed above. The winds continued to veer becoming easterly at 1500 m. The easterlies extended up to around 2500 m. where they continued to veer becoming northwesterly in agreement with the upper air flow described above.

The easterlies from 1500 to 2500 meters were probably a direct result of the high pressure to the northeast of the Persian Gulf interacting with the mountains of the southern shore of Iran and Pakistan. This interaction resulted in a lee trough over the Persian Gulf and GOO and east-west orientated isobars along the aforementioned mountain range. Figure 3.2 shows that the topography in this region is mostly between 1000 and 2000 meters. The lee trough probably disappears above these mountains and the resulting winds become more geostrophic as expected at the southern end of a high pressure region. In addition, it is also possible that these mountains help maintain a thermal difference between the cold dry air of the continent and the warmer moist air over the Arabian Sea. This thermal gradient would add a easterly thermal wind vector that could help explain these easterlies.

The temperature and dew point plot displayed in Figure 5.11 shows a deep, well mixed boundary layer with a top at around 1100 m. As mentioned in the previous chapter, the layer of easterly winds appear to be bringing fairly substantial moisture with them. The result was a very weak trapping layer from 1100 m. to 1200 m.

Three hours later, both the Lake Erie and the Silas Bent launched soundings in the same general position. The layer of easterlies was still present but it was thicker, starting at around 1000 m. These low level easterlies appear to have slightly drier air associated with them. This caused a 100 m. thick trapping layer centered near 750 m. as shown by the Silas Bent's 06Z sounding (Figure 5.12).

The soundings start to show a sea breeze effect in their lower level winds by 12Z 13 Feb. An indication of how far south the layer of easterlies extends is given by soundings launched from the Silas Bent and Lake Erie. Figure 5.13 shows where the 12Z 13 Feb. soundings were launched while Figures 5.14 and 5.15 are the plots of the soundings from the Lake Erie and Silas Bent respectively. The low level winds for the Lake Erie are out of the northwest which, given the ship's location, gives onshore winds into Oman. In addition, the layer of easterlies has disappeared. The boundary layer top is down to around 700 m. causing a trapping layer at the same height. The Silas Bent, around 40 nm to the north, still shows a layer of easterlies. This soundings low level winds are generally out of the west due to an onshore component given to the surface wind by the sea breeze effect much like that shown in Figure 5.7. This sounding also indicates a weak trapping layer at around 800 m.

The trapping layer in these soundings appears to have reached its maximum strength at 15Z 13 Feb. The Silas Bent's sounding at this time (Figure 5.16) shows that the low level

winds have a substantial onshore component (Figure 5.7) presumably due to the sea breeze being at its maximum. The top of the boundary is fairly well defined with some capping subsidence. This subsidence was probably enhanced by the sea breeze return allowing the strong trapping layer seen in the M unit profile. As the evening progressed the sea breeze effect decreased and by 21Z the duct had disappeared resulting in normal refractive conditions.

The sounding launched from the David R. Ray at 03Z 14 Feb. (Figure 5.17) showed that the Northeast Monsoon had finally set in (see Figure 5.8). Winds at the Silas Bent's position were out of the northeast from the surface to 2400 m. These direct off shore winds whose source region was well inland resulted in a very dry atmosphere immediately above the surface and were reflected in the temperature-dew point plot of the sounding. As a result, there is no trace of a trapping layer anywhere in this sounding but there more than likely would have been an evaporation duct present.

These conditions continued well into the daylight hours, until around 12Z. At this time the sounding from the Silas Bent began to show a sea breeze effect in its low level winds. By 15Z the sea breeze was in progress as shown by the Silas Bent's sounding at this time (Figure 5.18). Once again, the sea breeze return caused in low level subsidence over the GOO resulting in a fairly well defined boundary layer top and corresponding trapping layer at around 600 m. This trapping layer persisted into the night as the northeasterly winds reasserted themselves. As the boundary layer cap was forced down, the trapping layer got

lower and lower, eventually resulting in the surfaced based duct seen in the 21Z 14 Feb. sounding from the Silas Bent (Figure 5.19). By 00Z 15 Feb. the trapping layer much weaker as the offshore winds continued to dry out the boundary layer.

In general, the land/sea breeze appears to play a major role in the formation of trapping layers in the Gulf of Oman. In this section the movement of dry air from both southern Iran and Oman was shown to be offshore at night due to a land breeze effect. This tends to dry out the lower layers and destroys any trapping layer that may have been present due to a marine layer. During the day, on the other hand, it appears the sea breeze causes the formation of a marine layer allowing a trapping layer to reform.

C. SHORT SHAMAL EVENT

1. Synoptic Weather

Surface winds in the GOO became more easterly by 03Z 15 Feb. as shown in the streamline analysis for this time in Figure 5.20. This was caused by a low pressure system with an associated upper level short wave trough moving into southern Iraq and Kuwait from the eastern Mediterranean. This evolution is apparent in the 00Z 15 Feb. NORAPS surface and 500 mb. analysis (Figures 5.21 and 5.22). Surface winds in the GOO were still offshore as expected with the high pressure still dominating northeast Iran, Afghanistan, and southern Russia. However, instead of flowing generally southward and then being channeled out of the northwest by the Hajar Mountains, surface winds turned easterly in the GOO and were drawn over the Omani Peninsula and into the Persian Gulf (Figure 5.20).

This synoptic situation caused the southeasterly winds in the Persian Gulf known as Kaus winds which generally precede a Shamal. This particular Shamal, however, was not as

strong as the one discussed previously. Instead, this system followed a recognized variation in the typical synoptic sequence of a Shamal. Perrone (1979) states,

> If the surface lows and their associated upper air troughs traverse west to east through, or just to the north of, the northern Gulf without sufficient intensity to draw cold air southward to the rear of the surface low, only a brief period of gale force north westerlies, confined to the northern Gulf, may result.

This low pressure passed just to the north of the Persian Gulf weakening as it did so. Figure 5.23 presents the 0546 15 Feb. DMSP infrared image for the Persian Gulf region. It clearly shows the low and associated cold front. However, unlike the previous system , it is clear that the frontal band was fairly narrow and apparently dissipating at this point. By 12Z 16 Feb. the surface low has almost disappeared and the upper level flow is zonal (Figures 5.24 and 5.25). Figure 5.25 shows that the strongest part of the upper level short wave trough was well into southern Russia. This would seem to indicate that the surface low weakened because it lost its upper level support. Even though the surface low did fill, it did manage to establish the mountain lee trough along the eastern shore of the Persian Gulf and into the GOO (Figure 5.24).

The lee trough produced during this short lived Shamal event was not as strong at its maximum intensity as the trough of the previous chapter. However, higher pressure ridging extending from the northwest along the eastern half of the Saudi Arabian peninsula caused the lee trough to be shifted slightly eastward with a corresponding increase in the pressure gradient as shown in the NORAPS surface pressure analysis for 15Z 16 Feb. (Figure 5.26). This resulted in the jump in wind speed seen in the time series of Figure 5.10 at this time. Figure 5.26 shows this tighter gradient located over southwestern Iran along the eastern coast

of the Persian Gulf. This indicates that the model may have been slow in predicting the strength of the high pressure system as it moved down the east coast of the Saudi Arabian Peninsula. Even with a tighter pressure gradient, the sea breeze signal existed as shown in the 15Z 16 Feb. surface streamline analysis shown in Figure 5.27. While the surface wind flow in the GOO (and the Persian Gulf for that matter) is generally out of the northwest, there is a distinct onshore component to the wind. The surface pressure pattern in Figure 5.26 persisted for the pretty much the rest of the exercise resulting in surface flow as shown in Figure 5.27 during the day. At night the land breeze effect would resume resulting in general flow as shown below in Figure 5.28. However, at the very end of the exercise, high pressure to the northeast of the Persian Gulf began to reassert itself by ridging down into southeast Iran and western Pakistan as the Northeast Monsoon began to reform.

2. Upper Air and Refraction

The effect the new low pressure system positioned just north of the Persian Gulf had on low level winds can be seen in the 03Z 15 Feb. launched from the Silas Bent (Figure 5.29). The lower level winds were still offshore as would be expected at this time but they show a distinct easterly influence. There is still a hint of a trapping layer at around 400 m. but the offshore winds have continued to dry out the boundary layer making the trapping layer weaker.

A significant change took place in the wind profiles starting at 09Z 15 Feb. A layer of light and variable northerly winds developed in the soundings starting at about 600 m. extending up to about 1500 m. These northerly winds are more directly from offshore and therefore brought with them a dry tongue of air. This caused the development of an initially

weak trapping layer at around 500 meters. By 15Z 15 Feb. the ships were mostly reporting light and variable winds in the GOO. Figure 5.30 is the sounding launched from the Lake Erie at this time. A layer of northerlies still present but now extending from around 250 m. up to around 600 m. The westerly winds below 250 m. are probably due to the sea breeze effect. A shallow boundary layer formed topped by dry air and a slight inversion. This led to a fairly strong trapping layer and produced a duct that almost reached the surface.

As already mentioned, this Shamal event was not as strong as the system discussed previously. The pressure gradient over the GOO became very weak during the switch over from southeasterly Kaus winds to northwesterly Shamal winds. This allowed a northwesterly confluent asymptote due mainly to a land breeze and down slope winds to form during the nighttime hours of 15 Feb. into the morning hours of 16 Feb. The Lake Erie's sounding form this time is shown in Figure 5.31. It shows that a fairly well mixed boundary layer topped by a slight subsidence inversion still exists resulting in a fairly strong trapping layer. The subsidence inversion at around 3700 meters indicates that the upper level ridge and its associated negative vorticity advection is reasserting itself at this time also. This upper inversion was strong enough to cause a trapping layer.

The Shamal winds do not begin to appear until around 12Z 16 Feb. This is reflected as an increase in wind speed in Figure 5.10 at this time. By 15Z the sounding from the Lake Erie clearly shows the low level winds increase in speed in response to high pressure intensifying over the eastern Saudi Arabian discussed earlier (Figure 5.32). The boundary

layer is more shallow than in the previous sounding so the trapping layer is lower (top at 300 m.) resulting in a surface based duct which remained present at least until 18Z according to another sounding from the Lake Erie at that time.

The 21Z 16 Feb. sounding from the Silas Bent shows that by this time the boundary layer had deepened back up to around 600 m. and that the atmosphere just above the boundary layer had become more moist and well mixed. This caused the trapping layer to become higher and weaker resulting in an elevated duct centered around 500 m (Figure 5.33). This tendency for the boundary layer to be less well defined continued until 09Z 17 Feb. when it had all but disappeared (Figure 5.34) resulting in normal refractive conditions.

The boundary layer reappeared just three hours later as shown by the 12Z 17 Feb. sounding from the David R. Ray (Figure 5.35). At this time the low level winds in the boundary layer had a stronger westerly component than previous soundings. Starting at around 500 m. they began to veer more out of the north up to around 1500 m. Above 1500 m. the winds were again out of the northwest. The formation of a boundary layer was probably due to a combination of dry air brought offshore by the layer of northerly winds and a subsidence due to the sea breeze return. Also, the upper level subsidence had also pushed down far enough to cause an additional trapping layer at 1300 m. By 18Z the boundary layer had shallowed to around 200 m. causing a strong trapping layer and surface based duct.

Into the night, winds below 2500 m. weakened as the lee trough began to break down and the high pressure intensified over Iran, Afghanistan, and southern Russia as discussed above. This caused the boundary layer to deepen with the associated trapping layer becoming higher and weaker. The boundary layer and associated trapping layer remained in all of the

soundings until after 12Z 18 Feb. By the end of the exercise, the Northeast Monsoon had completely reestablished itself as the dominate regime. This is indicated in the low level winds of the last sounding of the exercise at 18Z 18 Feb. (Figure 5.36). At this time the David R. Ray was just inside the Strait of Hormuz. The low level winds shown in the sounding are out of the northeast. This direction is consistent with a land breeze and topographic channeling that would be expected during the Northeast Monsoon in this area.

In general, a short Shamal, such as the one just described seems to favor the formation of a marine layer and associated trapping layer in the Gulf of Oman. This is probably due to the fact that during the Shamal, the source region for much of the low level air is the Persian Gulf where it gathers increasing amounts of moisture. This keeps the marine layer from drying out even at night when dry land breeze air from southern Iran is moving out over the GOO. It is not until the very end of the exercise that the Northeast Monsoon appears to be reasserting itself and is able to once again dry out the lower levels and eliminate the trapping layer.

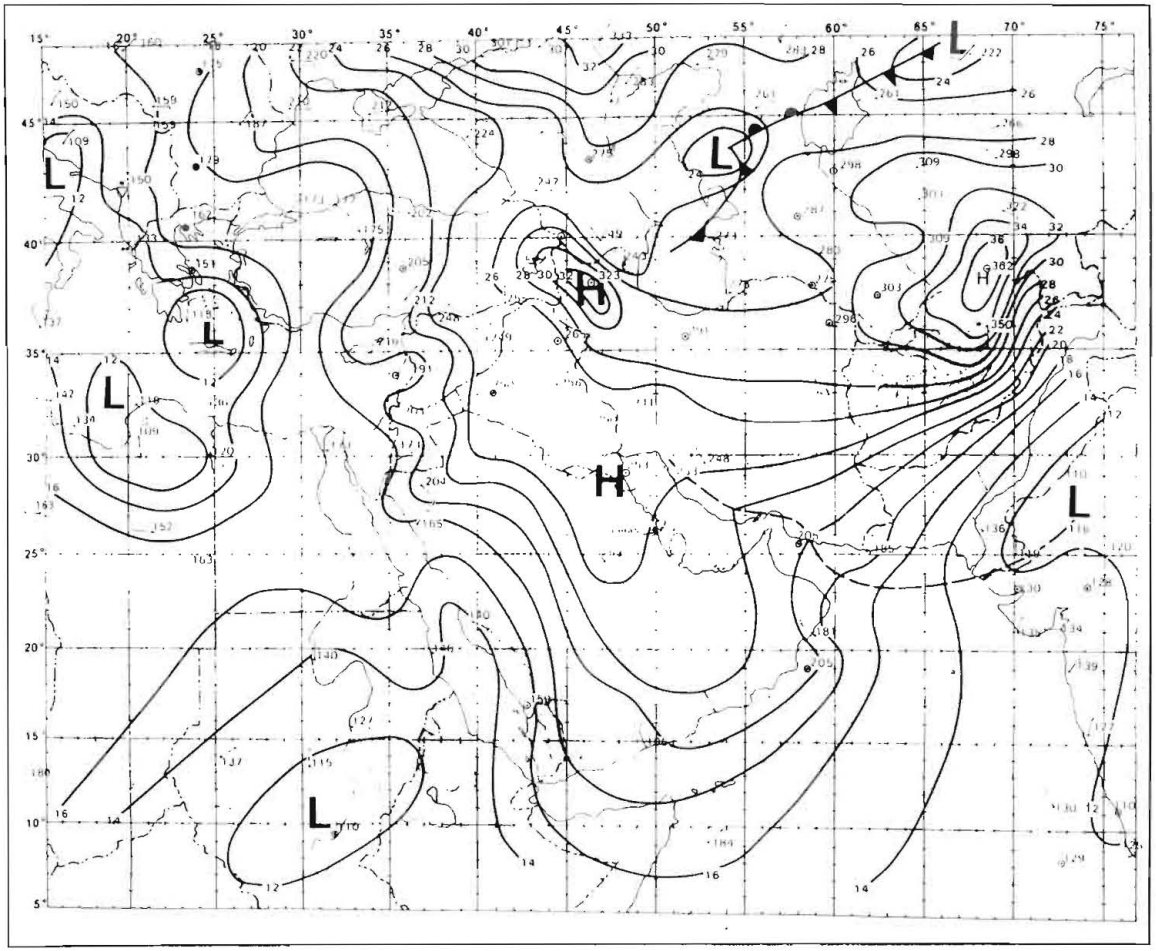

Figure 5.1 00Z Surface Pressure Analysis from 20 Jan., 1973. This is a typical surface pressure pattern for the Northeast Monsoon (from Perrone, 1979).

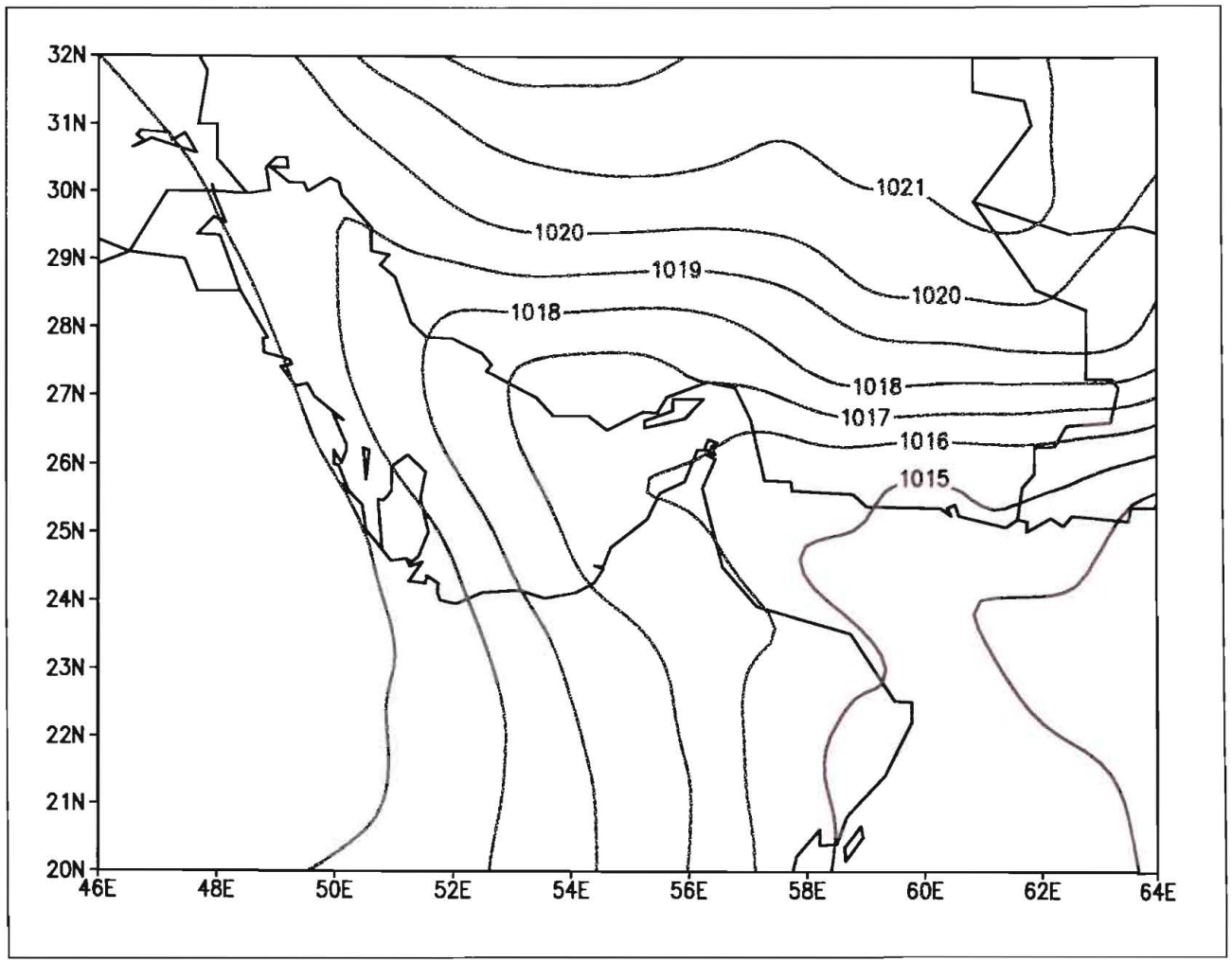

Figure 5.2 NORAPS (τ=15 hr.) 03Z Sea Level Pressure for 13 Feb., 1995.

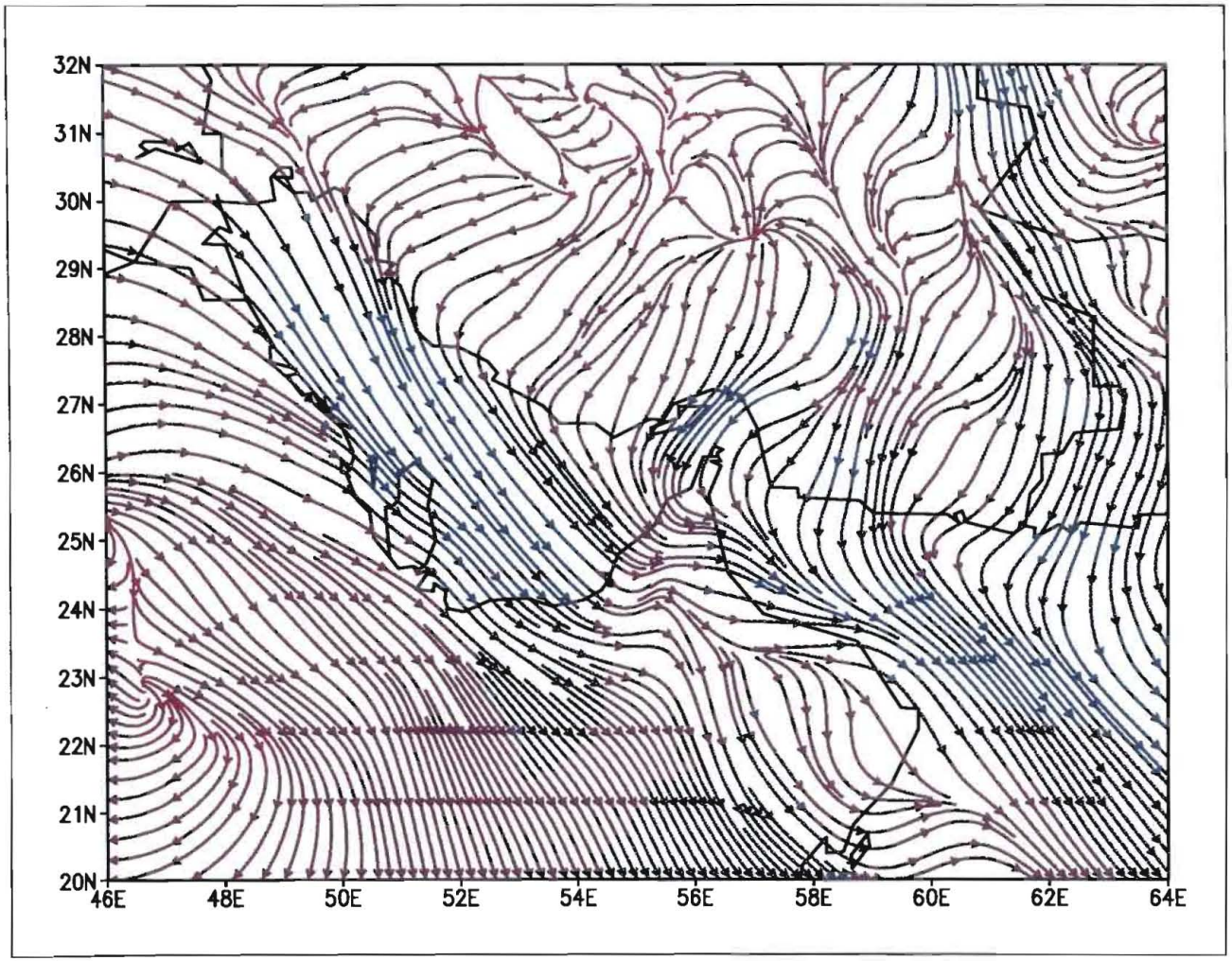

Figure 5.3 NORAPS (τ=15 hr.) 03Z Surface Streamlines for 13 Feb., 1995.

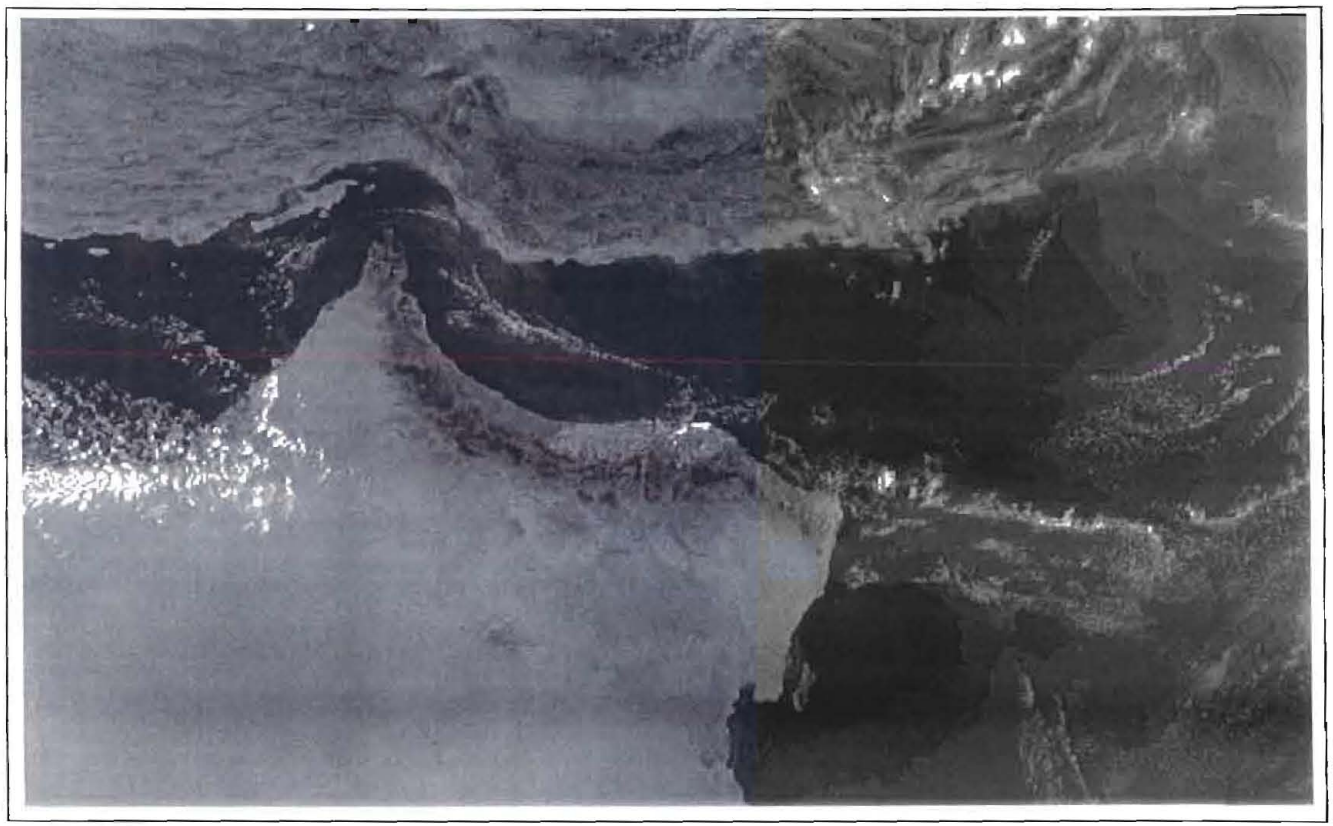

Figure 5.4 0611Z DMSP Visual Image form 13 Feb., 1995.

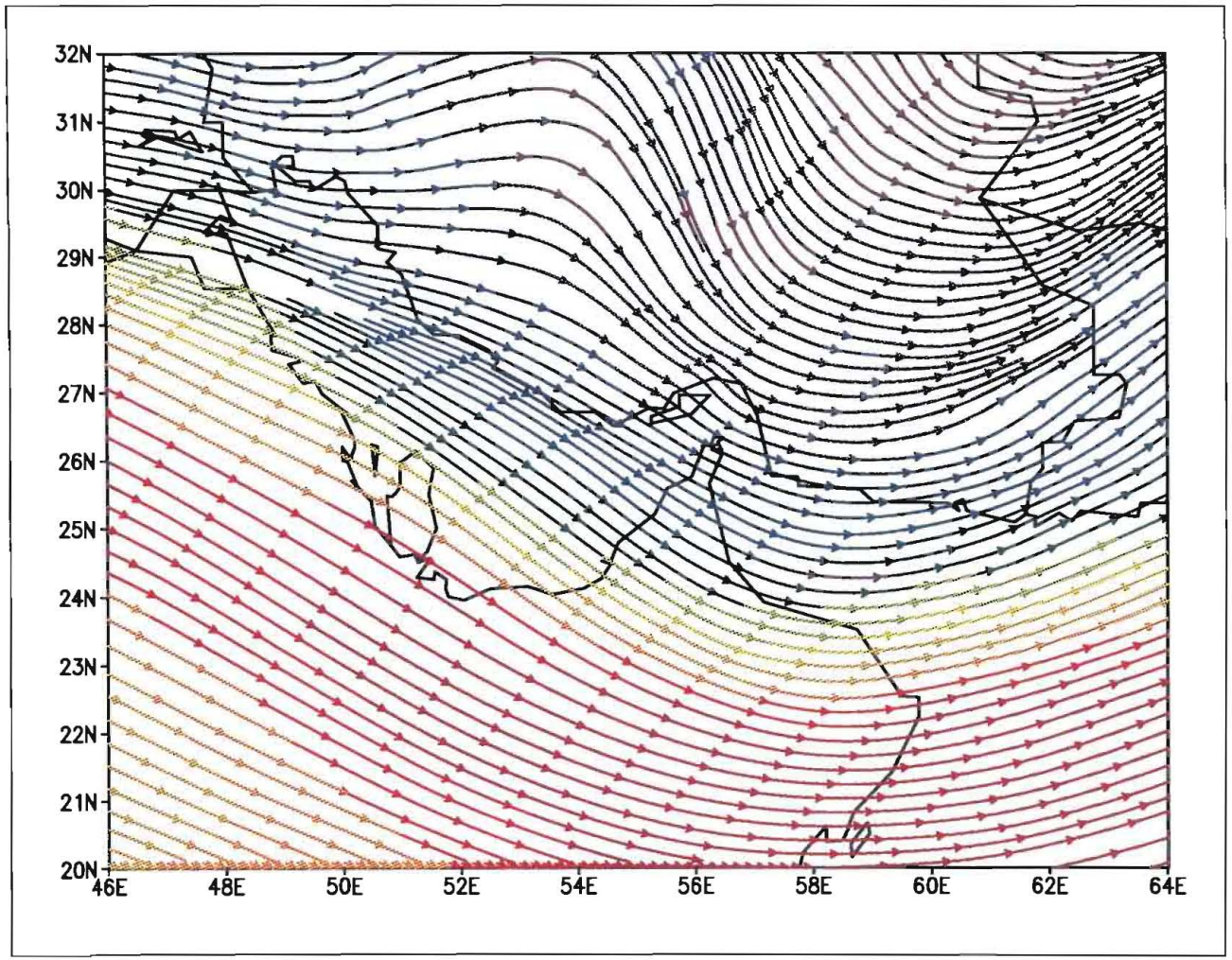

Figure 5.5 NORAPS (τ=15 hr.) 03Z Streamlines at 5500 m. for 13 Feb., 1995.

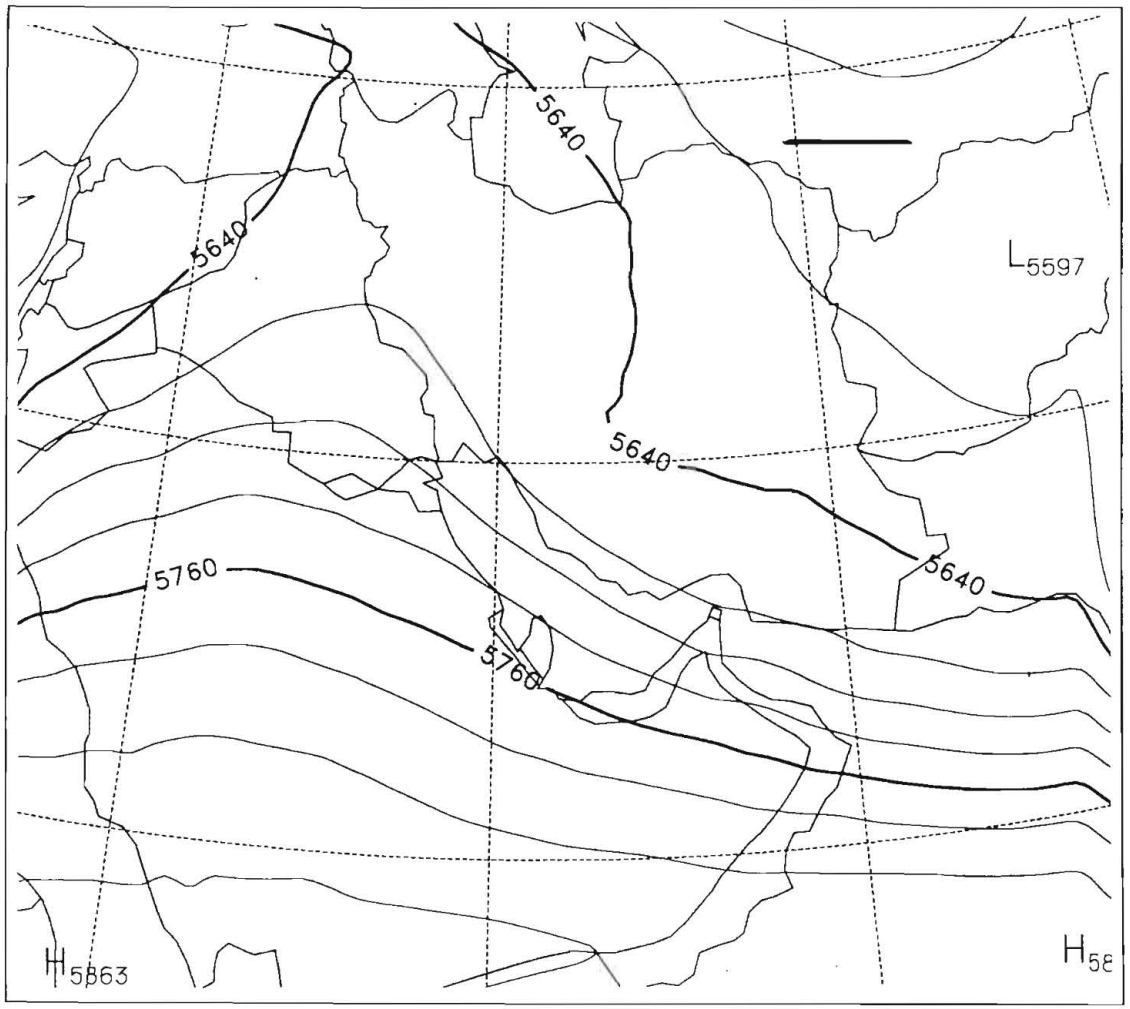

Figure 5.6 NORAPS 00Z Mean Sea Level Pressure Analysis for 14 Feb., 1995.

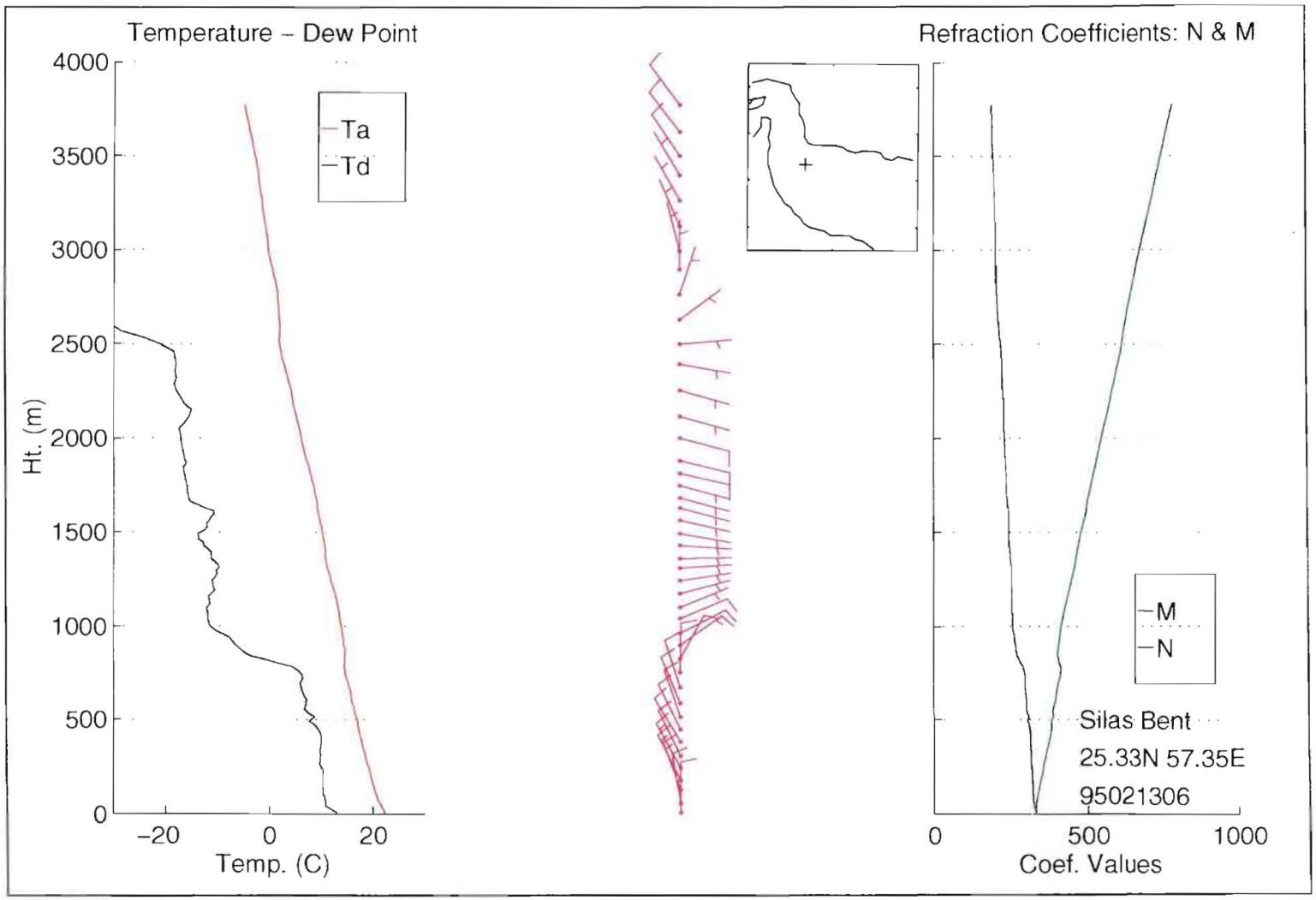

Figure 5.12 06Z Radiosonde Launched from the Silas Bent on 13 Feb., 1995.

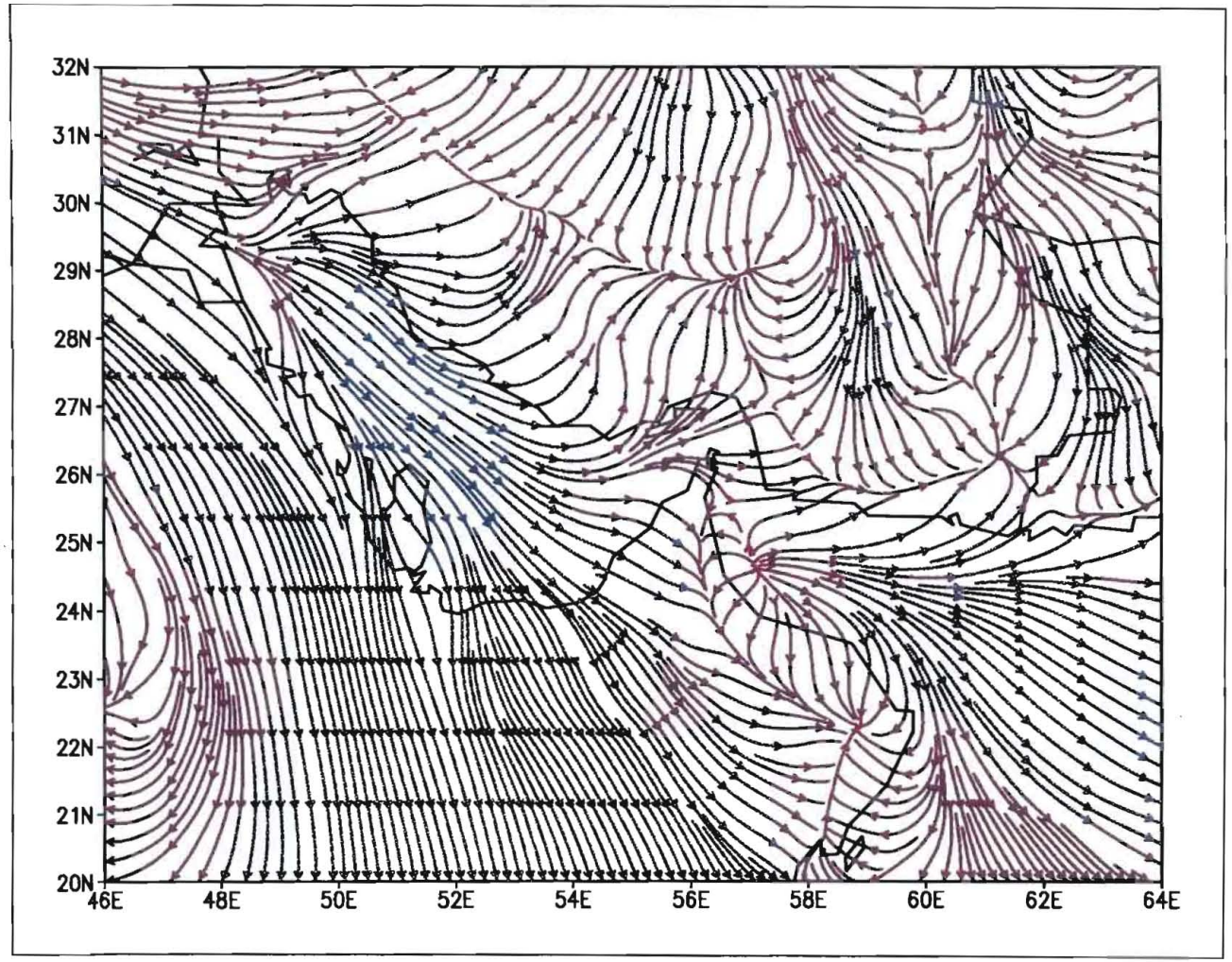

Figure 5.7 NORAPS (τ=15 hr.) 15Z Surface Streamlines for 13 Feb., 1995.

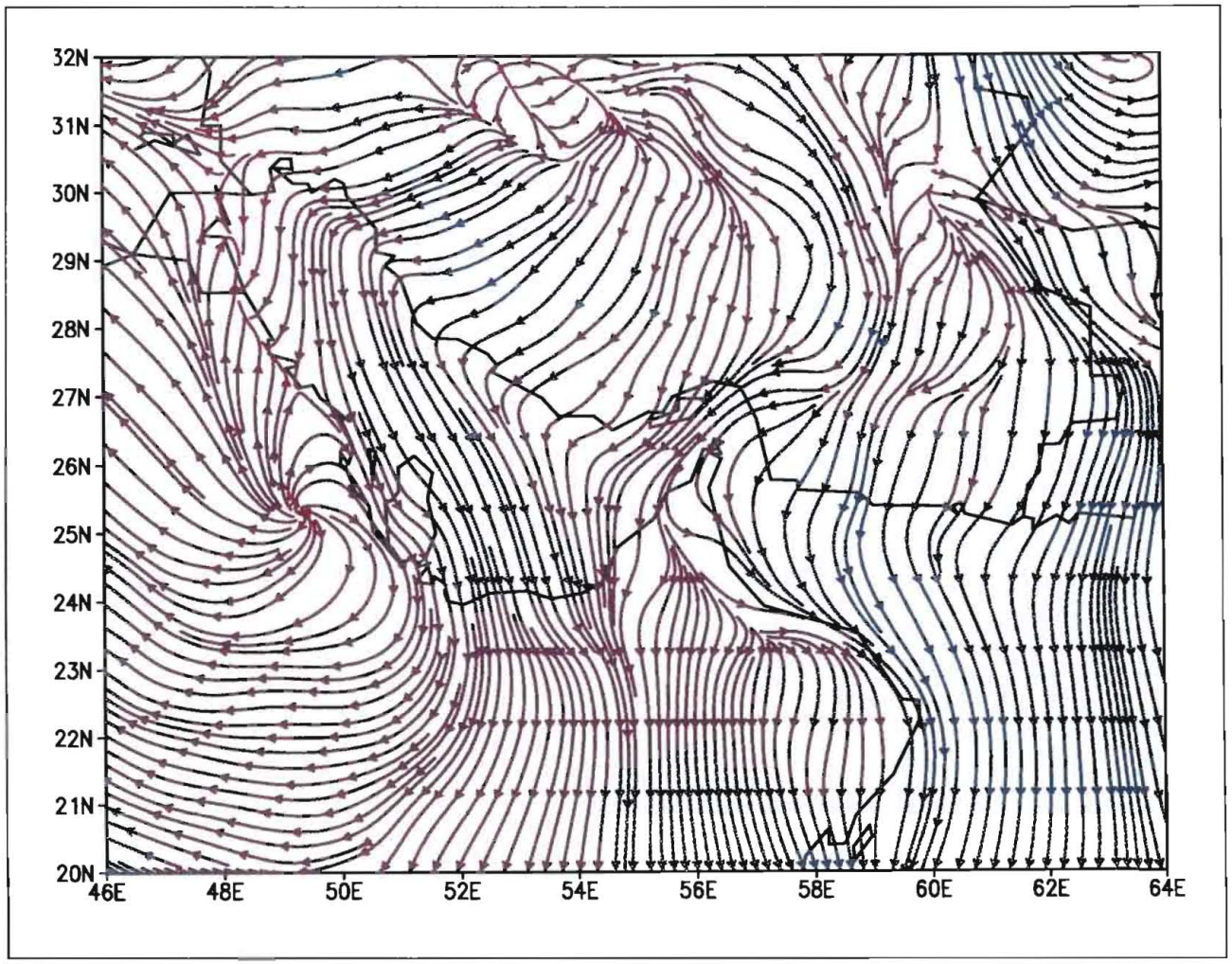

Figure 5.8 NORAPS (τ=15 hr.) 03Z Surface Streamlines for 14 Feb., 1995.

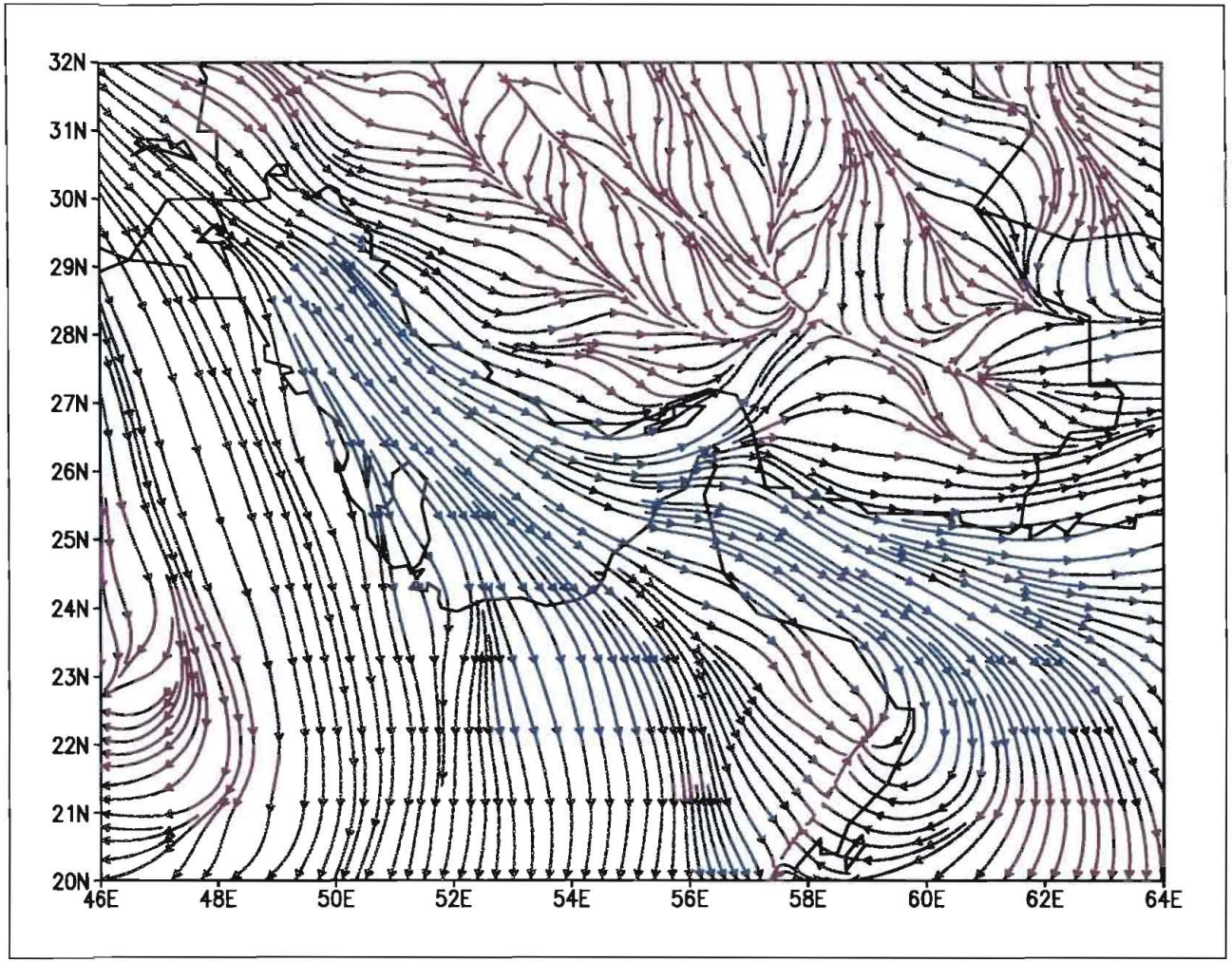

Figure 5.9 NORAPS (τ=15 hr.) 15Z Surface Streamlines for 10 Feb., 1995.

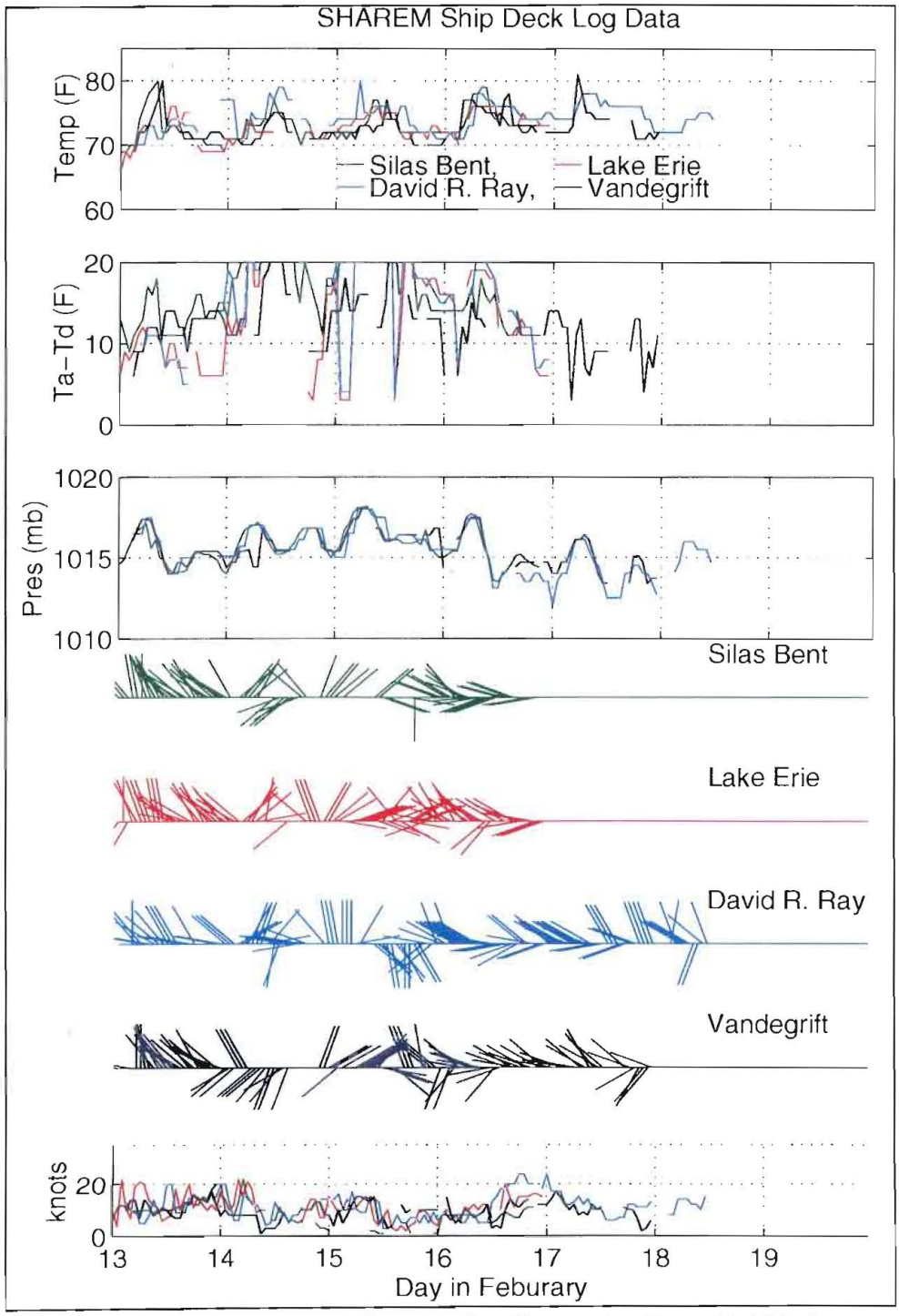

Figure 5.10 SHAREM Ship Surface Weather Observation Data: 13-19 Feb., 1995.

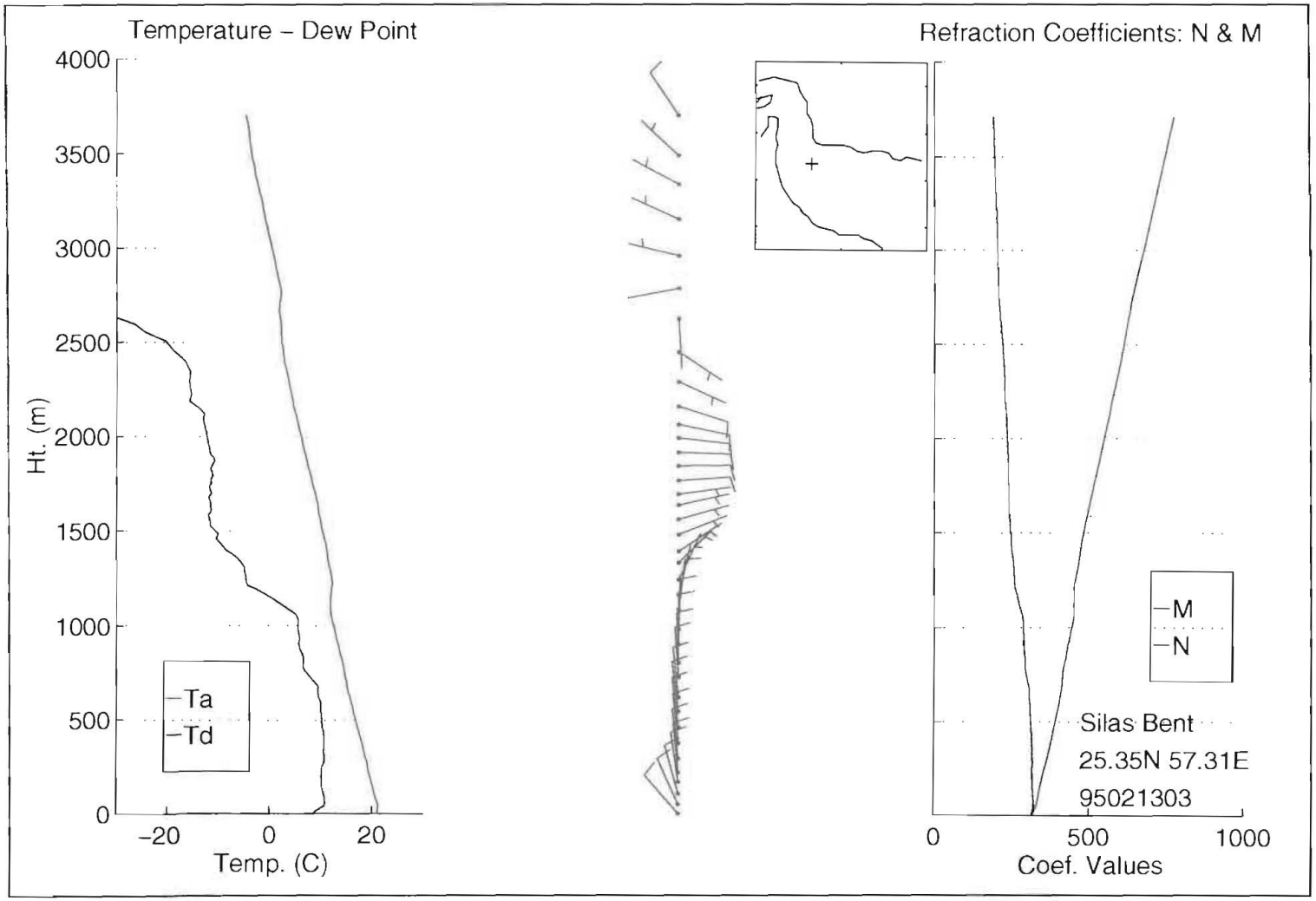

Figure 5.11 03Z Radiosonde Launched from the Silas Bent on 13 Feb., 1995.

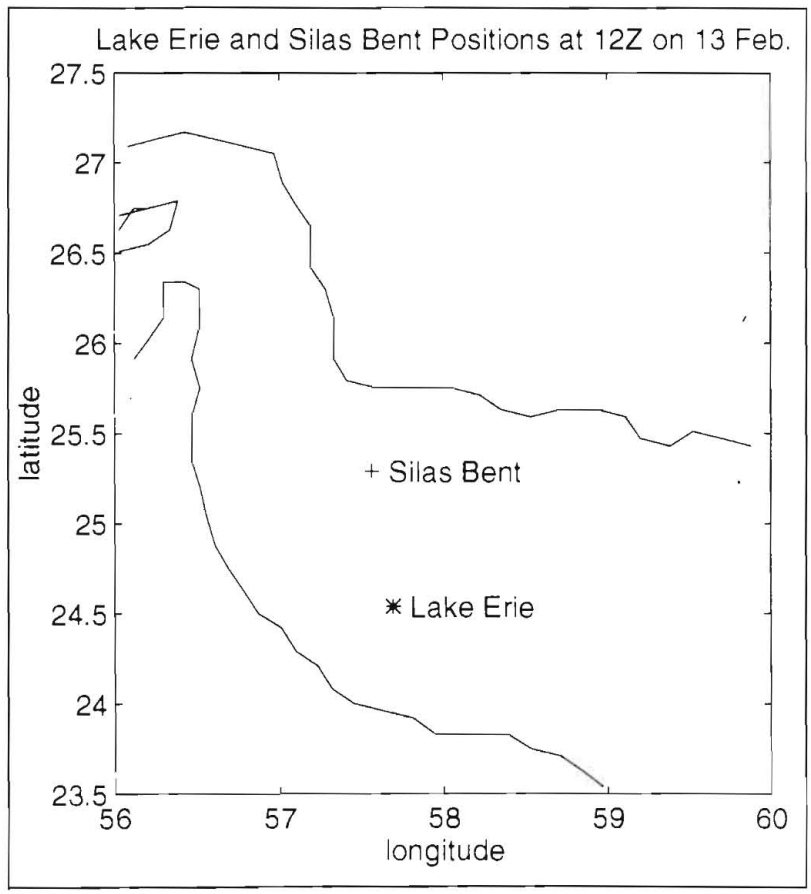

Figure 5.13 Lake Erie and Silas Bent Positions at 12Z on 13 Feb., 1995

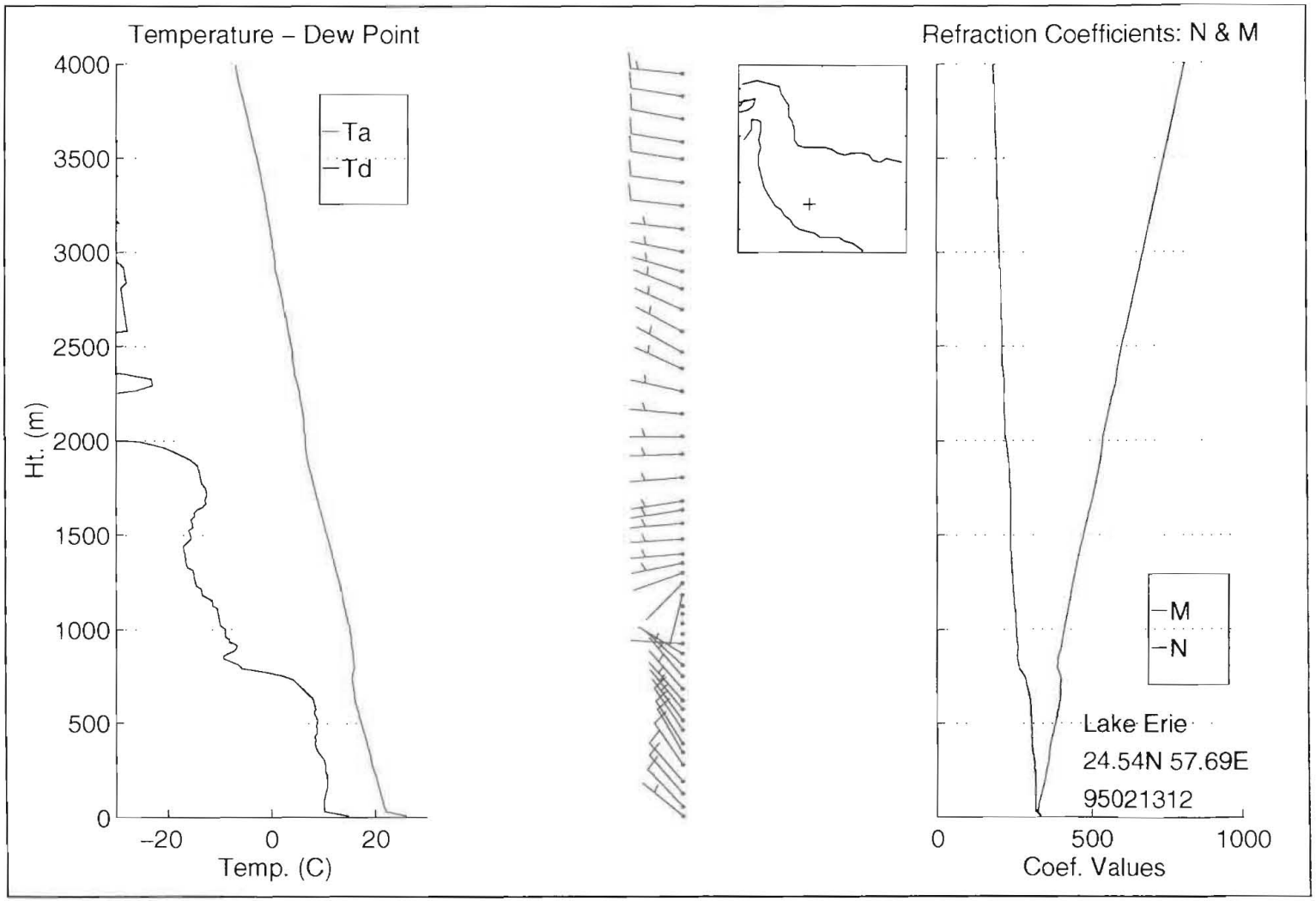

Figure 5.14 12Z Radiosonde Launched from the Lake Erie on 13 Feb., 1995.

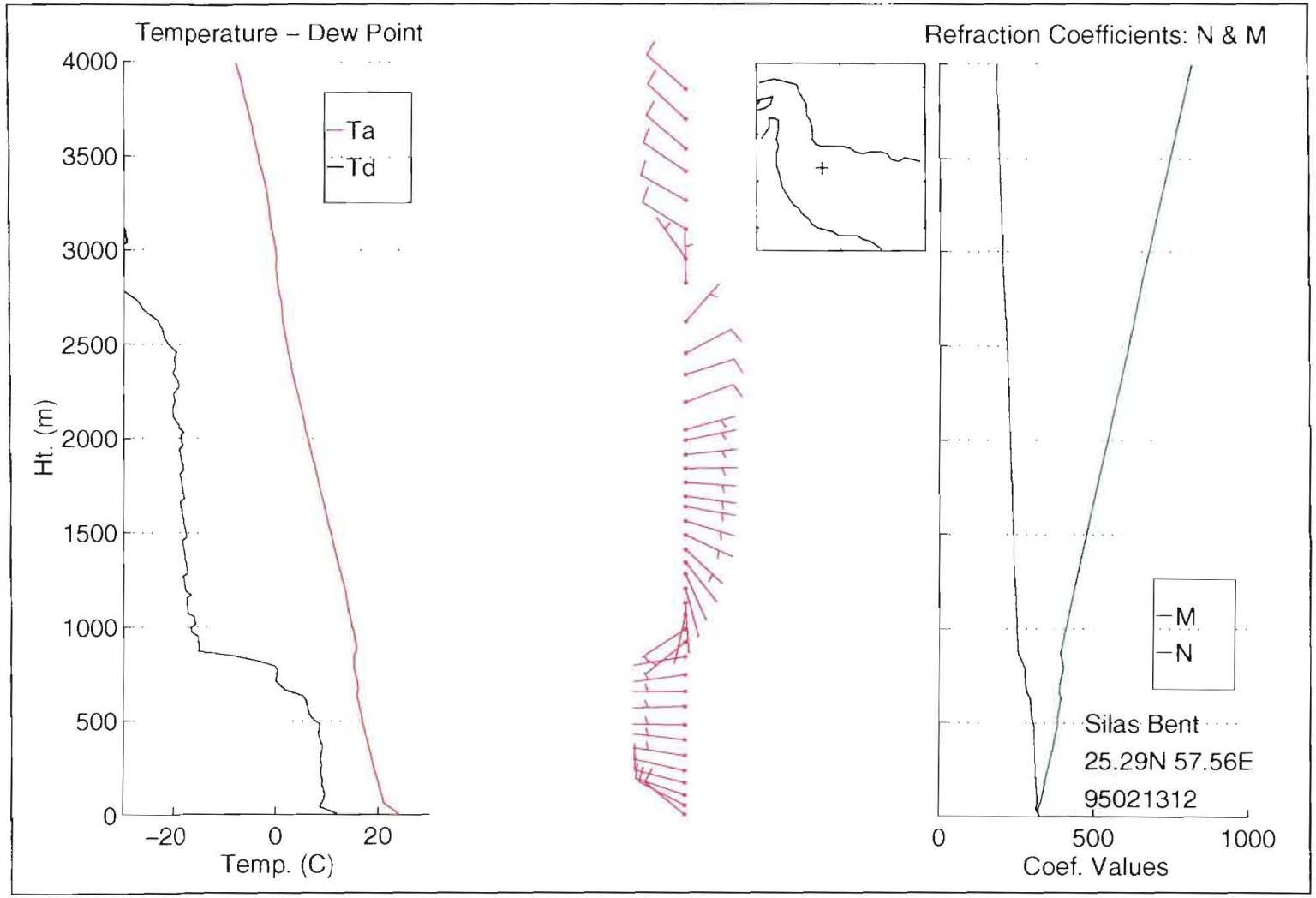

Figure 5.15 12Z Radiosonde Launched from the Silas Bent on 13 Feb., 1995.

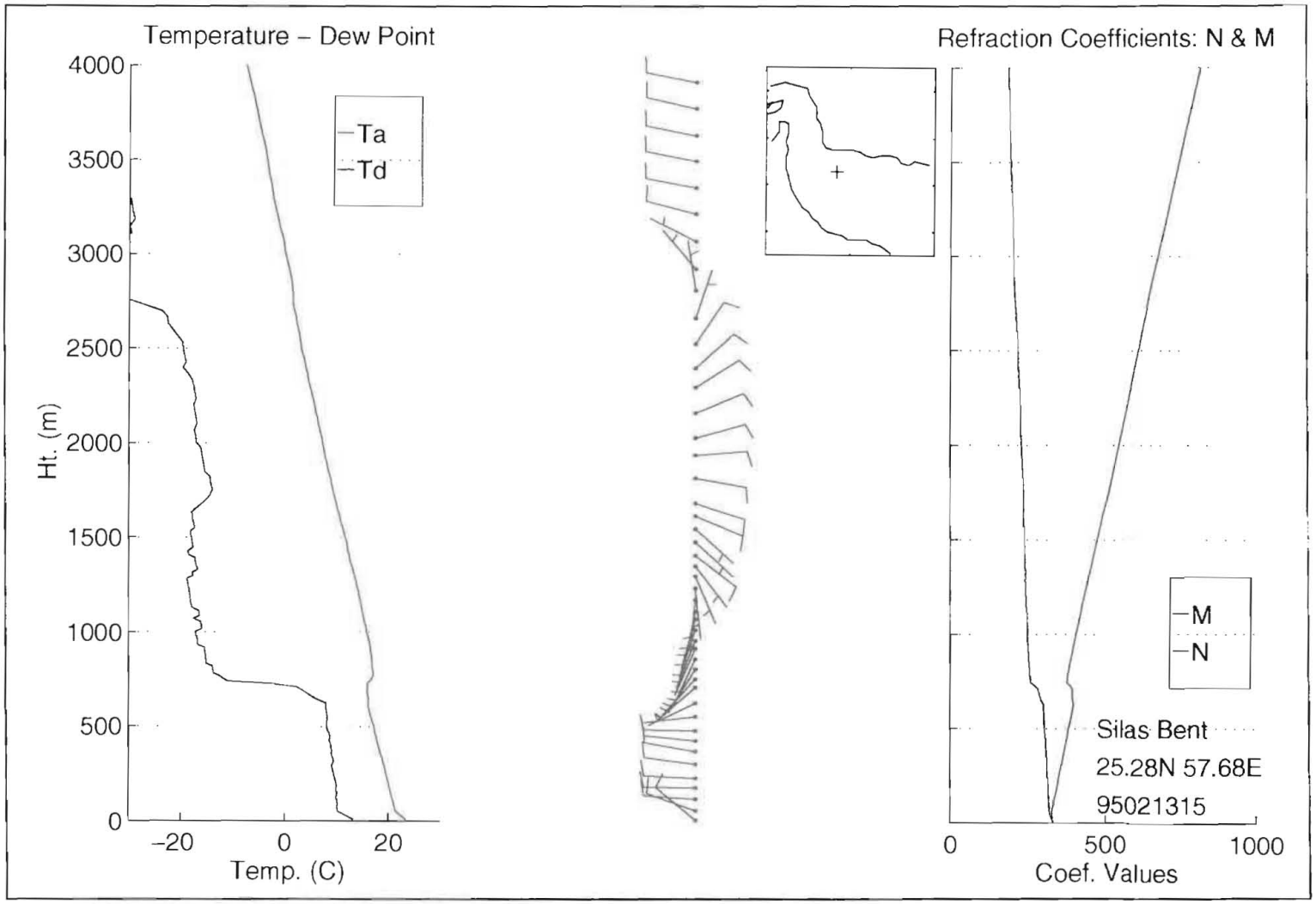

Figure 5.16 15Z Radiosonde Launched from the Silas Bent on 13 Feb., 1995.

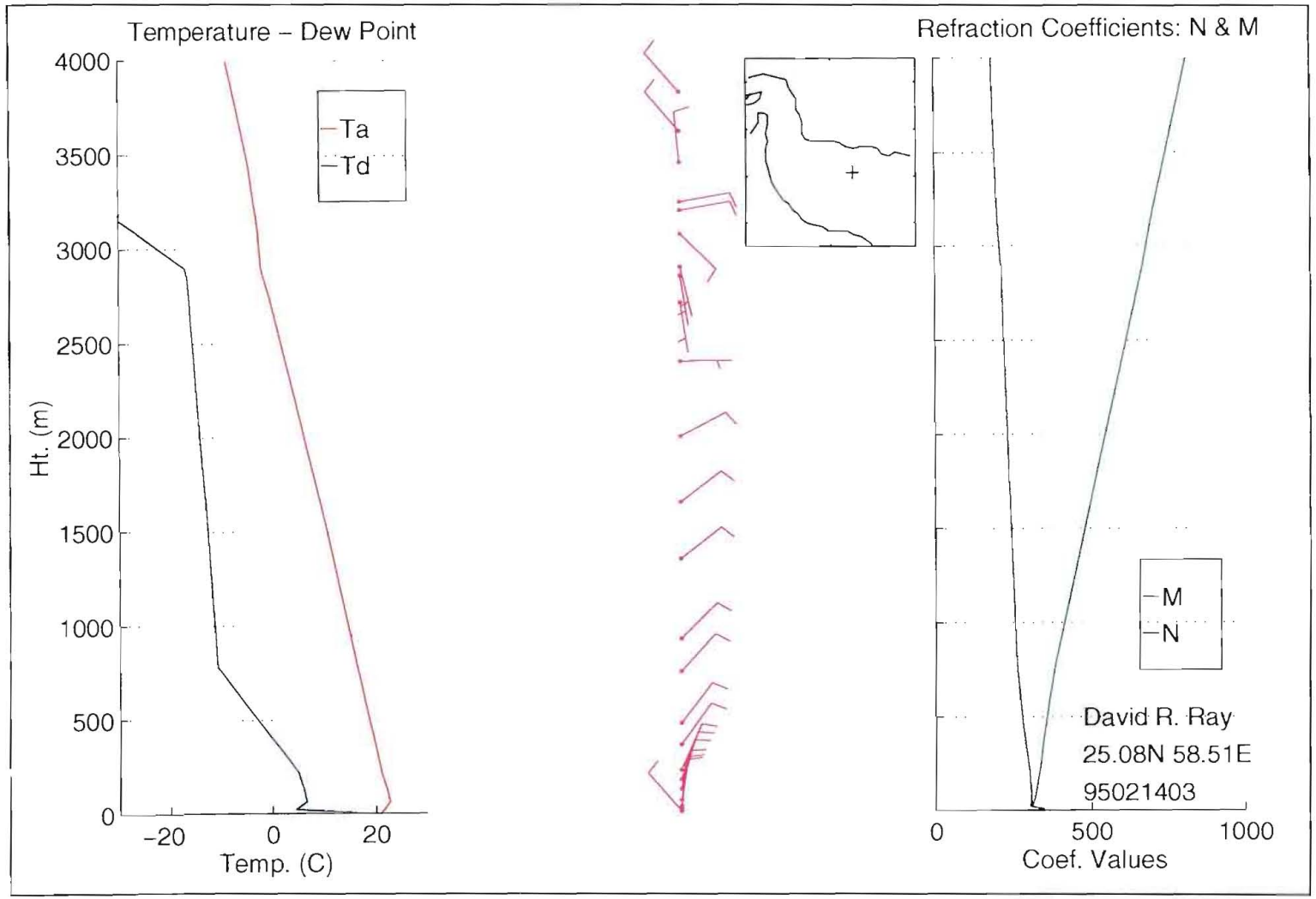

Figure 5.17 03Z Radiosonde Launched from the David R. Ray on 14 Feb., 1995.

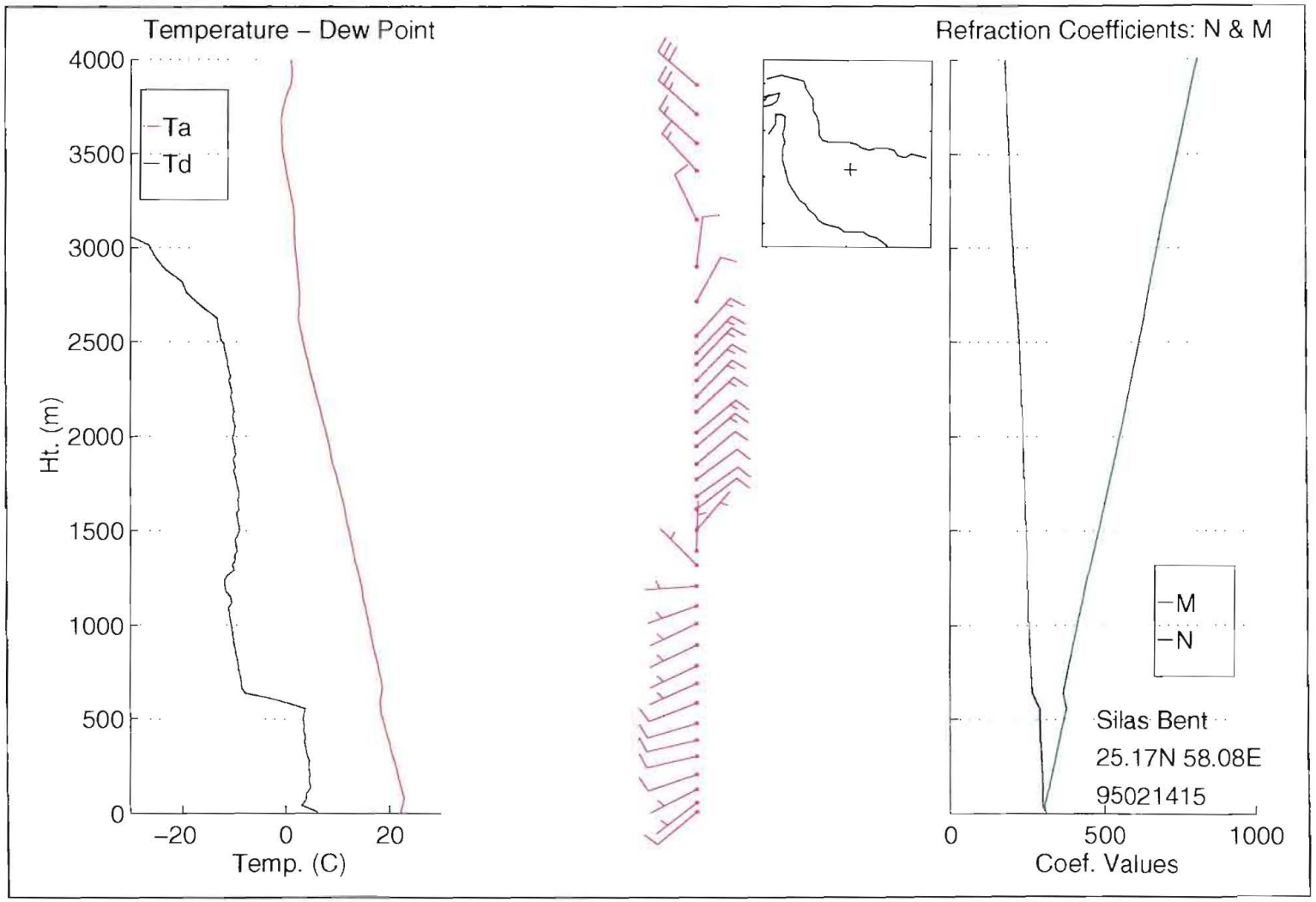

Figure 5.18 15Z Radiosonde Launched from the Silas Bent on 14 Feb., 1995.

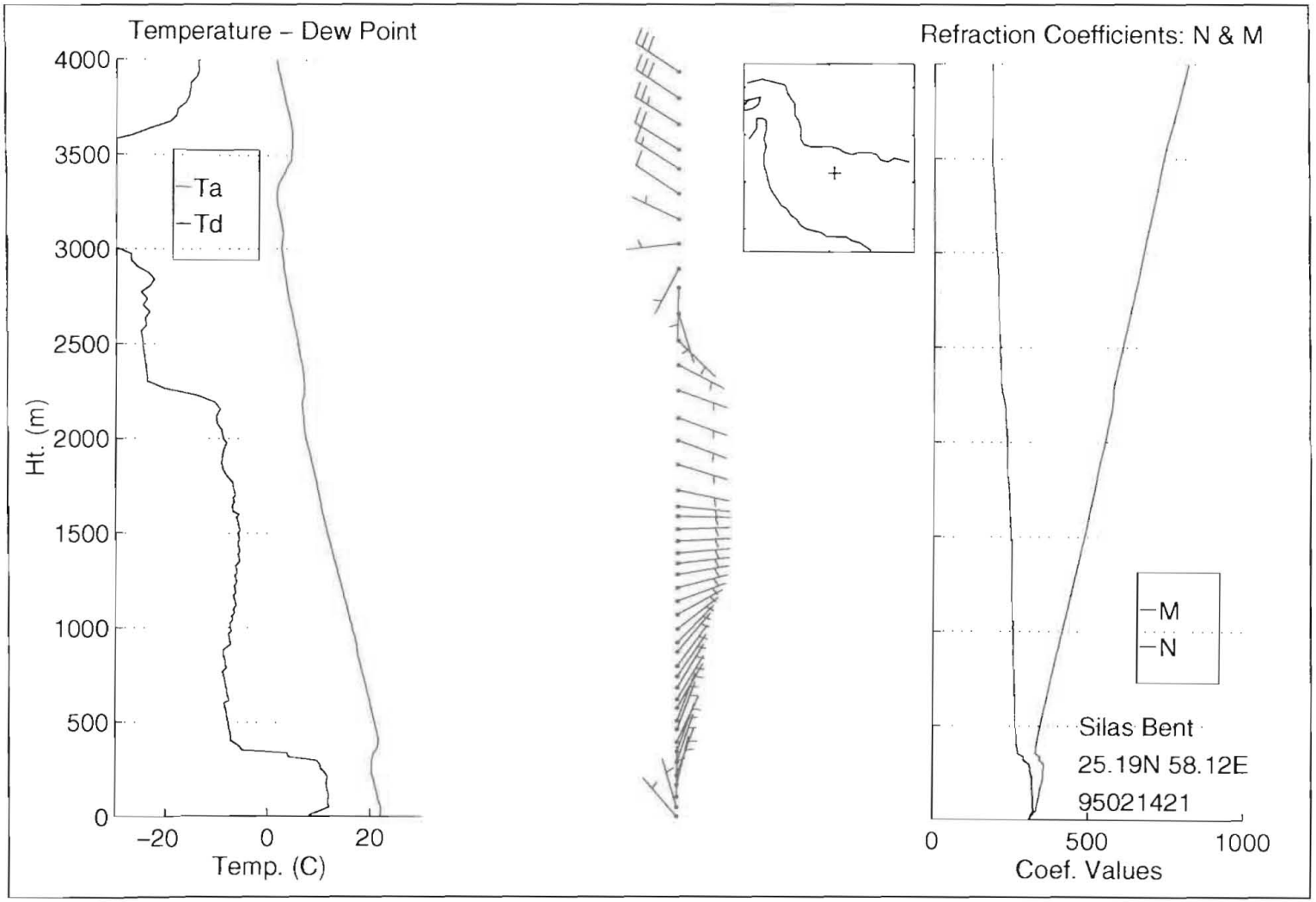

Figure 5.19 21Z Radiosonde Launched from the Silas Bent on 14 Feb., 1995.

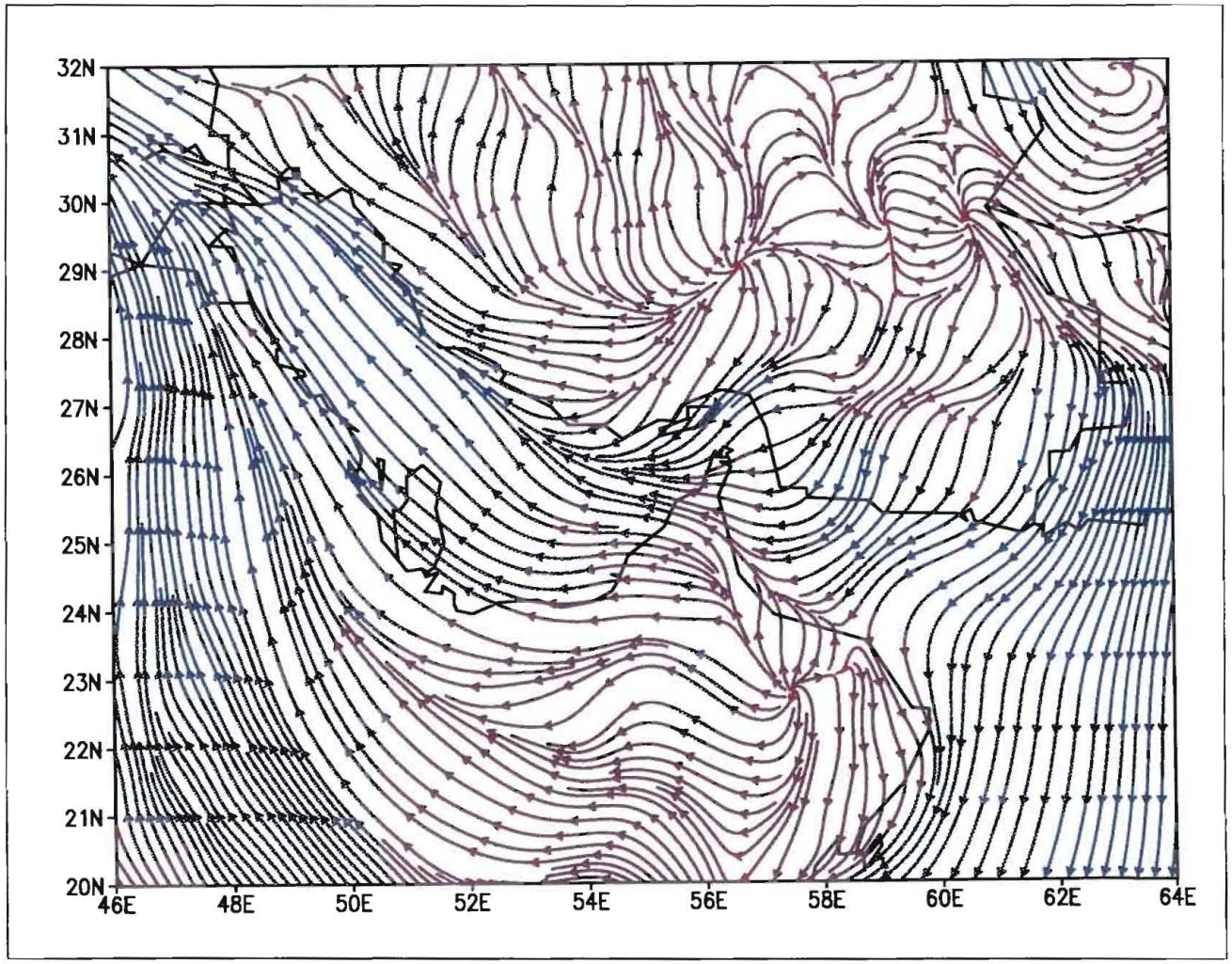

Figure 5.20 NORAPS (τ=15 hr.) 03Z Surface Streamlines for 15 Feb., 1995.

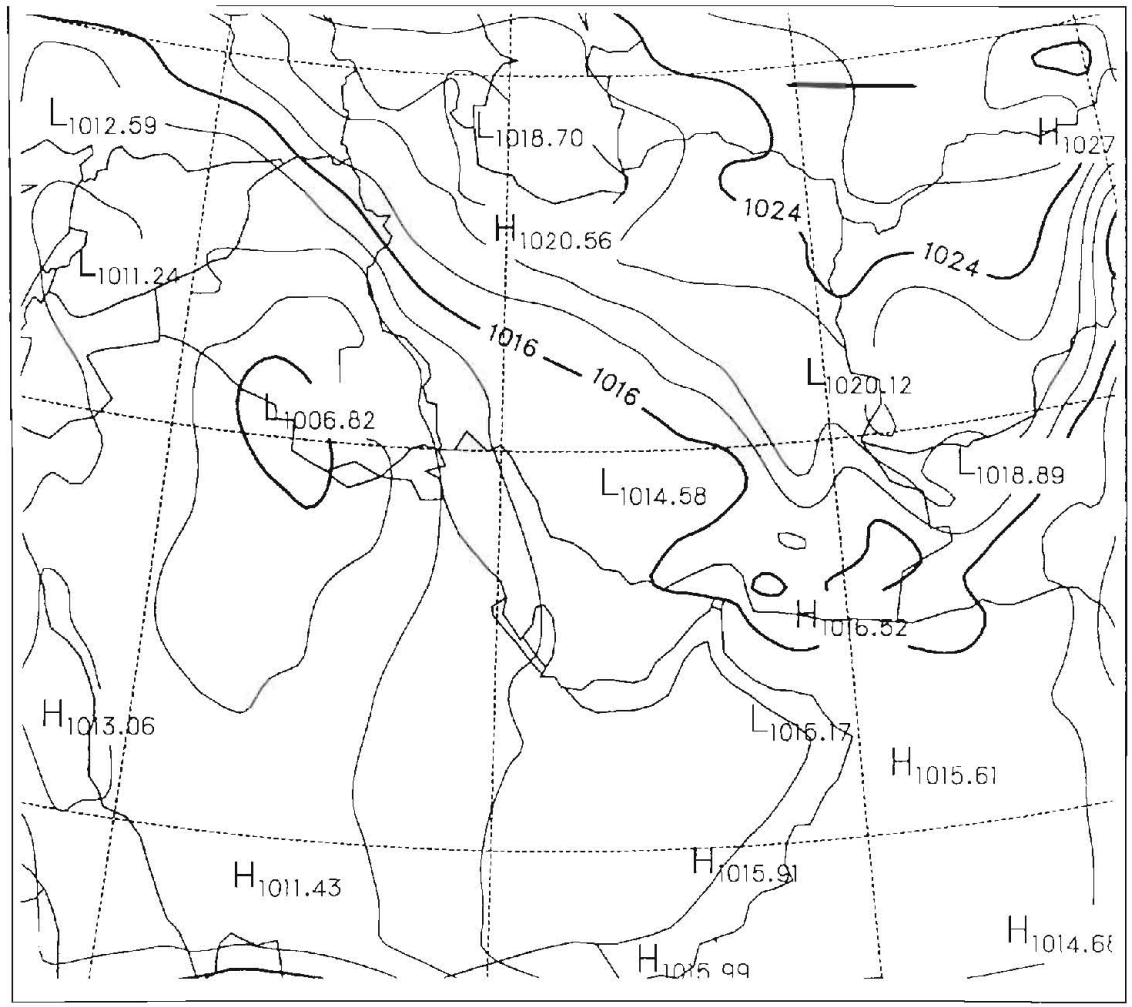

Figure 5.21 NORAPS 00Z Mean Sea Level Pressure Analysis for 15 Feb., 1995.

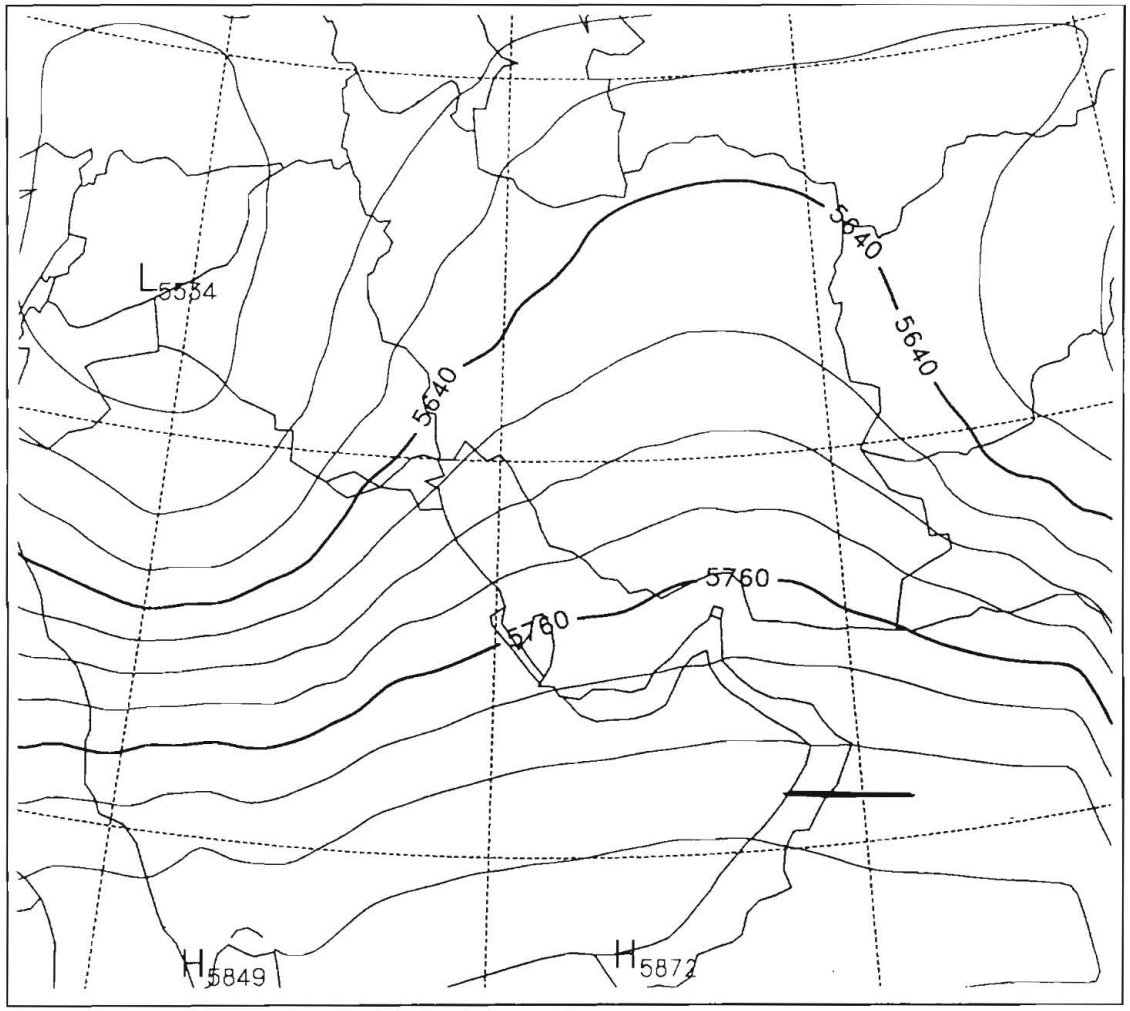

Figure 5.22 NORAPS 00Z 500 mb. Height Analysis for 15 Feb., 1995.

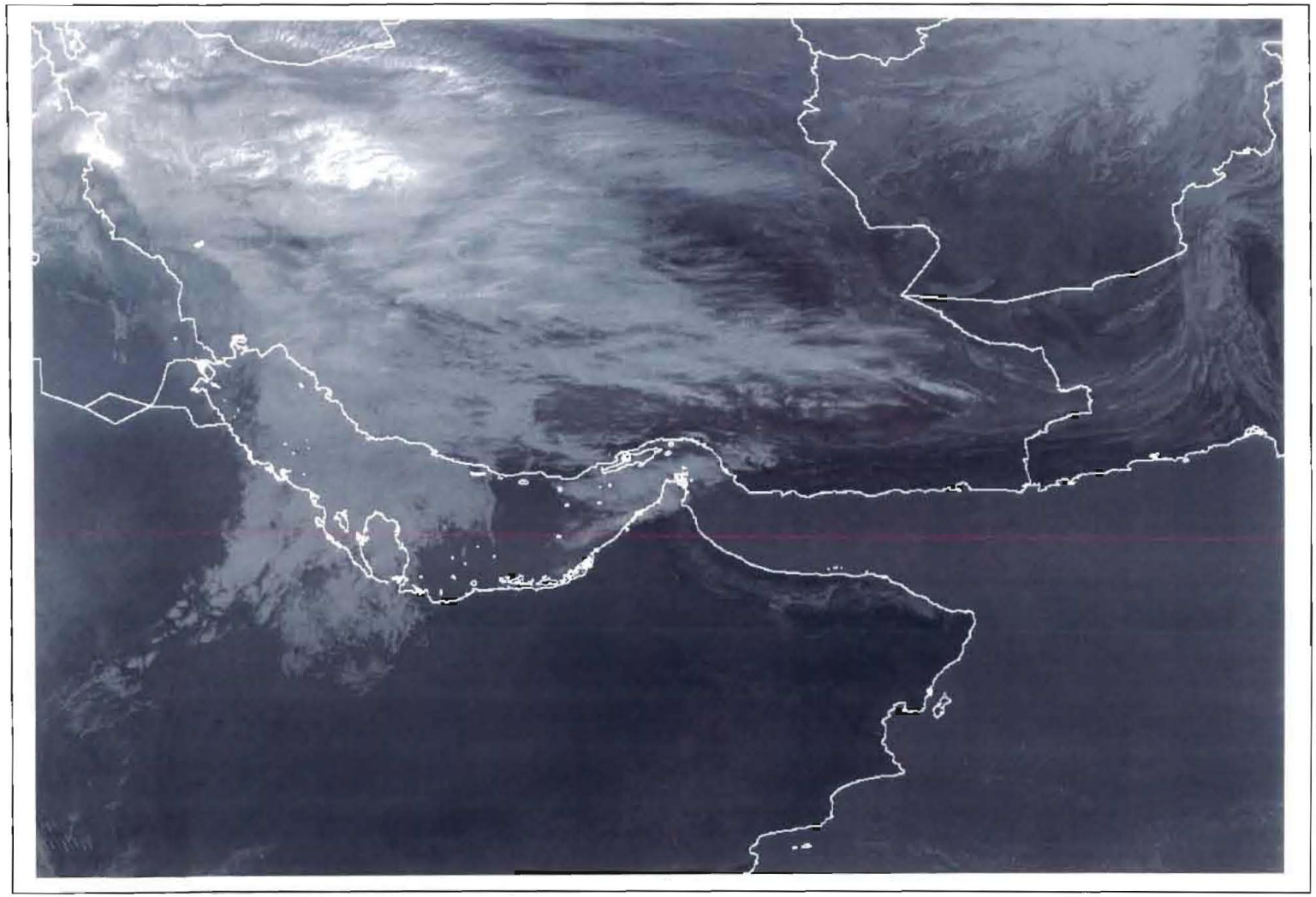

Figure 5.23 0546Z DMSP Infra-red Image on 15 Feb., 1995.

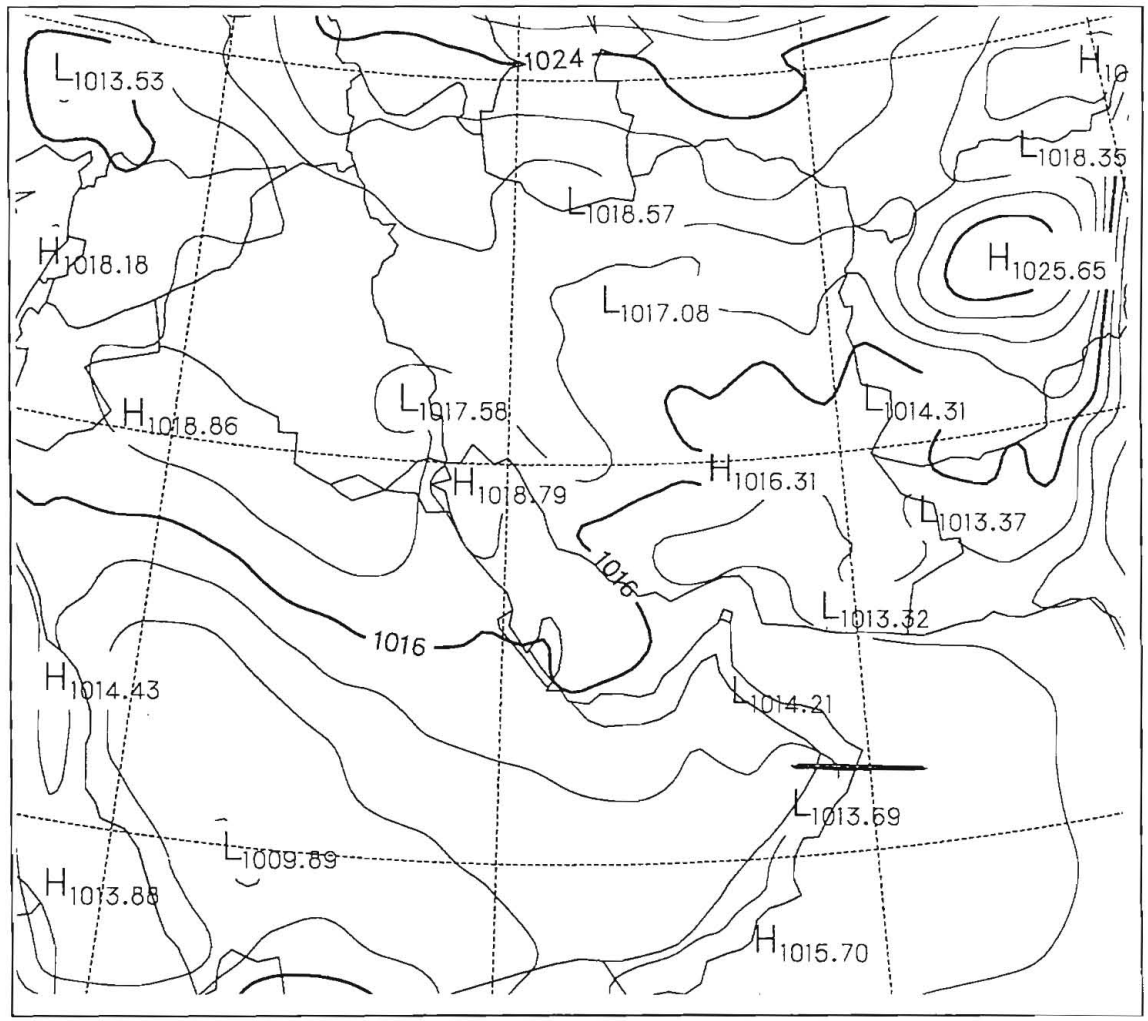

Figure 5.24 NORAPS 12Z Mean Sea Level Pressure Analysis for 16 Feb., 1995.

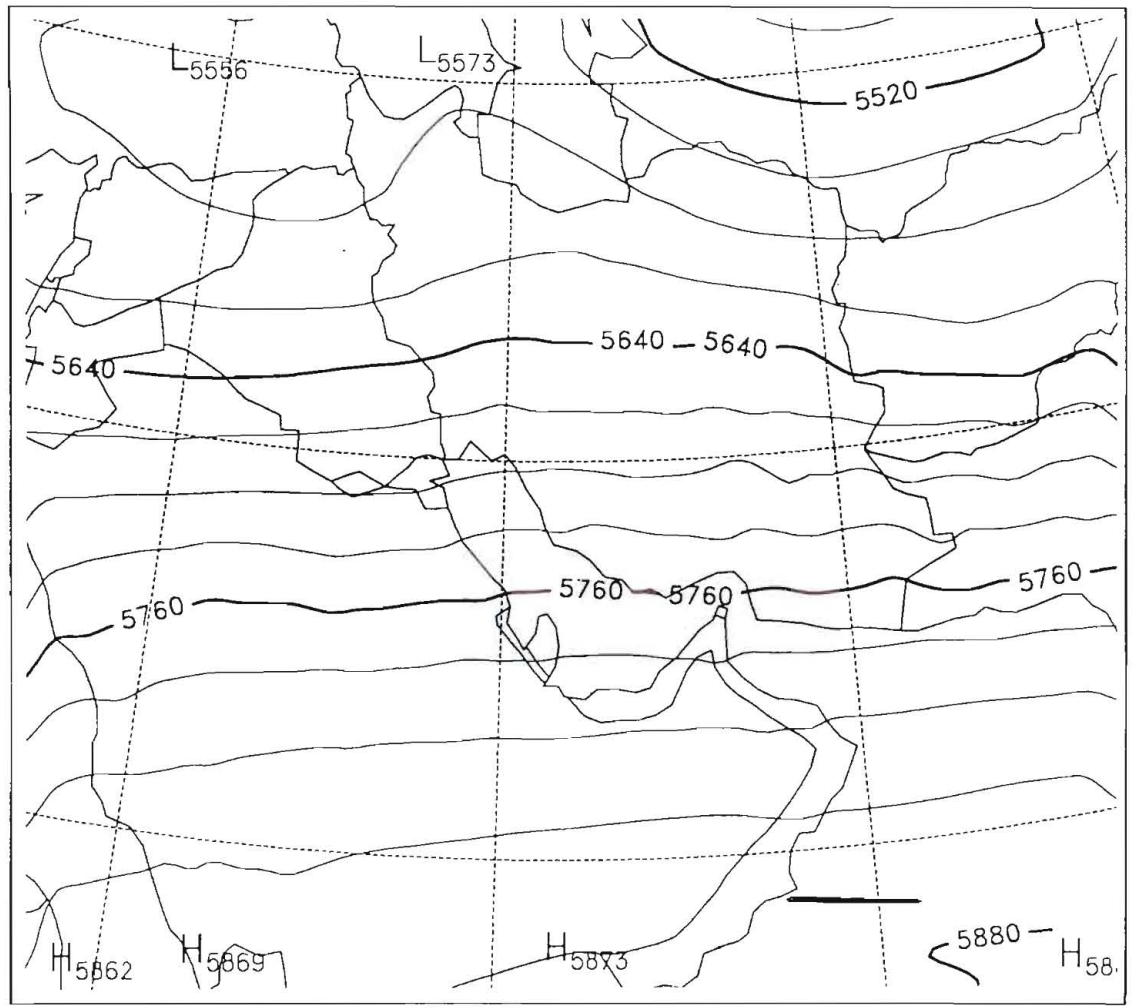

Figure 5.25 NORAPS 12Z 500 mb. Height Analysis for 16 Feb., 1995.

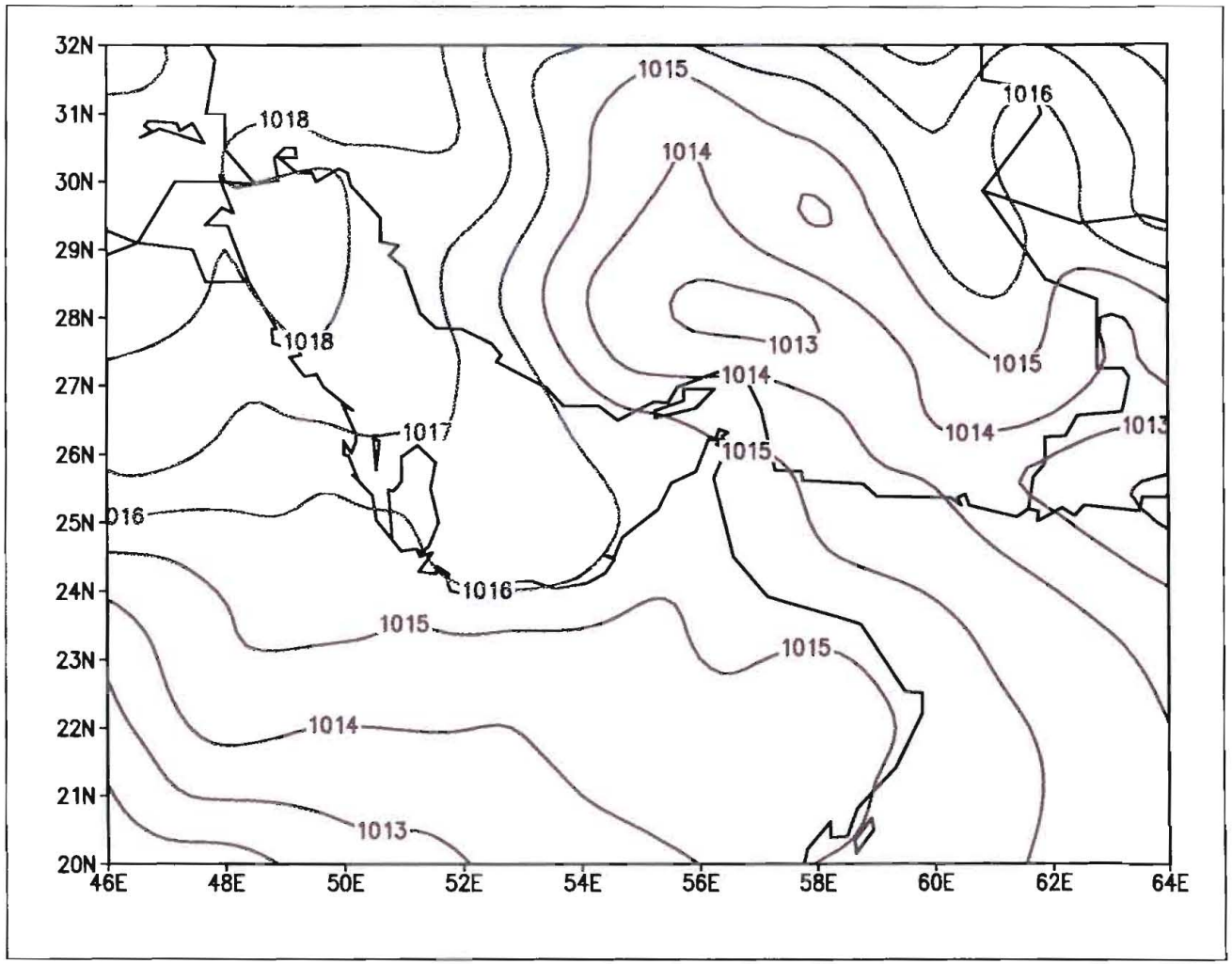

Figure 5.26 NORAPS (τ=15 hr.) 15Z Sea Level Pressure for 16 Feb., 1995.

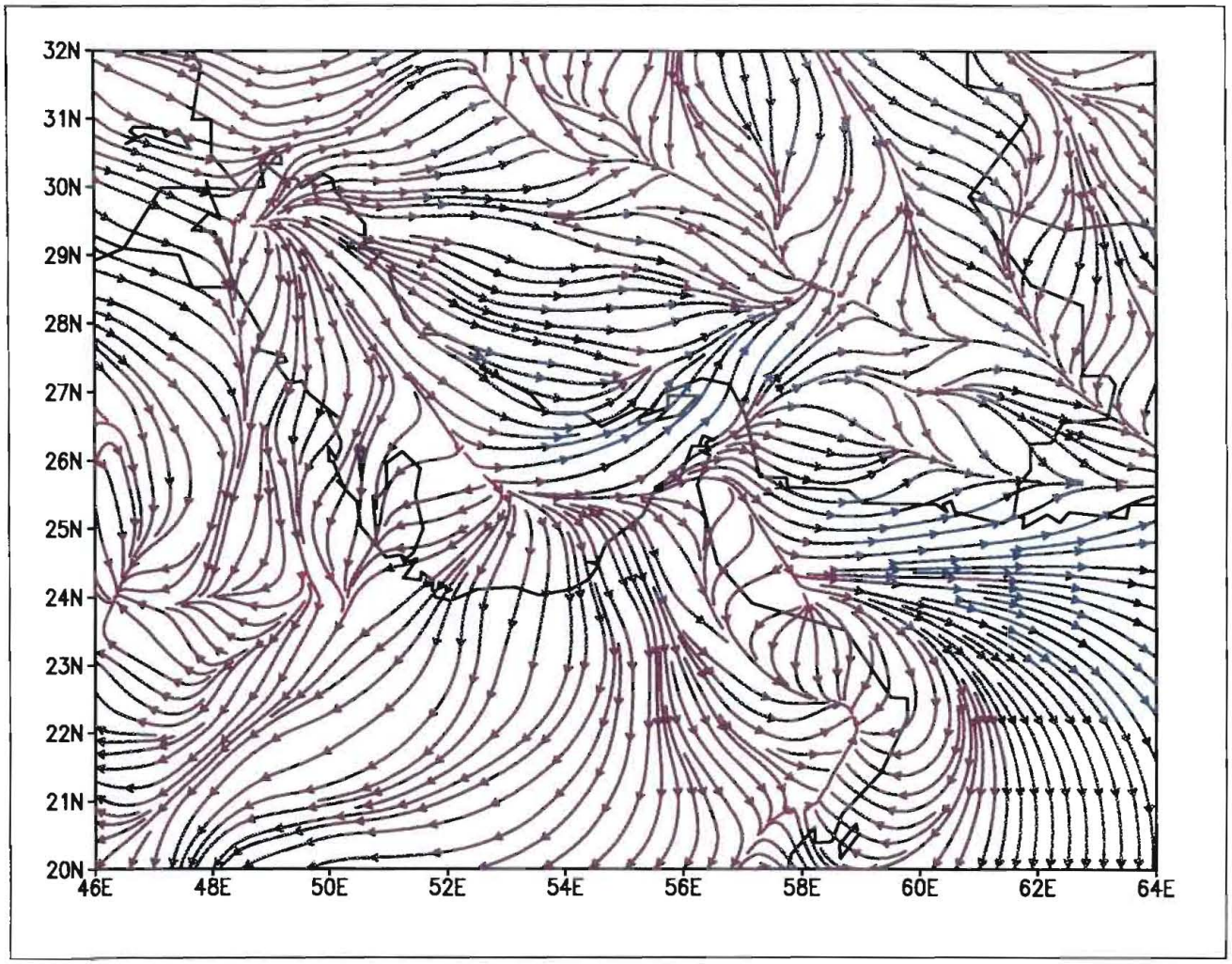

Figure 5.27 NORAPS (τ=15 hr.) 15ZSurface Streamlines for 16 Feb., 1995.

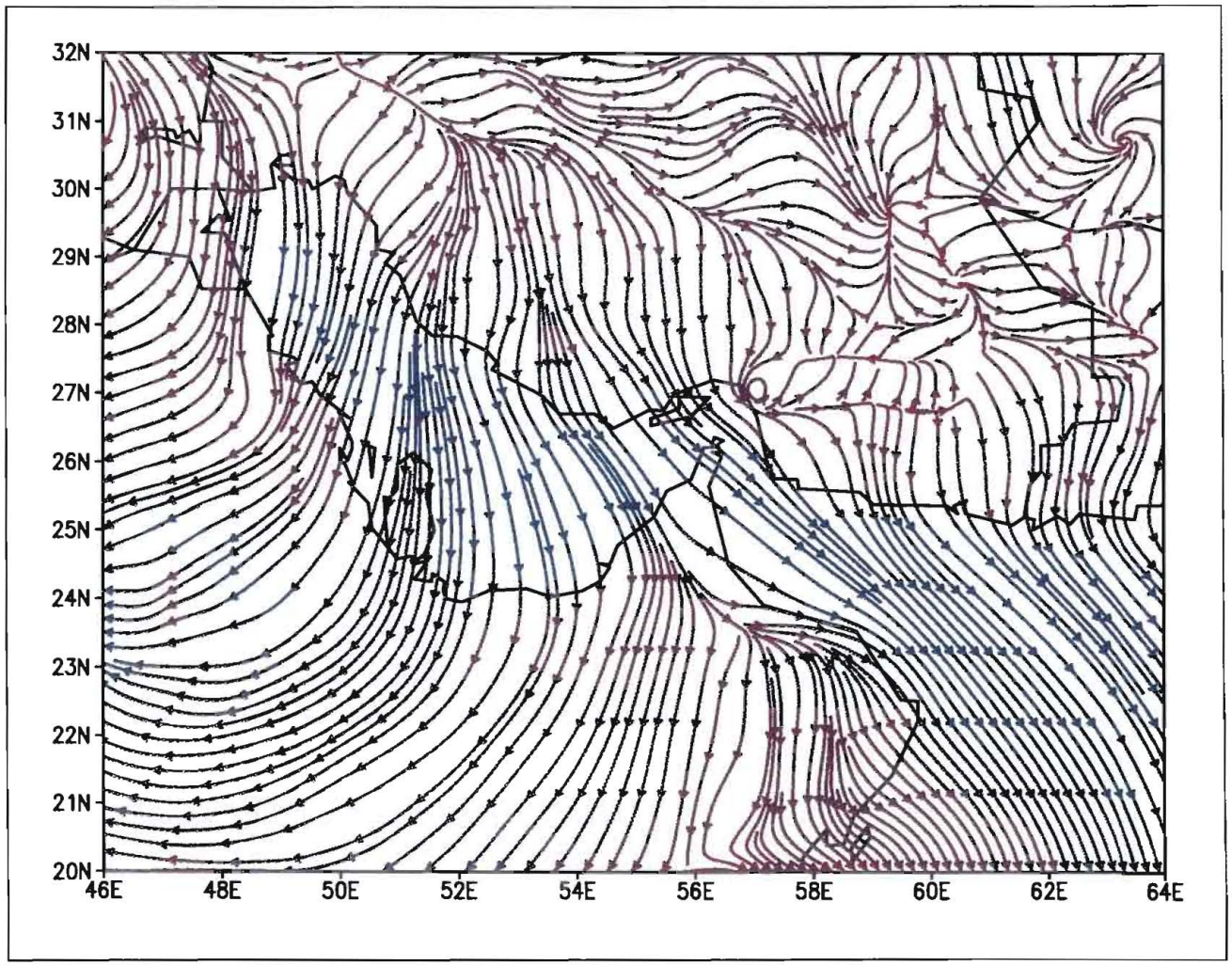

Figure 5.28 NORAPS (τ=15 hr.) 03Z Surface Streamlines for 17 Feb., 1995.

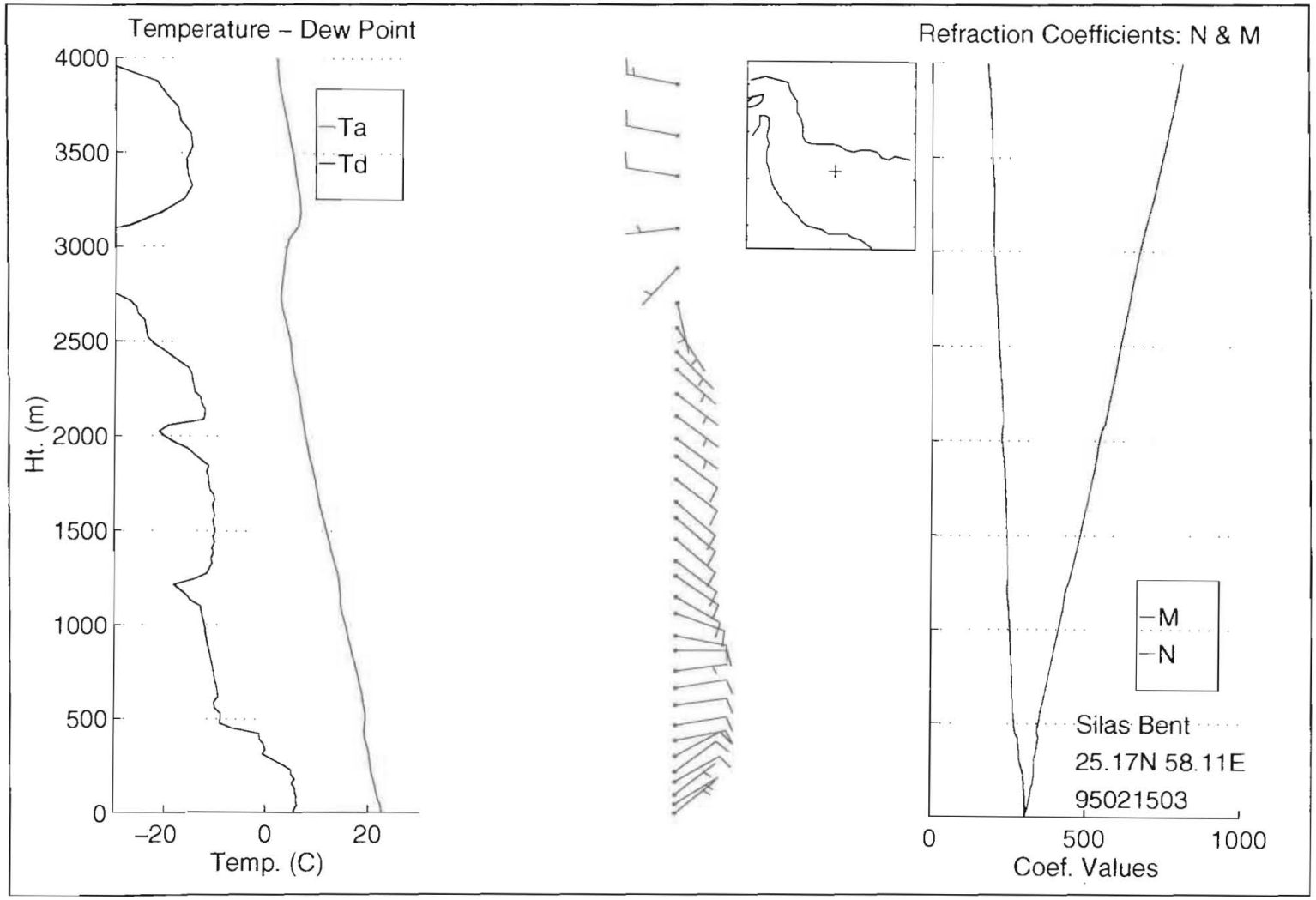

Figure 5.29 03Z Radiosonde Launched from the Silas Bent on 15 Feb., 1995.

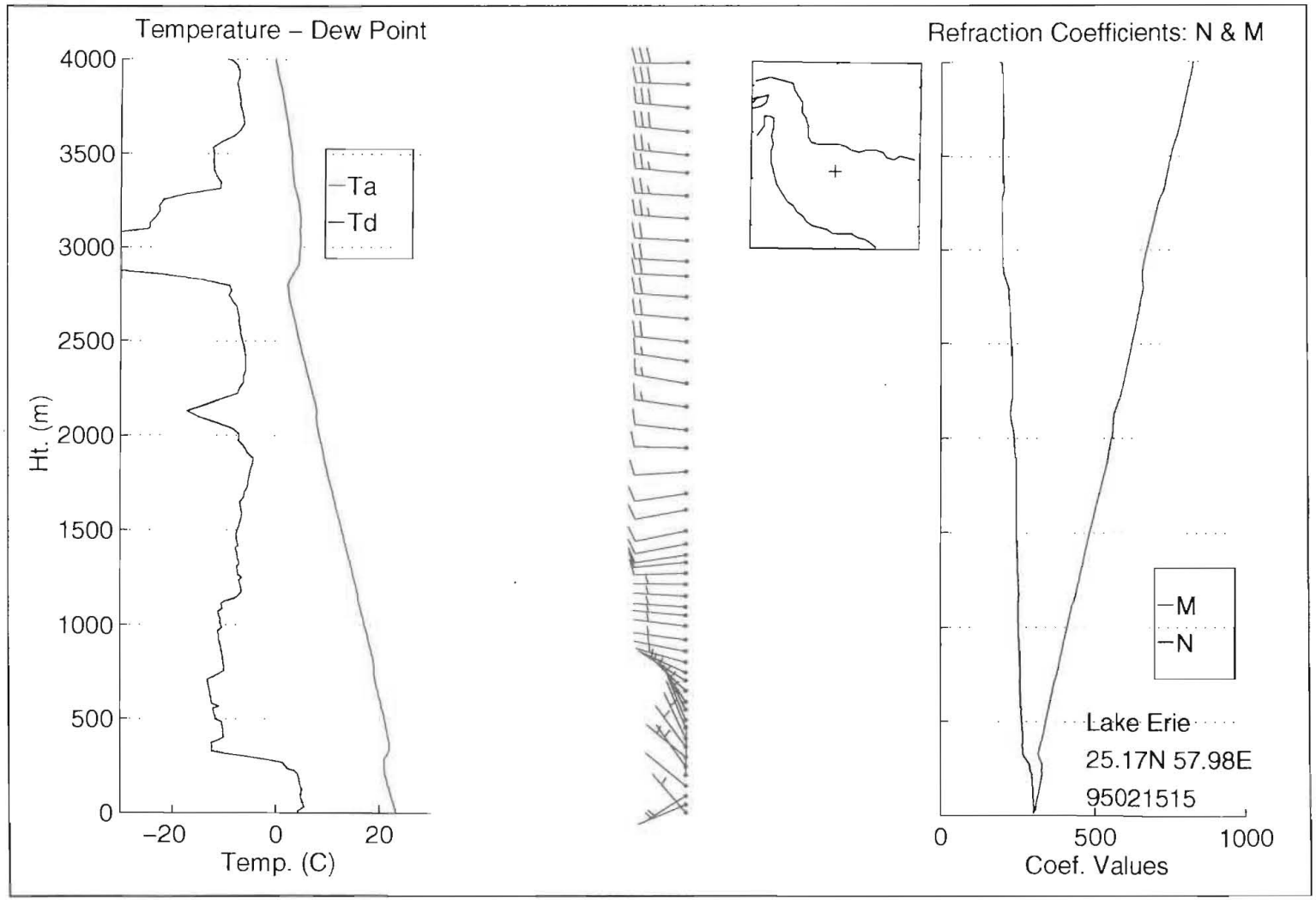

Figure 5.30 15Z Radiosonde Launched from the Lake Erie on 15 Feb., 1995.

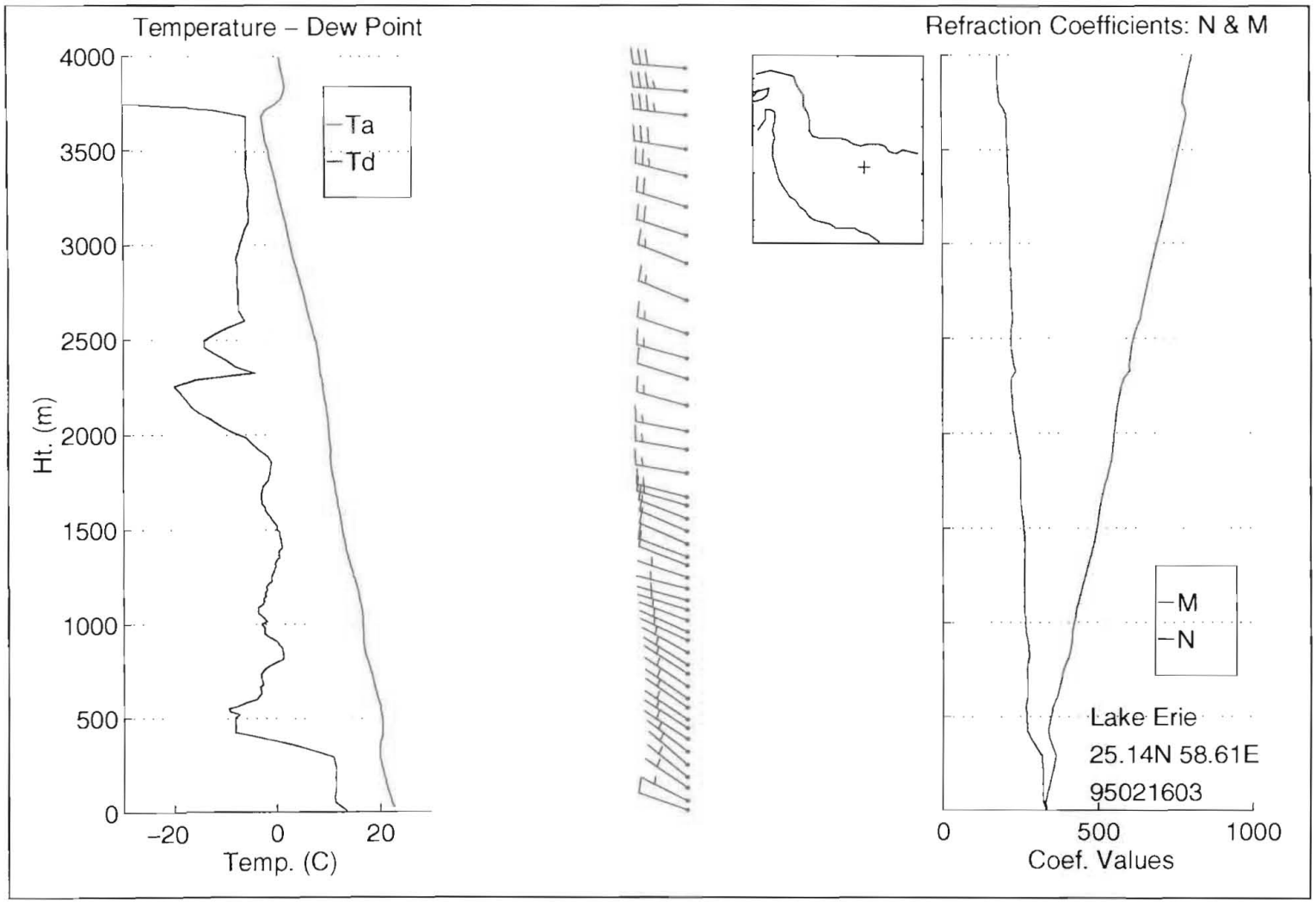

Figure 5.31 03Z Radiosonde Launched from the Lake Erie on 16 Feb., 1995.

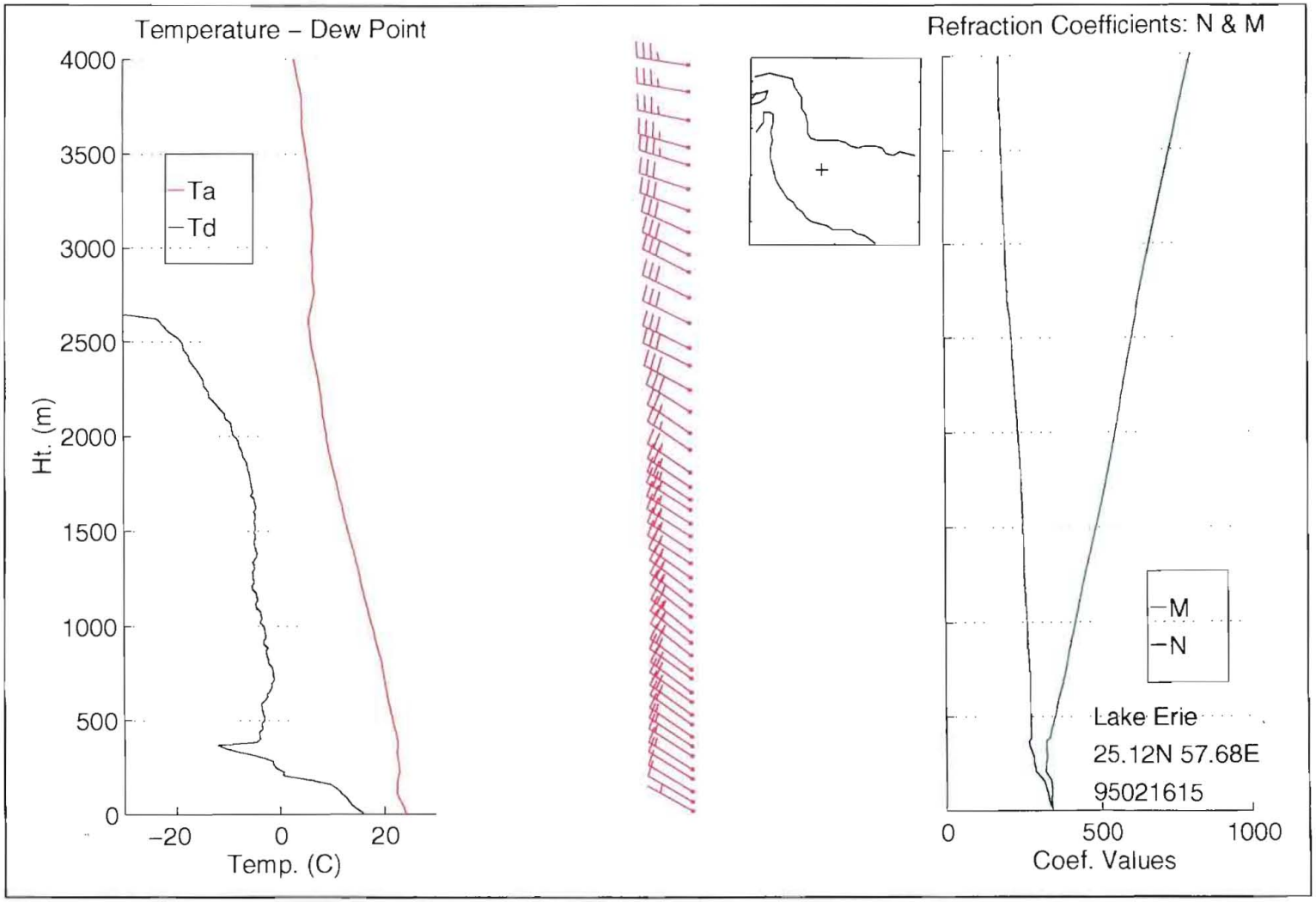

Figure 5.32 15Z Radiosonde Launched from the Lake Erie on 16 Feb., 1995.

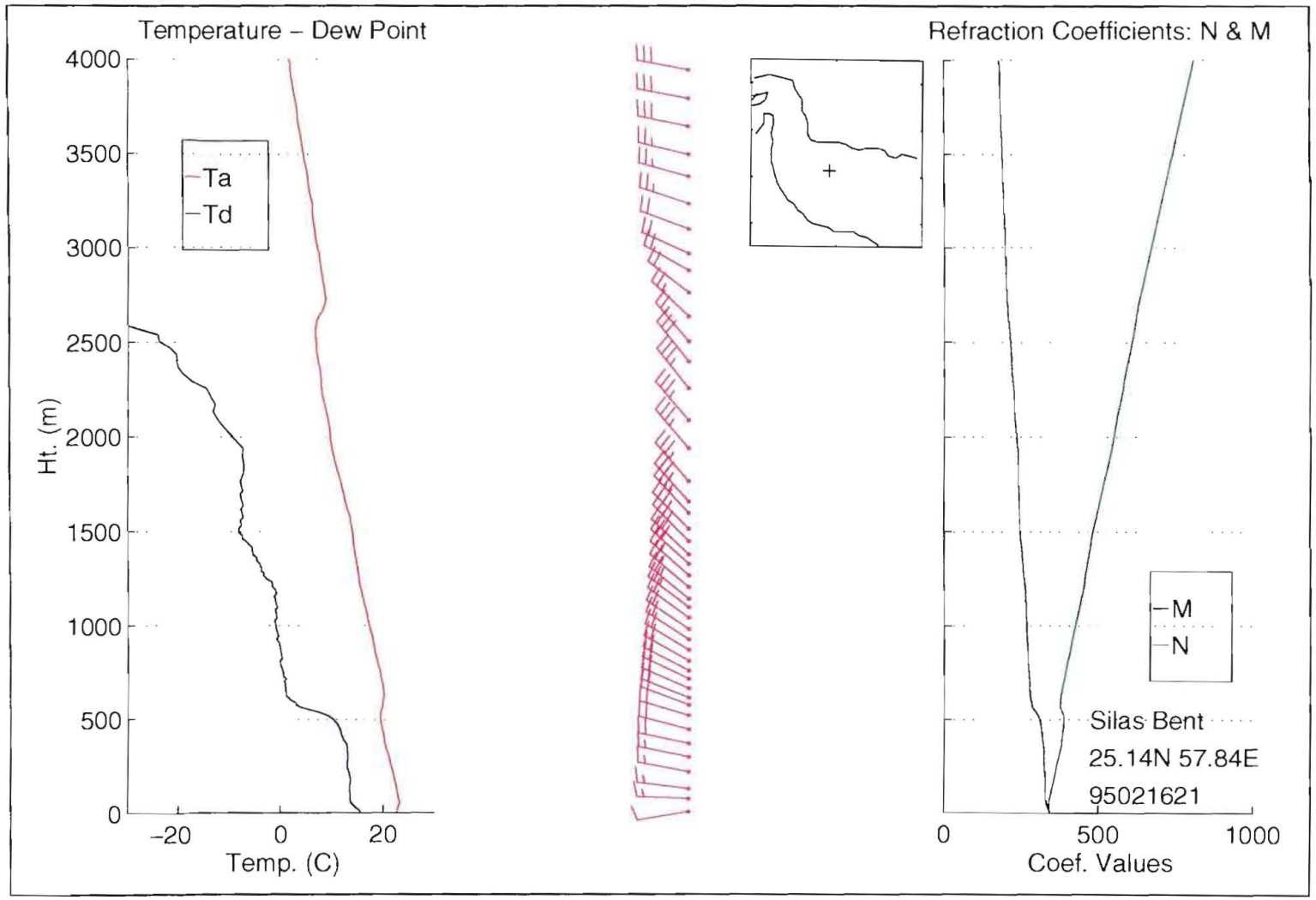

Figure 5.33 21Z Radiosonde Launched from the Silas Bent on 16 Feb., 1995.

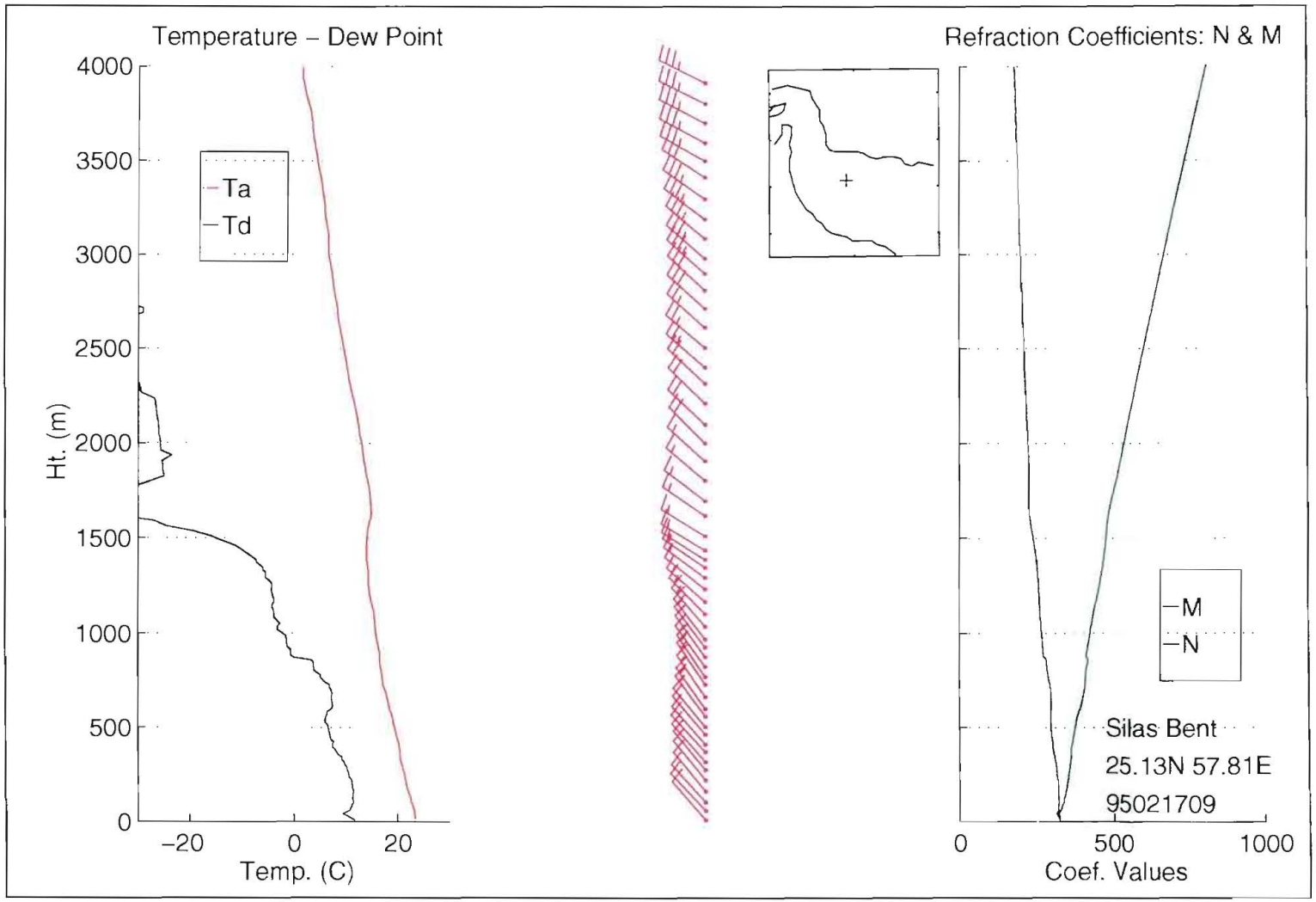

Figure 5.34 09Z Radiosonde Launched from the Silas Bent on 17 Feb., 1995.

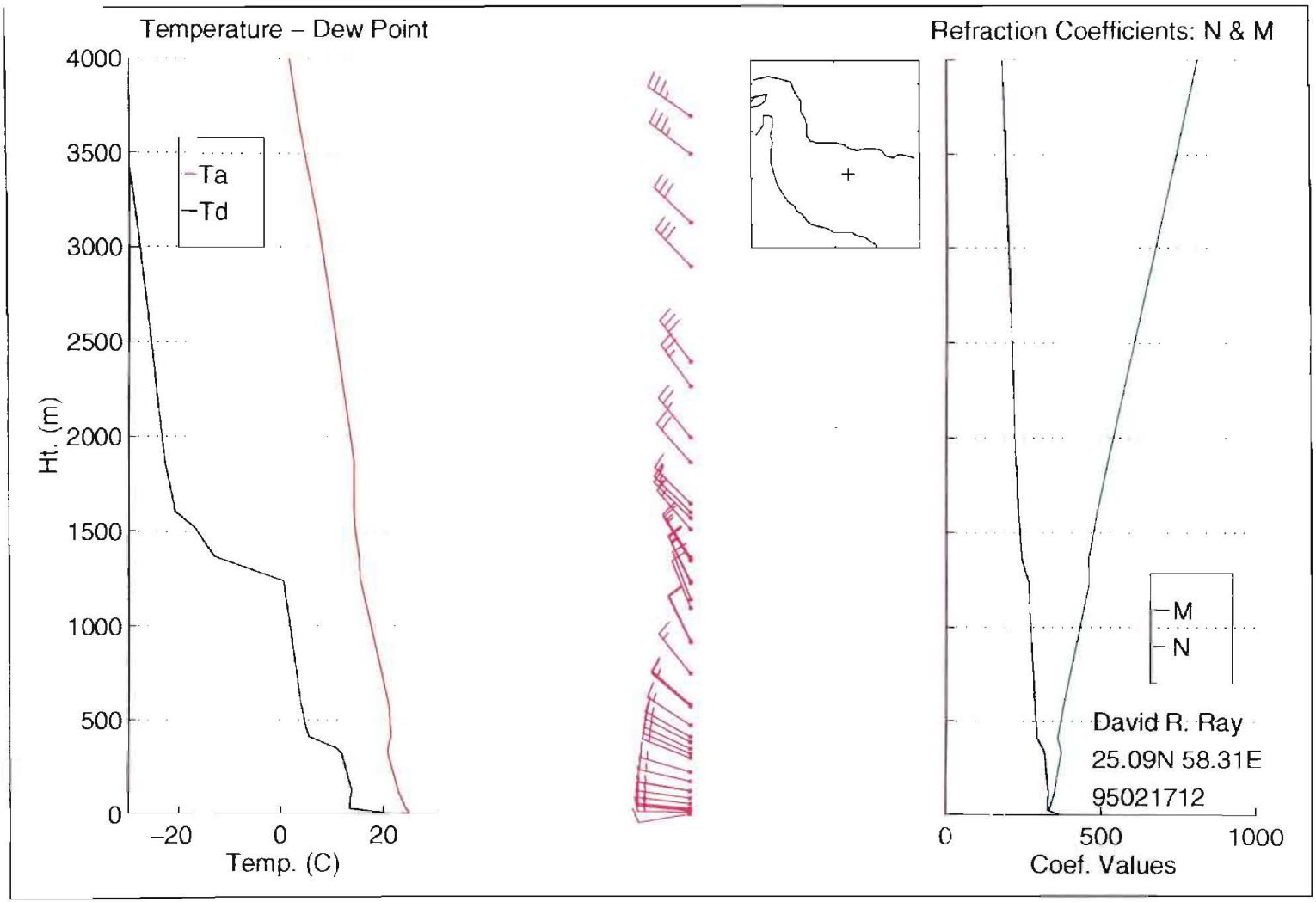

Figure 5.35 12Z Radiosonde Launched from the David R. Ray on 17 Feb., 1995.

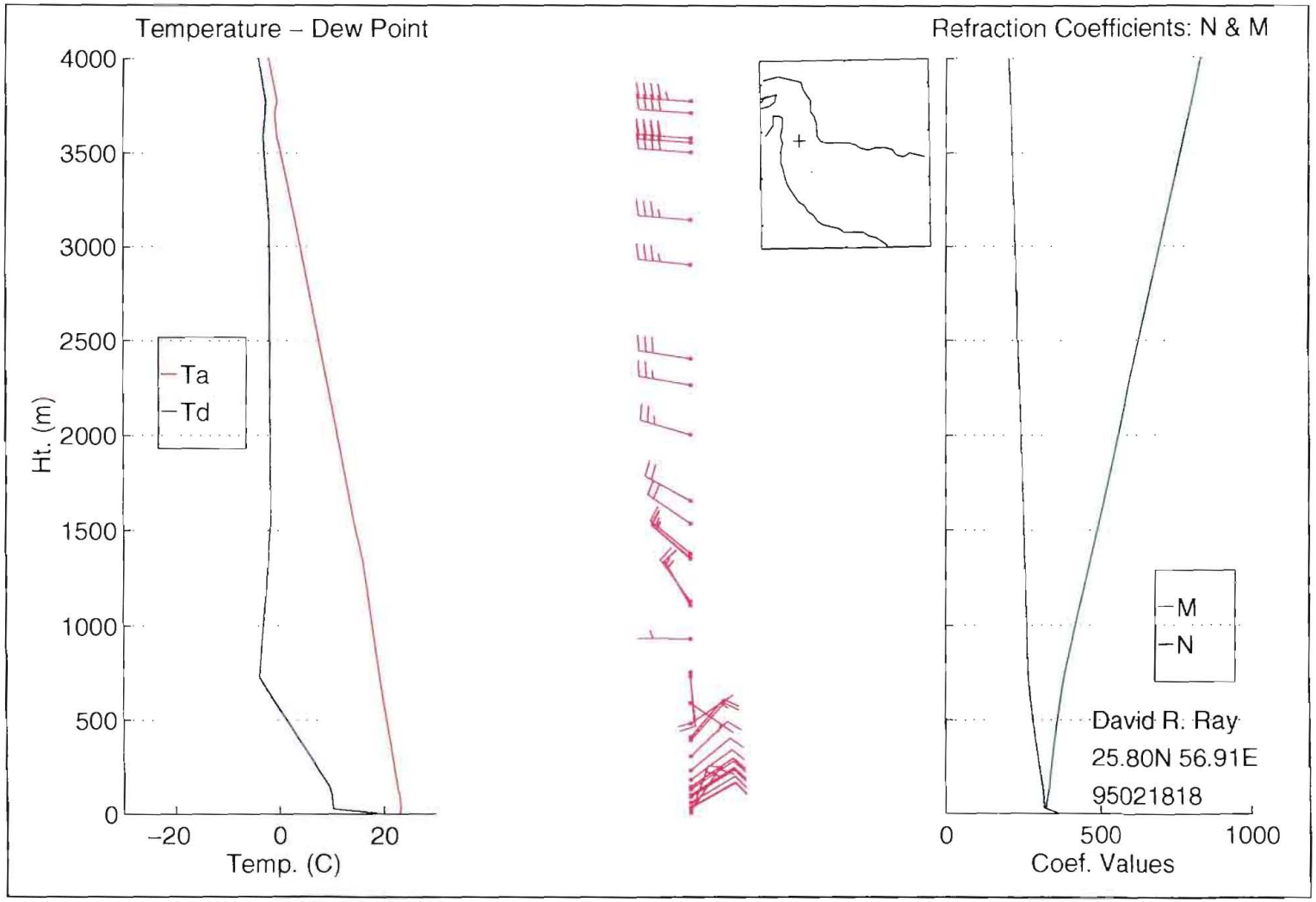

Figure 5.36 18Z Radiosonde Launched from the David R. Ray on 18 Feb., 1995.

VI. CONCLUSIONS AND RECOMMENDATIONS

This thesis investigated the reasons for the variability of atmospheric refraction in the Persian Gulf and Gulf of Oman seen during SHAREM 110. It was shown that operationally significant changes to vertical profiles of M can occur in small periods of time and over relatively short distances. Topography and its effects on the direction of low level wind flow can play a large role in variations of profile properties. Land/sea breeze effects were capable of modifying low level wind flow which, in turn, could greatly affect how a vertical profile of M would appear, especially in the Gulf of Oman. Specifically, four different weather regimes and their influence on atmospheric refractivity were discussed in this thesis. The first two were in the Persian Gulf and the other two were in the Gulf of Oman.

The first regime described was the Kaus wind period in the Persian Gulf which typically precedes the onset of a Shamal. Examples presented showed how these southeasterly winds are channeled by the local topography, especially in the southeastern portion of the Persian Gulf where SHAREM 110 was conducted. The in situ sounding data and NORAPS model data showed how large differences in atmospheric moisture characteristics could exist over a relitively short horizontal distance resulting in large differences in the strength and altitude of trapping layers. The atmosphere became more and more mixed and elevated moisture gradients disappeared with the approach of a frontal system.

The second regime that occured during the Persian Gulf portion of SHAREM 110 was the Shamal. These strong northwesterly winds dominated the region for almost five days.

The changes in atmospheric refractivity during this time period seemed to be the most "predictable" than during any other period. Changes in M were primarily due to synoptic scale forcing (i.e. large scale subsidence associated with negative vorticity advection aloft and development of a surface mixed layer) and was exhibited in all of the soundings.

The situation was somewhat different for the third regime, the transition to the Northeast Monsoon, which occurred in the Gulf of Oman. By this time, the Shamal had weakened significantly. The effects of the land/sea breeze became more noticeable in the low level flow and the soundings. At night very dry air from both coasts of the Gulf of Oman moved out over the water under the influence of a land breeze. These off shore winds were drier and stronger than when the Northeast Monsoon was fully developed. This led to decreasing moisture in the lower levels causing the elevated trapping layer to disappear. The sea breeze contributed to the reformation of a mixed boundary layer during the day allowing trapping layers to once again form.

The fourth regime was a short Shamal event and also occurred in the Gulf of Oman. This regime appeared to support the production of a marine layer and associated trapping layer. This was probably due to the moist air from the Persian Gulf which flowed into the Gulf of Oman during this period had a long fetch over water. This tended to permit the well mixed boundary layer to remain even at night when dry land breeze air from both shores would mix with this moister air.

The consequences of varying refractive conditions such as those described in this study are critical to coastal operations. Many of the changes in refractivity described from the SHAREM 110 data set took place over much shorter time periods than twelve hours.

They would have been missed by naval units launching soundings at the normal synoptic times of 00Z and 12Z each day. It was only because such a large effort was expended to launch soundings at much smaller intervals that it was possible to observe the changes in refraction documented in this thesis.

Knowledge of such a quickly changing refractive environment is very useful to an operational commander. Questions such as battle group vulnerability and at what level a strike mission should be flown could be answered confidently. The key to this capability lies in developing an EM/EO support system that is capable of quickly and accurately displaying real-time and predicted environmental information. Hence, this is the very reason for the existence of the SHAREM series of exercises.

In addition to the large amount of environmental data collected during SHAREM 110, a large number of actual detection ranges for various targets with various radars was also recorded. Future studies should include comparing the upper air profiles collected during this exercise with predicted NORAPS profiles. Both of these types of profiles could then be placed into the Navy's RPO program and the resulting predicted detection ranges could be compared with the actual ranges. This would give some insight on the seccess of the EM/EO support system used during SHAREM 110.

LIST OF REFERENCES

Brody, L.R., 1977: Meteorological Phenomena of the Arabian Sea, NAVENVPREDRSCHFAC AR 77-01, 188pp.

Craigie, K.M., 1993: Assessment of Atmospheric Influence on Surveillance Radar Performance in Littoral Zones, Master's Thesis, Naval Postgraduate School, Monterey, California, 73 pp.

Dalton, J.H., 1994: Forward...From the Sea, Library of Congress no. VA 58.4 053 1994, 10 pp.

Farrell, R. J., 1988: The Persian Gulf Region - A Refractivity Study, USAFETAC TN-88/004, 71 pp.

Hubert, W.E., Hull, A.N., Morford, D.R., and Englebretson, R.E., 1983: Forecasters Handbook for the Middle East/Arabian Sea, NAVENVPREDRSCHFAC CR 83-06, AD-A134312, 165 pp.

O'Keefe, S., 1992: ...From the Sea - Preparing the Naval Service for the 21st Century, Library of Congress no. VA 58.4 053 1992, 17 pp.

Perrone, T.J., 1979: Winter Shamal in the Persian Gulf, NAVENVPREDRSCHFAC TR 70-06, 172 pp.

Walters, K.R., and Sjoberg, W.F., 1988: The Persian Gulf Region - A Climatological Study, USAFETAC TN-88/002, 62 pp.

INITIAL DISTRIBUTION LIST

		No. Copies
1.	Defense Technical Information Center 8725 John J. Kingman Rd., STE 0944 Ft. Belvoir, VA 22060-6218	2
2.	Library, Code 13 Naval Postgraduate School Monterey, California 93943-5101	2
3.	Commander Space and Naval Warfare Systems Command (PMW-175) Washington D.C. 20363-5100 Attn: CAPT R. Hillyer	1
4.	Naval Research Laboratory Naval Postgraduate School Annex Monterey, California 93940-5006 Attn: A. Goroch, Code 7543	1
5.	Naval Research Laboratory Naval Postgraduate School Annex Monterey, California 93940-5006 Attn: J. Cook, Code 7542	1
6.	Naval Research Laboratory Naval Postgraduate School Annex Monterey, California 93940-5006 Attn: L. Phegley, Code 7542	1
7.	Professor K. Davidson Meteorology Department, Code MR/DS Naval Postgraduate School Monterey, California 93943-5002	2
8.	Proffessor C. Wash Meteorology Department, Code MR/DS Naval Postgraduate School Monterey, California 93943-5002	2

9. Analysis & Technology, Inc. 1
2341 Jefferson Davis Highway
Suite 1250
Arlington, VA 22202
Attn: M. Pastore

10. LT David J. Byers, USN 1
U.S. Naval European Meteorology and Oceanography Center
PSC 819, Box 31
FPO AE 09645-3200